October 12, 1989

A study of η production in 530 GeV/c Hadronic Interactions

A Dissertation Presented
by
Christopher B. Lirakis
to
The Department of Physics

Submitted in partial fulfillment of the requirements for the degree of Doctor of Philosophy in Physics in the Graduate School of Arts and Sciences of Northeastern University.

---

* Work supported by NSF grant number

October 12, 1989

A study of π° and η production in 530 GeV/c Hadronic Interactions

C.B. LIRAKIS
Northeastern University Department of Physics
360 Huntington Avenue, Boston Massachusetts

ABSTRACT

We present a measurement of η production in 530 GeV/c proton , and π^- collisions on beryllium targets. The production is studied with respect to transverse momentum, P_T . The $\gamma\gamma$ decay mode is presented. Data presented were from 530 GeV/c $\pi^{\pm}$, P, *and* K^- on beryllium and copper targets. The transverse momentum, range studied is from 4.0 – 8.0 GeV/c . A measurement of the differential cross section $E\frac{d^3\sigma}{d^3p}$presented as a function of transverse momentum. The production of η to π° is examined as a function of P_T . Data were gathered during the 1987/88 run of Fermilab Experiment 706. The data were gathered from the E706 apparatus made up of a charged particle spectrometer and a large highly segmented liquid argon calorimeter. The trigger for data aquisition was for local depositions of high P_T energy in the electromagnetic calorimeter.

---

† in residence at Fermi National Accelerator Laboratory.

Northeastern University

Graduate School of Arts and Sciences

A study of η production in 530 GeV/c Hadronic Interactions

Author: Christopher B. Lirakis

Department: Physics

Approved for Thesis Requirements of the Doctor of Philosophy Degree.

Thesis Committee	Date

Department Head	Date

Acknowledgements:

First and foremost I would like to thank my wife Eleanor for helping me with this long and difficult process. I am quite sure that this thesis has been as difficult for her as it has been for me. I would also like to thank my daughter Elizabeth for taking my mind off physics and teaching me how to play again.

I would also like to thank the entire E706 collaboration. Without the help of every person this entire project would not have been possible.

I would like to take this space to thank the Department of Energy and National Science Foundation who footed the bill.

I would like to thank George Ginther for his support and sharing his experience with me. I would like to thank Marek Zielenski for teaching me tricks of the trade. I would like to thank fellow graduate students John Mansour, Dane Skow, and Eric Prebys for their friendship. I would like to thank Bud Dickerson for leading me astray when I needed it. Special thanks to Bill DeSoi who made so many nice figures that I took from him.

I would like to thank the Northeastern Professors, Bill Faissler, David Garelick, Mike Glaubman, and George Alverson for their aid in completing this project. I would like to thank Bill for reading each page of this thesis more than once. I would like to thank George for his guidance as an advisor and as a friend.

Thanks to Takahiro Yasuda for helping me get it all together.

Special thanks also to Tom Ferbel who first advised me to quit physics then later reversed his decision and talked me into joining the experiment.

Both my father and mother deserve a great deal of credit since they always encouraged me to find things out. They also put up with a great deal of my early experimentation. I a quite sure that they have both had shortened life spans due to the many heart stoppers I may have caused in my adventures.

Biographical Data

Christopher B. Lirakis

EDUCATION

Phd. Physics Sept. 1989	Northeastern University
M.S. Physics 1984	Northeastern University
B.S. Physics 1982	University of Rochester

POSITIONS HELD

5/83-Present.	Research Associate, Northeastern University Boston, Ma. 02115

Currently, in residence at Fermi National Accelerator Laboratory analyzing data from experiment E706.

9/82-5/83	Teaching Assistant, Northeastern University Boston, Ma. 02115
4/82-9/82	Field Technician, Science Applications Inc. Corp. Newport, R.I. 02840
9/80-9/81	Technician, U. of Rochester, Department of Physics Gravity Wave Lab. Rochester, N.Y. 14627

PUBLICATIONS and PRESENTATIONS

C. Lirakis et al., " A Comparision of π^0 η and η' Production in 530 GeV/c Hadronic Interactions ", APS spring Meeting, May 4, 1989.

PERSONAL

Date of birth December 8, 1959.

Place of birth Fall River, Massachussetts.

Current age 29, Married, 1 child.

Table of Contents

FIGURE CAPTIONS

TABLE CAPTIONS

1: MWPC lower left corner, facing downstream, location and acceptance.

2: Steel absorber plate beam aperture.

3: Cookies and their sections.

4: Hadron Calorimeter Front pulser cable connections.

5: Hadron Calorimeter Back pulser cable connections.

6: Pads not covered by pulser.

7: Pads not covered by pulser. continued

8: Pads not covered by pulser. continued

9: Pads not covered by pulser. continued

10: Pads not covered by pulser. continued

11: Table showing data broken down by beam polarity, run number, target, and Live Triggerable Beam, LTB. The Target CuBe represents the copper beryllium target mentioned in chapter 2. Set E does not include the spill scaler corrections.

12: The effects of Various Cuts on the Data Sample

13: Calorimeter geometric acceptance and reconstruction efficiency, for P_T from 3.5 to 7.5 and rapidity from -1.0 to 0.6.

14: Errors on table above.

15: Acceptance in finer bins for forward region.

16: Errors on table above.

17: Cerenkov and veto wall scaler values.

18: Upstream latch house scalers, beam and interaction definitions.

19: Faraday room scalers, pretriggers and triggers .

1. The Physics of E706.

The experiment described here was designed to measure direct photon processes. Contained in this chapter is a short discussion on this process. A direct photon is a photon which comes from the primary interaction of the particle constituents, that is, from the quarks and gluons that make up the beam and target particles. E706 is a fixed target experiment designed to measure these processes.

1.1. QCD AND DIRECT PHOTONS.

Quantum chromodynamics, QCD, is the theory that describes the strong interactions. It is modeled after quantum electrodynamics, QED, which describes the electromagnetic interaction. QCD differs from QED in size of the coupling constant and in the behaviour of the interactions as a function of distance. The concept of distance is coupled with the energy transfer in the interaction or Q^2 . Q^2 is the energy flow of the interaction and is proportional to the transverse momentum, P_T of the scattered products. The coupling constant for QED is α_{em} , and the coupling constant for QCD is given by α_s . A full discussion of these theories is beyond the scope of this document.* For very large momentum transfer, Q^2 , solutions for QED diverge. This is the opposite for QCD which diverges at low Q^2 . It was pointed out by Gross and Wilczek[1] that the solutions for α_s converged sufficiently well at high Q^2 that perturbative QCD is permitted. It can be easily seen in the dependence of α_s on Q^2 by

$$\alpha_s(Q^2) = \frac{12\pi}{(33 - n_f)\ln(\frac{Q^2}{\Lambda^2})} \tag{1.1}$$

where n_f is the number of quark flavors and Λ is the scale factor, that

---

⋆ A more complete discussion may be referenced in Quantum Electrodynamics, R.P. Feynman, Copyright 1961, W.A. Benjamin, Inc. ISBN 0-8053-2501, and Gauge Theories of the Strong, Weak, and Electromagnetic Interactions, Chris Quigg, Copyright 1983, The Benjamin-Cummings Publishing Co., Inc., ISBN 0-8053-6020-4.

α_s diverges rapidly at low Q^2 . This motivates us to study QCD at large Q^2 or proportionally high P_T . Quarks and gluons in QCD demonstrate asymtoptic freedom as seen in equation (1.1)which shows that as $\alpha_s(Q^2) \rightarrow 0$ that $Q^2 \rightarrow \infty$, and $\alpha_s(Q^2) \rightarrow \infty$ as $Q^2 \rightarrow 0$. This implies that α_s becomes quite large at large distances. This model explains the behaviour of scattered partons to fragment or hadronize, that is, the free quarks or gluons tend to become particles quickly by interacting with the vacuum state. Probing the structure of the incident or target particles requires large Q^2 . The dominant reaction to study for proton or meson on target is

$$pp \rightarrow jet + jet,$$

where the jets are the fragmented partons. The jet jet cross section is proportional to α_s^2. The four vector of the jet is closely related to that of the parent parton. Studying this process may lead to better understanding of the underlying parton-parton scattering process. This is difficult to do since we do not yet understand the fragmentation process, and it is experimentally difficult to separate out the jet. The jet identification algorithm has a tendency to bias the results. It is easier to study the direct photon process

$$pp \rightarrow \gamma + X$$

since the photon couples in an electromagnetic manner and is a clean signal. This does have the disadvantage that the cross section is proportional to $\alpha_s \alpha_{em}$, thus is down from the jet jet process by 2 orders of magnitude. The direct photon cross section is given by

$$E\frac{d^3\sigma}{d^3p} = \sum \int dx_a dx_b G_{\frac{a}{A}}(x_a, Q^2) G_{\frac{b}{B}}(x_b, Q^2) \frac{\hat{s}}{\pi} \frac{d\sigma}{d\hat{t}}(ab \rightarrow \gamma + X)\delta(\hat{s} + \hat{t} + \hat{u}) \quad (1.2)$$

where the caret has been added to denote the parton-parton subprocess, and the G are the structure functions governing the parton distribu-

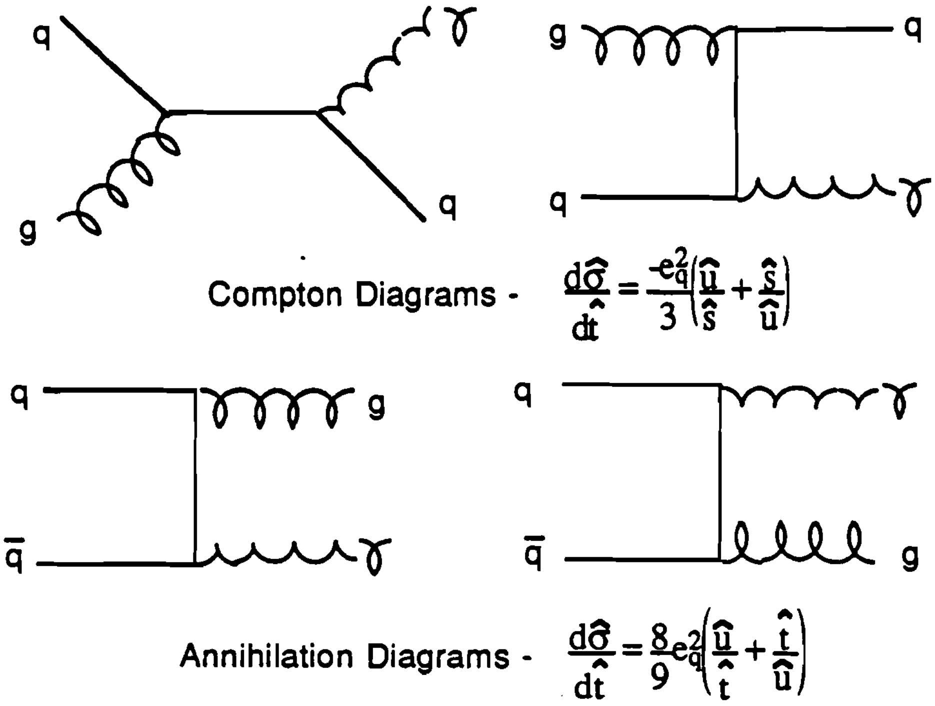

Figure 1: Feynman diagrams of A) Compton and B) Annihilation processes

tions.[2] This may be shown graphically in figure 1. These Feynman diagrams schematically represent to first order the direct photon processes. The Compton process has two partons scattering, and the annihilation process has a quark-antiquark annihilation. The crossed diagrams, where the incoming partons are exchanged in essentially the same process, also contributes.

Direct Photons and Quark Charge.

In proton, nucleon collisions at low Q^2 , the Compton process is dominant while at higher Q^2 the annihilation process dominates. This is brought about by contributions from valence quarks at high Q^2 . The annihilation process also dominates in pion beams, $\pi^{\pm}$. Pion beams also have the interesting property that the ratio of direct photon cross sections is $\frac{1}{8}$.

$$\frac{E\frac{d^3\sigma}{d^3p}(\pi^+ \to \gamma + X)}{E\frac{d^3\sigma}{d^3p}(\pi^- \to \gamma + X)} \approx \frac{1}{2}(\frac{e_d}{e_u})^2 = \frac{1}{8} \tag{1.3}$$

Equation (1.3)shows that the difference comes from the quark charge since the π^+ meson contains a $u\overline{d}$ and the π^- contains a $\overline{u}d$ combination and the process is electromagnetic. The direct photon is electromagnetically coupled to the quark, thus the quark charge enters into the equation.[3]

Direct Photon to π° Ratio.

The direct photon cross section can be compared to the jet cross section by comparison of direct photon to π° cross section. It is expected in QCD that the ratio

$$\frac{\sigma(AB \to \gamma + X)}{\sigma(AB \to \pi^\circ + X)}$$

should be one for lower P_T values and rise for higher values. This is expected because quark-gluon scattering is expected to dominate at large values of Q^2 . Thus in a direct photon event the away side jet is initiated by a quark whereas a π° away side jet could be either a quark or a gluon fragmenting. The gluon fragmentation is expected to be much softer in nature than quark fragmentation.[4]

Two Direct Photons.

Since the experiment is designed to study direct photons we may also study the process,

$$\sigma(AB \to \gamma\gamma)$$

although this is difficult to extract from the background. To compare the cross sections for direct photon with double direct photon, we replace the accompanying quark/gluon with another photon in the previous Feynman diagrams and we get

$$\frac{E\frac{d^3\sigma}{d^3p}(\pi^- \to \gamma\gamma)}{E\frac{d^3\sigma}{d^3p}(\pi^- \to \gamma + X)} \approx \frac{3}{4}(\frac{\alpha_e m}{\alpha_s})e_u^2 = \frac{1}{3}\frac{\alpha_e m}{\alpha_s} \tag{1.4}$$

and

$$\frac{E\frac{d^3\sigma}{d^3p}(\pi^+ \to \gamma\gamma)}{E\frac{d^3\sigma}{d^3p}(\pi^+ \to \gamma + X)} \approx \frac{3}{4}(\frac{\alpha_e m}{\alpha_s})e_d^2 = \frac{1}{12}\frac{\alpha_e m}{\alpha_s} \tag{1.5}$$

where e_u and e_d are the up and down quark charges respectively. This process is suppressed by another two orders of magnitude with respect to the direct photon process.

Gluon Fragmentation Functions.

Studying the jet on the away side of a direct photon may yield a determination of the gluon structure function. Additionally, if the direct photon cross section is compared with the jet-jet cross section, a fragmentation function for the quark/gluon may be extracted. The photon-jet inclusive cross section is given by

$$\frac{d\sigma(AB \to \gamma + h + X)}{dy_1 dy_2 dp_t^2 dz} = \sum x_a x_b G_{\frac{a}{A}}(x_a, Q^2) G_{\frac{b}{B}}(x_b, Q^2)$$

$$\times \sum \frac{d\sigma}{d\hat{t}}(ab \to \gamma + jet) D_{h/j}(z) \tag{1.6}$$

where y_2 is the away side rapidity and z is the fraction of the jet momentum carried away by the hadron. Dividing equation (1.6) by (1.2) will eventually yield the gluon fragmentation function $D_{h/g}(z)$.[5]

Gluon Structure Functions.

Comparisons of data from p vs $\pi^\pm$ should yield changes in the direct photon cross section. The types of interactions that take place in each is different. Since the pion beams contain antiquarks, we expect the dominant process to be annihilation. In in proton beams we expect the process to be compton and changing to annihilation at higher Q^2 . Subtraction of these processes should yield the gluon content of the pions by comparing the results to the structure functions of the proton.

1.2. BACKGROUNDS TO DIRECT PHOTON PROCESSES.

The direct photon process seems ideal to study the underlying theories of QCD, but it is experimentally quite hard to isolate a direct photon signal from the background. Any process which is electromagnetic in nature is a potential source of background. Sources include hard bremsstrahlung from target particles, or from the primary interaction, and asymmetric decays of neutral mesons. Other sources are brought about by experimental considerations, like beam halo muons. Muons in the beam halo, discussed in the equipment and trigger chapters of this thesis, arise from a nonperfect beam production. These muons travel parallel to the beam and simulate high P_T objects. Additionally, a small contribution is made from Drell-Yan type decays, in which one or both leptons are misidentified.

Decays of Neutral Mesons

The neutral mesons π° η, η', ρ, ω, and ϕ may all contribute in their electromagnetic decay modes. This arises when one of the photons produced is not detected or reconstructed. Particularly energetic π° events can cause the two decay photons to coalesce within the detector, to appear as one photon. The primary source of background are π° 's. η decays play a secondary background, although the contribution is reduced by a branching ratio of $\approx$ 0.4 and production ratio of $\frac{\eta}{\pi^\circ}$ of 0.5. The two photon decays contribute when the energy asymmetry,

$$Asymmetry = \frac{|E_1 - E_2|}{|E_1 + E_2|} \approx cos\theta_\gamma$$

is large, where θ_γ is the angle of the photon in the π° rest frame with respect to the laboratory direction of the π° . This argument is also true for η decays.[6] The analysis section involves the understanding of the $\eta \rightarrow \gamma\gamma$ decay mode. A cross section is measured at $\sqrt{s} = 530$ GeV/c . This is done partly because of a need to understand the backgrounds to the direct photon process, and partly because of the need to measure the η cross section at this energy and with meson beams. The analysis is also done to measure the production cross section for η at $\sqrt{s} =$ 31.6GeV/c which has not been done elsewhere.

1.3. SUMMARY OF PROPOSED PHYSICS.

E706 is was intended to measure the direct photon cross section in the X_T range from 0.19 to 0.5. The objective is was to experimentally study QCD. The results of this study should yield:

- a direct photon cross section,
- gluon structure functions for pions and protons,
- a understanding of quark and gluon fragmentation.[7]

2. The Meson West Spectrometer.

The FermiLab Meson West fixed target experimental hall housed two experiments. The first physical experiment was E706 which will be described in full. Experiment 672 followed E706 in physical location. An overall view of the entire spectrometer can be seen in figure 2. E672 was designed to study massive dimuon pairs. It was a simple apparatus consisting of a toroidal magnet for bending charged muons, and a set of multiwire chambers before and after the toroid for position detection. E706 served as a target and hadron shield for E672.

The E706 portions of the spectrometer consisted of a beam transport system, a charged tracking system, a liquid argon calorimeter, and a forward calorimeter. The charged tracking system was made up of silicon microstrip detectors, an analyzing magnet, and multiwire proportional chambers. The liquid argon calorimeter, LAC, was made up of two sections. The first section was designed to detect gamma rays and electrons. The second section was designed to detect hadrons. The forward calorimeter was designed to detect particles produced at small angles in the interaction. These units made a multiparticle spectrometer for experiment E706 having a 4 π solid angle coverage in the center of mass. Each element of the spectrometer will be described in some detail in the following sections of this chapter. The main focus will be on the construction of the hadron calorimeter, HAC. The coordinate system for the experiment was centered on the beam. The beam defined the Z axis of a conventional Cartesian coordinate system. X was defined as the horizontal plane and Y the vertical. References to distance here are along the z axis and given from the defined origin to be at the target. This system and scale may be seen in figure 3.

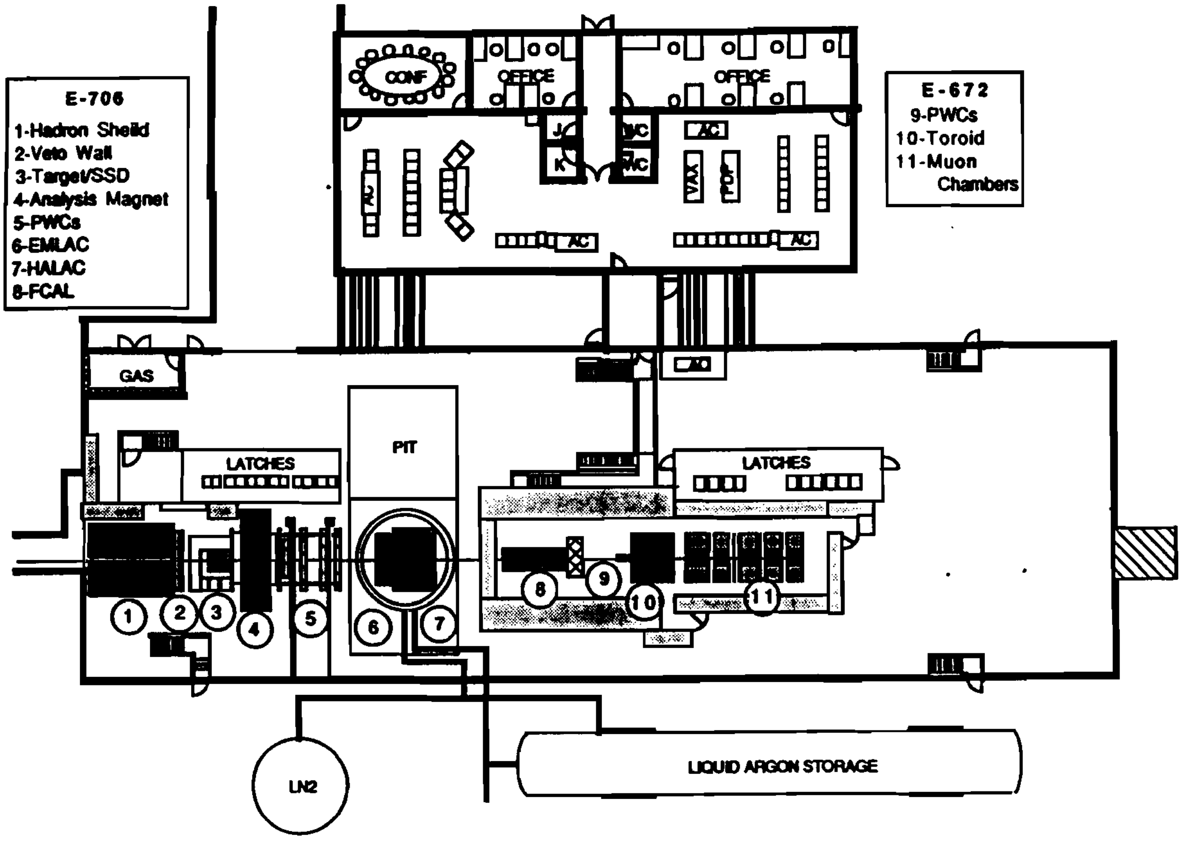

Figure 2: The Meson West Experimental Hall
Legend identifies Experimental Apparatus.

2.1. OVERVIEW OF BEAM TRANSPORT.

The Meson West beam line provided E706 with a stream of particles. The beam line consisted of two sections. A beam of primary protons of 800 GeV from the Fermilab Tevatron was transported in the primary beam line to the production target. The protons were delivered for a

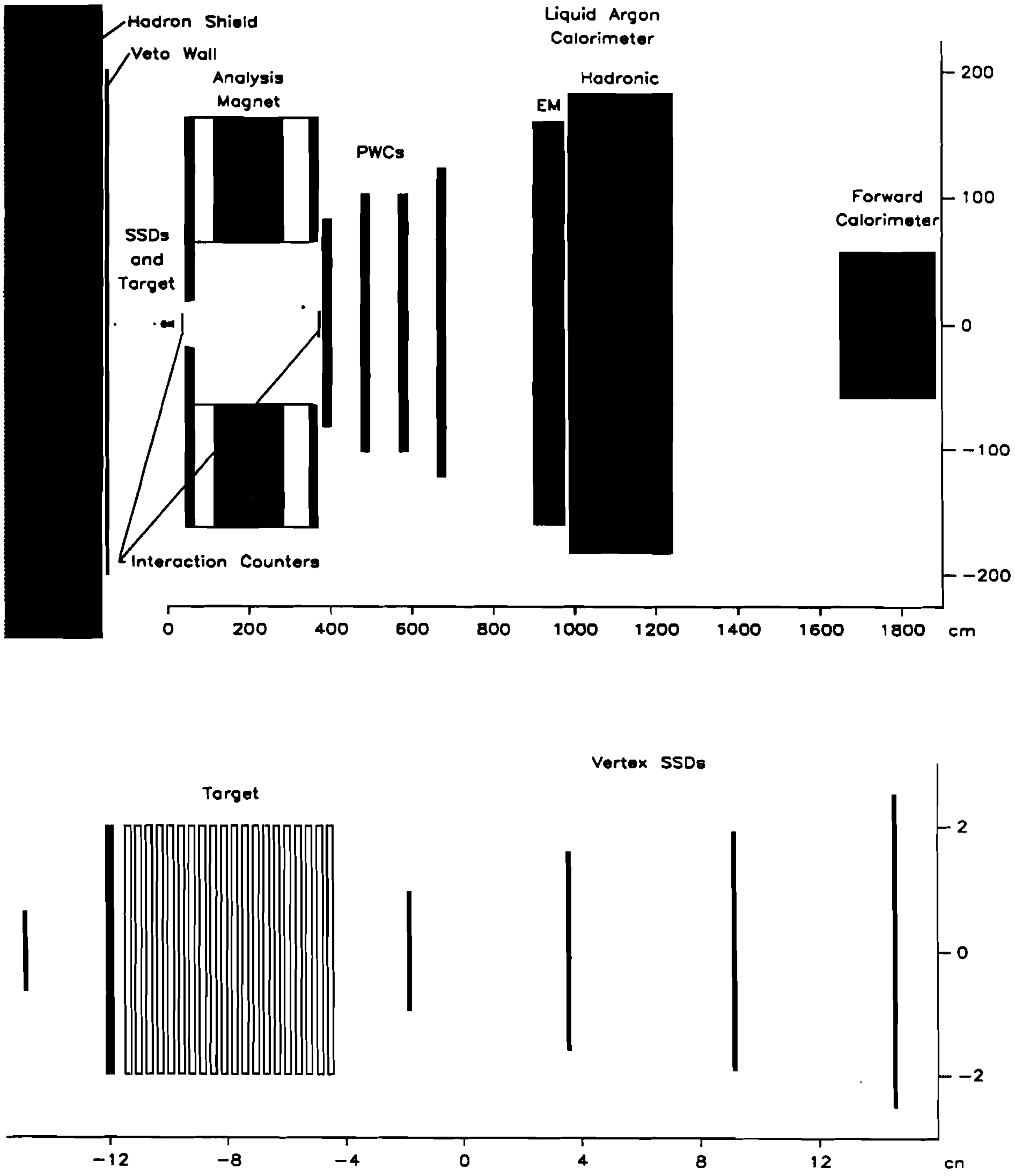

Figure 3: The experimental layout with a scale in cm.

period of 23 seconds, a spill. There was a 37 second regeneration time between spills for a total period of 60 seconds. The microstructure of the primary beam was related to the accelerator clock which resulted in buckets of protons with a nominal separation of 19.9 ns. The beam of primary protons hit a 0.75 interaction length production target of aluminum to produce a secondary beam of protons, pions and kaons. The secondary beam line, discussed here, transported the secondary protons, pions and kaons to the E706 experimental target. The secondary beam was made up of a momentum selecting dipole pair at the production target followed by a double focus beam transport system shown in figure 4. The buckets had a 10% occupancy with 1% chance of double occupancy. The beam line could be run with either polarity of particle over a momentum range 400 to 600 GeV/c. The data presented here were taken with a 530 GeV/c momentum beam. For reasons of radiation safety the production angle was changed from $0mr$ for negative beam to $1.4mr$ for positive beam. A parallel section of 41 meters was included to allow for a differential cerenkov counter for beam particle identification.

capital C ?

The Cerenkov counter operated with an acceptance of $5mr$. It was filled with helium gas at about 4 PSIA. This pressure was varied to identify the desired particle type. A large background contribution to the direct photon events were muons and hadrons at large radial distance from the beam and in time with an interaction in the target. These would appear to the trigger as a high transverse momentum objects and fake the signal on which we wished to trigger. These muons and hadrons were produced at the production target or when the beam scraped something in the beam line. Three efforts were made to reduce this background. First, muon spoilers were included in the beam line. The beam traveled inside a vacuum pipe of 2 inches diameter embedded in the spoiler. Outside of the vacuum pipe was soft steel wound with a copper coil to make an electromagnet. The magnetic field was high inside the steel and low in the beam volume, and was oriented to sweep the muons away from

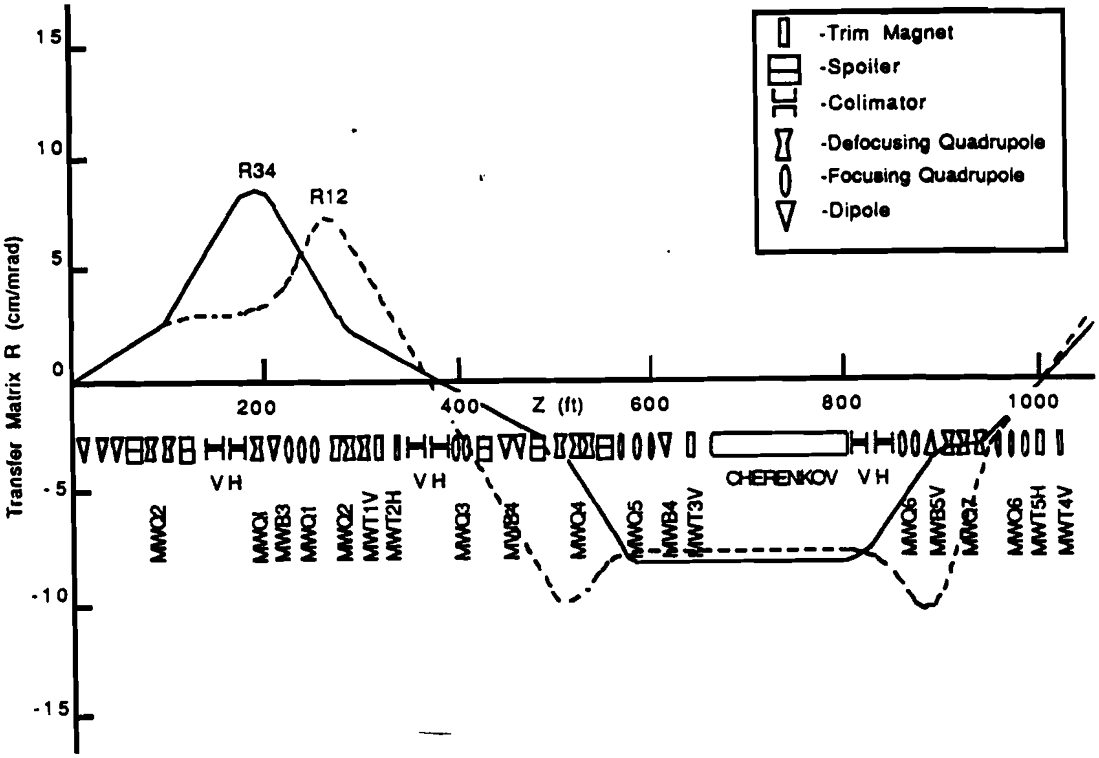

Figure 4: The Meson West Secondary Beam Line.

the beam. Second, a steel cube 3 meters on a side was located just inside the experimental hall. This shield was to absorb some of the debris from the primary target traveling parallel to the beam line. This shield was meant primarily for the hadronic debris. The third was two walls of scintillation counters, veto walls, which were designed to detect any minimum ionizing particle traveling parallel to the beam. They covered the X-Y surface of the steel shield on the downstream side. The veto walls will be described in the trigger section of this document.

2.2. SILICON STRIP DETECTOR AND TARGET SYSTEM.

The target region was covered upstream and downstream by X-Y pairs of silicon strip detectors or SSD's. The combined SSD and target system is shown in figure 5. All of the SSD's have a $50\mu m$ pitch and a thickness of $250 - 300\mu m$. During the data run there were 7 pairs of modules, with 7120 strips instrumented. Each plane, two planes per module, was referred to by a number starting with 1 at the upstream end where the beam entered the system. There were three pairs upstream of the target for beam track information. The remaining four pairs were downstream of the target for vertex reconstruction. The first four pairs of X-Y SSD's were of overall size 3 × 3 cm. The remaining three were 5 × 5 cm. Because of the cost the downstream 5 × 5 cm modules were not fully instrumented, rather the outermost strips were left inactive.

The target was placed between plane 6 and plane 7 of the silicon system. The target was segmented to aid in the reconstruction of vertices. It was expected that interactions would primarily come from the target material rather than air. The target initially consisted of 20 $2mm$ thick beryllium segments separated by $1.6mm$ gaps. During the course of the run, two $0.8mm$ thick copper segments separated by $1.6mm$ were placed upstream of the beryllium stack with a $3.2mm$ gap.

2.3. ANALYSIS MAGNET.

The analysing magnet was a 400 ton rectangular block of steel with a hole in the middle. The maximum possible field was 15.2 KG. It was configured as a dipole with the bend in the x-plane. Either end of the magnet had steel slabs, mirror plates, attached to help confine the return field to the magnet. The aperture was slightly smaller than the total acceptance of the apparatus that followed, 35.6 × 25.4 cm at

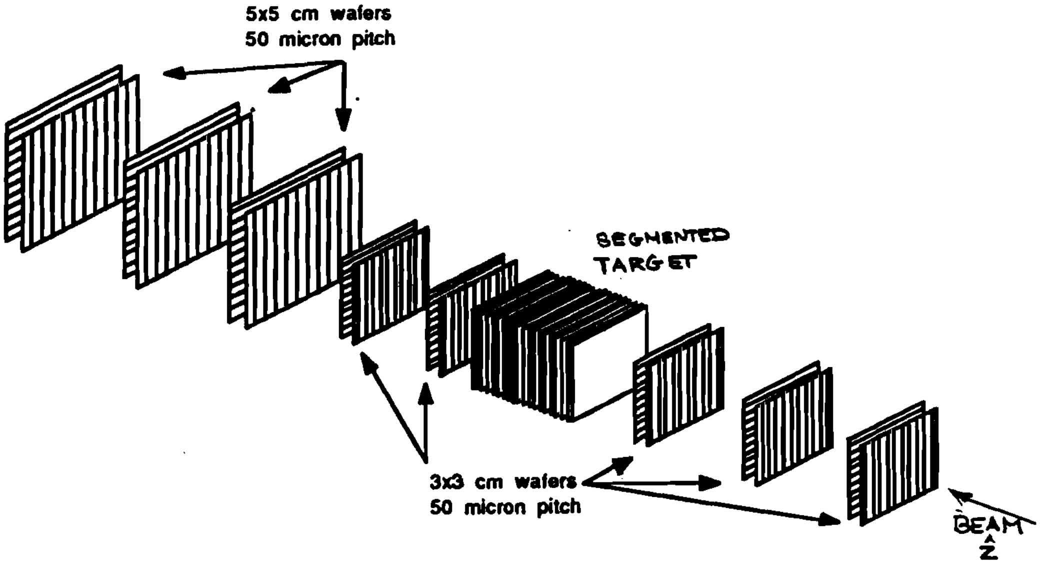

Figure 5: SSD and target section.

downstream end, and 137.2 × 124.5 cm at upstream end. It was run nominally with 450 MeV/c P_T kick.

2.4. PROPORTIONAL WIRE CHAMBERS.

The Multi-Wire Proportional Chambers, hereafter called MWPC, were made up of 4 modules situated downstream of the magnet. Each module was subdivided into 4 planes, X, Y, U, and V as shown in figure 6.

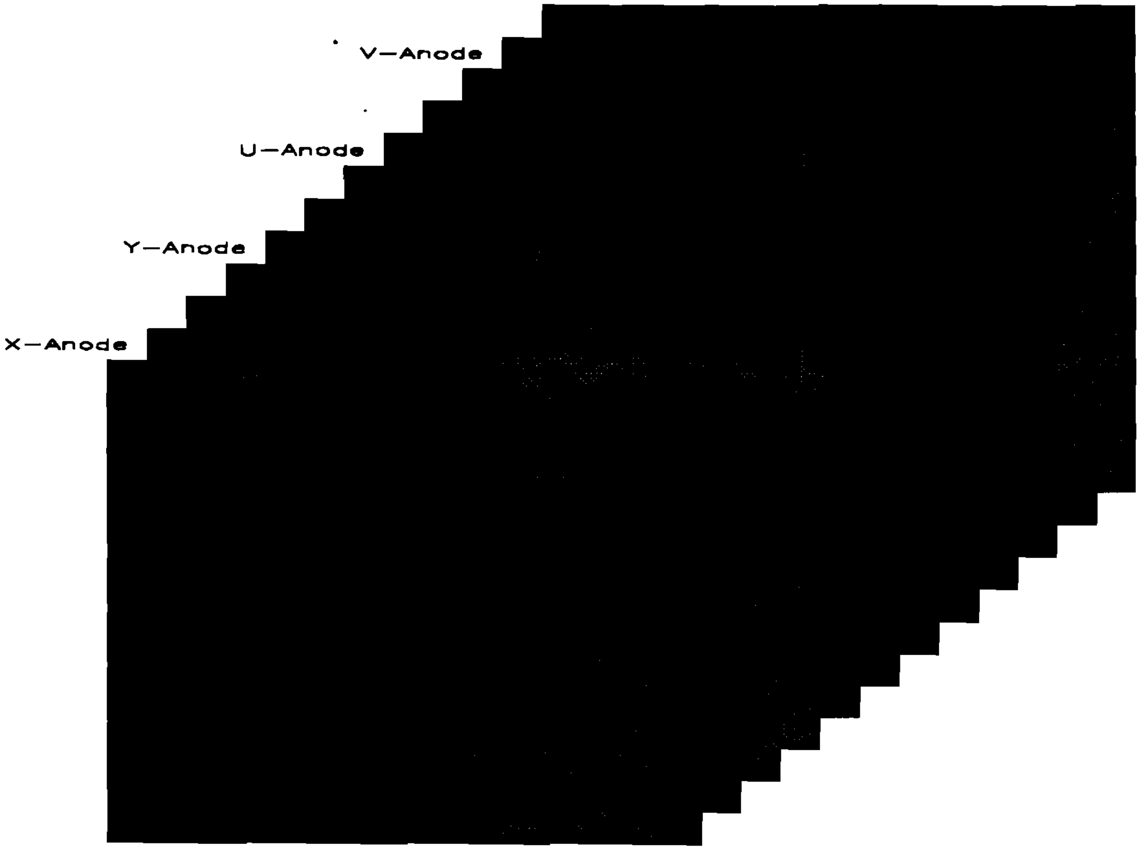

Figure 6: A detail of E706 MWPC.

The X and Y planes within a module correspond to the conventional

Cartesian coordinate system. The U and V planes formed 3 4 5 and 4 3 5 right triangles respectively to the X, Y system. The U and V planes were necessary to resolve ambiguities in the tracking and to increase the overall tracking efficiency of detection. The transforms are given by

$$U = \frac{4}{5} \times X + \frac{3}{5} \times Y,$$

and

$$V = \frac{-3}{5} \times X + \frac{4}{5} \times Y.$$

The number of wires per plane varied from 480 to 1120.* The modules were labeled from 1 to 4 starting from the magnet and going downstream. The planes within a module were labeled from 1 to 16 in the same order. Each module had a slightly different acceptance as documented below.

⋆ See E706 internal memo number 137 for complete details.

Plane	Name	Location (cm)		Angle (mr)	
		X	Y	X	Y
1	X1	-81.15	-60.96	229	175
2	Y1	-81.28	-60.83	229	173
3	U1	-65.88	-60.96	-	-
4	V1	60.75	-60.96	-	-
5	X2	-101.47	-101.60	220	220
6	Y2	-101.60	-101.47	220	220
7	U2	-65.88	-101.60	-	-
8	V2	53.89	-101.60	-	-
9	X3	-101.47	-101.60	178	178
10	Y3	-101.60	-101.47	178	178
11	U3	-65.88	-101.60	-	-
12	V3	53.98	-101.60	-	-
13	X4	-121.79	-121.92	180	180
14	X4	-121.92	-121.79	180	180
15	X4	-86.20	-121.92	-	-
16	X4	74.30	-121.92	-	-

Table 1 The table shows the acceptance in mr with respect to the target.

The beam region of each MWPC was operated at a slightly lower high voltage than the rest of the chamber to reduce the efficiency of the chamber in this region.[†] This was achieved by use of a segmented cathode. The cathode spacing was maintained through the use of support wires, called garlands. These garlands were individually charged but still

---

[†] This definition of the beam region was module dependent.

caused some reduction in detection efficiency.[‡] The momentum resolution of the MPWC and SSD system was about $\frac{\delta P}{P} = 0.1\%$. Both the silicon microstrip detectors and the MWPC system used an electronic readout system designed and built by an industrial group, Nunamaker Electronics. The system consisted of preamplifier/discriminator cards mounted on the chambers. The latches and crates were located in a air cooled room away from the beam line. Each preamplifier card could accept 16 channels. Additionally, the card contained a discriminator circuit and a charge injection circuit. The output of the card was a differential Emitter Coupled Logic, ECL, signal that was transmitted via twisted pair flat cable to a latch/delay card in a CAMAC[§] crate in the latch house. The Nanometric system used their own non-CAMAC standard serial controller. Each latch module had 32 inputs and a 4 channel summed fast out on the front panel. The delays were set on a module basis by computer.

2.5. THE FORWARD CALORIMETER.

The forward calorimeter was made up of three sections of steel-scintillator stacks. The stacks were read out by wave shifter bars, BBQ doped rods, into photomultiplier tubes, PMT. The tubes are were in turn read out by a complex system of flash Analog to Digital Converters, ADC. The entire assembly was 10.2 interaction lengths of steel and 0.5 of acrylic scintillator. The details of construction are shown in figure 7 . Each stack ~~is~~ was made up of 32 steel-scintillator pairs. The steel ~~is~~ was a 45 inch diameter circle that ~~is~~ was 0.75 inch thick. Each steel plate and scintillator ~~has~~ had a 1.25 inch beam hole at its center. Each steel plate and scintillator

---

[‡] During the 1987/88 data run the voltage was such that the efficiency dropped to about 80% for ±10 wires about the garland.

[§] An acronym Computer Automated Measurement and Control, an industry computer bus and hardware standard, see CAMAC Instrumentation and Interface Standards, IEEE 1982, ISBN 0-471-89737-X, for a collection of papers describing the system.

pair ~~has~~ had a grid of 0.44 inch diameter holes drilled in it to accommodate the wave shifter bars. There were 76 holes on a 4.5 inch regular grid. The steel was interleaved with scintillator to produce light from showers in the calorimeter.

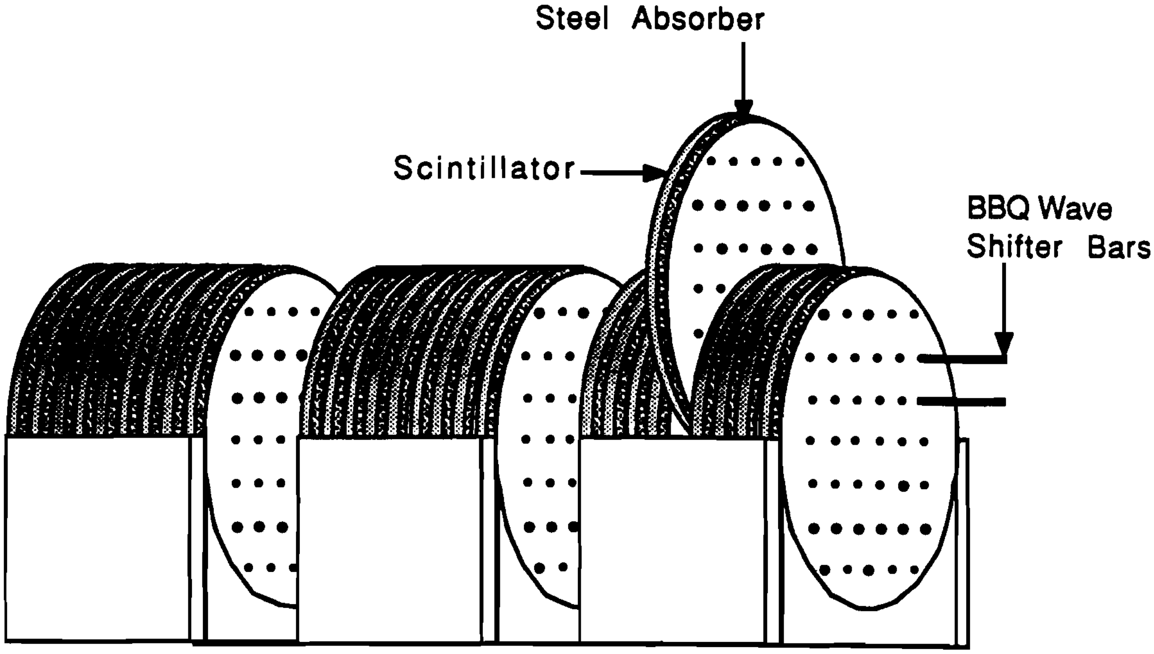

Figure 7: The construction details of the Forward Calorimeter.

The light produced in the scintillator was collected by the closest wave shifter rod and brought to the PMT at one end. The wave shifter also converted some of the shorter wavelength light into a longer wavelength where the PMTs were more sensitive. The amount of light produced was proportional to the amount of energy deposited. The readout for the calorimeter consisted of a 6-bit flash ADC for each channel. Each ADC continuously digitized at a rate of 80 MHz. The ADC's were operated in a logarithmic mode to accommodate the dynamic range of the PMTs. The resulting data were stored in a ring buffer in 64 time slices. This was necessary because of length of time to form the physics trigger. A physics trigger would cause the digitizing clock to stop and the entire 2.56 μsec history to be read for all 228 channels.[⋆] This entire buffer was stored on tape for every channel. In the offline analysis, events were reconstructed by position, timing and ADC values recorded.

2.6. THE LIQUID ARGON CALORIMETERS.

Liquid argon calorimeters were chosen for electromagnetic shower detector and hadronic shower detector. The calorimeters were designed to measure the energy of neutral particles by total absorbtion. During the process of absorbtion, charge was liberated in the liquid argon detection medium. It was this charge that was measured. Argon is liquid with a boiling point of 88° K. This necessitates the usage of a cryostat and cryogenic techniques. Liquid argon was chosen as a detection medium because it displayed a very uniform response to particle ionization. Additionally, due to the construction techniques employed, a fine spacial granularity was achieved. Some loss in overall energy resolution was seen as compared to conventional lead-glass or common scintillator. The calorimeters were submerged in liquid argon. The argon in a gap between radiator and charge collector served as an ionization medium. A particle entered the detector and converted in a cascade of electron-positron pairs for incident electrons and photons, or through nuclear

---

[⋆] E706 memo # 141 P. Lukens, K. Ruddick, The E706 forward Calorimeter.

break up for incident hadrons. This conversion made charged particles that traveled through and ionized the argon. The liberated electrons were guided to a patterned collector by an electric field. The details of construction and operation follow. The amount of charge collected was dependent on the electric field applied to drift the electrons, and the purity of the argon. Great care was taken during construction and argon transfer to prevent contamination. The detectors and vessel were meticulously cleansed to prevent this contamination. Dependence on collection voltage and impurities may be seen in figure 8. The first section of the calorimeters was the electromagnetic calorimeter, EMLAC. The EMLAC was designed to detect particles that interact in an electromagnetic manner, photons and electrons. The EMLAC was made up of lead sheets and Copper clad G-10[†] boards for the signal read out. A pattern based on a polar coordinate system was used for the signal readout boards. An exploded view of the EMLAC may be seen in figure 9 .

A photon entered the detector and underwent a electron-positron conversion in the presence of a lead nucleus. Electrons underwent a bremsstrahlung and subsequent pair creation. The resulting pair would bremsstrahlung and pair convert in a cascade fashion until the resulting particle was below production threshold, $2 \times M_e$. The resulting electrons and positrons would ionize the argon and the charge generated was collected and measured. ¶ The second section was a hadron calorimeter, HADLAC. The HADLAC was designed to detect charged and neutral hadrons and was constructed of steel plates and G-10 detector planes. The detector planes, called cookies, were a 7 layer laminate with a triangle pattern for charge collection. A view of the HADLAC may be seen in figure 10. Here, hadronic particles that made it through the EMLAC would

---

[†] G-10 is a fiberglass-epoxy combination used in conventional printed circuit boards. It is not to be confused with FR-4 which is similar in nature but contains a fire retardant. This fire retardant was found to contaminate liquid argon, hence FR-4 could not be used.

Figure 8: Graphs showing the dependence of charge collection on high voltage and equivalent oxygen contamination.

undergo nuclear breakup in steel nuclei. The resulting fragments would themselves break up more steel nuclei until capture was achieved. Some of the resulting fragments were charged and ionized the argon. The collected charge was proportional to the amount of energy deposited. The author spent the majority of his time in the construction of the HADLAC and will be describing it in some detail.

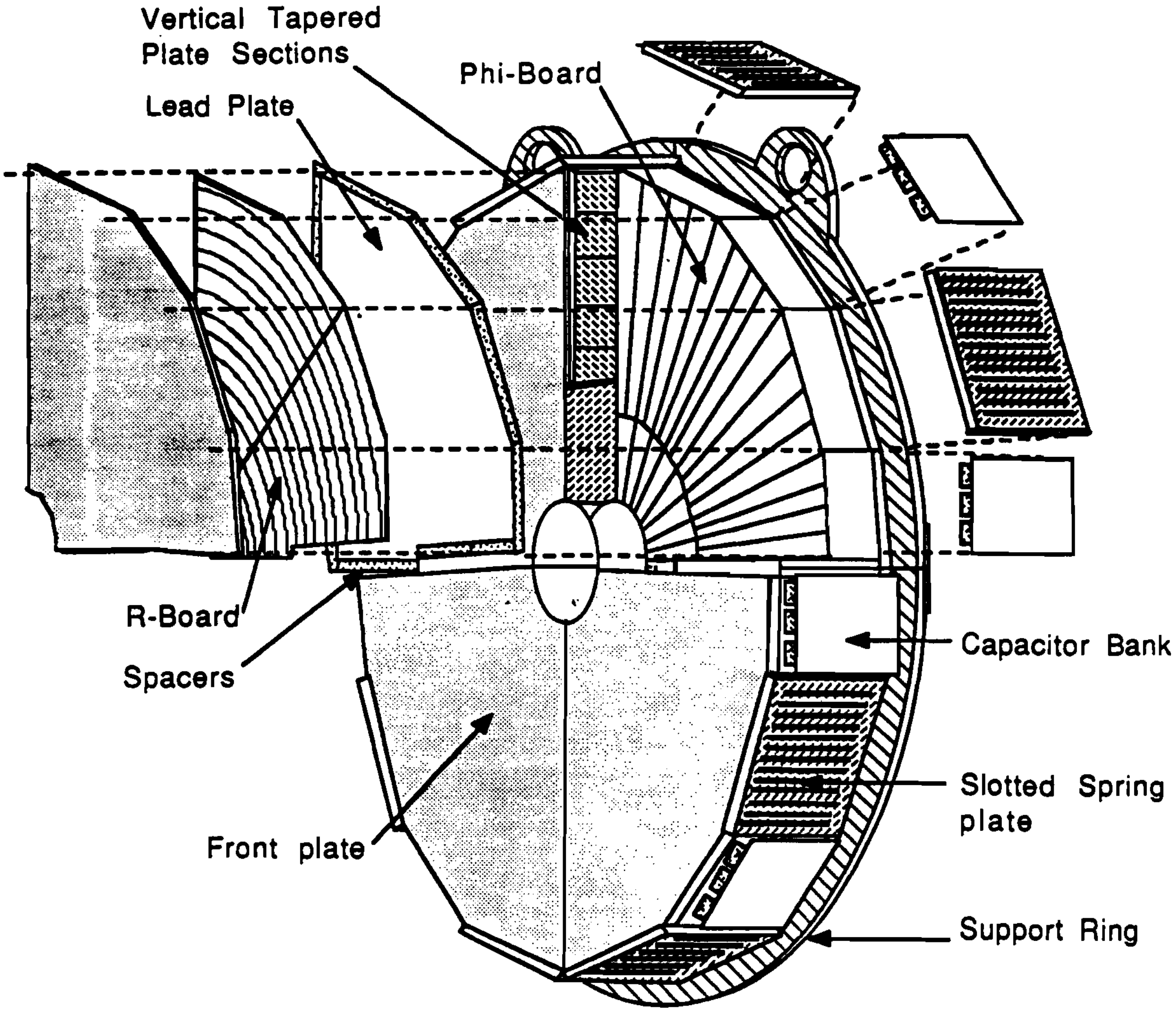

Figure 9: An exploded view of the EMLAC showing the details of construction and coordinate system.

don't you have to say where pictures like this came from.

The detectors were located in a common cryostat. The cryostat was suspended from a gantry. The first plane of the calorimeters, the face of the EMLAC, was located 9 meters from the experimental target. The calorimeters had an aperture of a circle with a radius of $1.6m$, which corresponded to an angular coverage from 40° to 138° in the center of mass frame or 77% of 4π solid angle for a 530 GeV incoming particle.

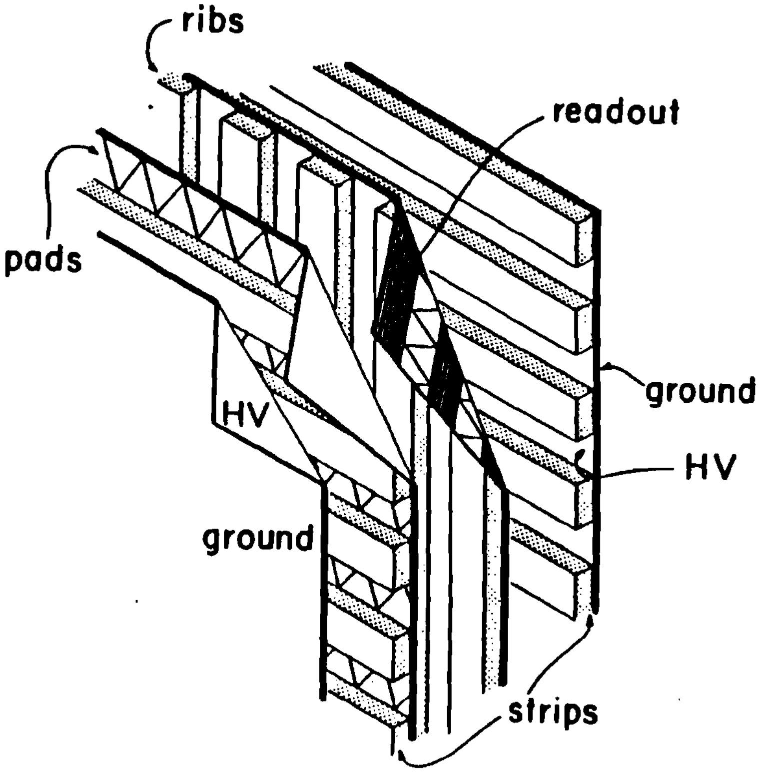

Figure 10: The Hadron calorimeter, showing the steel and charge collection pattern.

Both detectors had 40 cm diameter beam holes to avoid high rate forward going particles. The overall structure weighed 400 tons and contained 50000 liters of liquid argon.

The LAC Cryostat.

A cryostat was constructed of 316 stainless steel to contain the liquid argon and thermally isolated it from the outside world. The cryostat consisted of a cover plate or lid and a lower jacket. The lid was a cylinder of diameter 17 feet and with a flat top called the top hat. Eight rods came through the top of the cover plate and connected to steel box beams. The rods provided the support for the electromagnetic and hadron calorimeters. The box beams tied into the structure called the gantry. The gantry was an A-frame support structure. It transmitted the weight of the calorimeters to Hillman rollers on steel tracks in the floor. A cross sectional view in the y-z plane may be seen in figure 11. Motorized screws permitted movement transverse to the beam.

The lower half of the cryostat was a cylinder of diameter 17 feet with a rounded bottom. The detectors were first hung in place from the support rods. Then the lower portion of the cryostat was brought into place by four vertical screws. Three feet of insulation, made up of 6 inch thick PVC baffles interleaved with aluminized mylar, were located between the top of the liquid phase and the top flange of the cryostat. The insulation was supported from the bottom by an aluminum frame. The frame was supported from the cryostat lid by 10 evenly spaced half inch stainless steel threaded rods. Just below the insulation were two sets of copper cooling coils. The cooling coils were made up of copper tubing with copper fins on them. The total heat dissipation was calculated to be 30 KW. The first set of coils was made up of one ring and was meant to maintain the temperature and pressure during normal operation. The second set was made up of three rings and was designed for heavy heat load, for example during the cooldown phase. Each of the coils was attached to a vessel that maintained an even flow of liquid nitrogen at a specific temperature. The temperature of the nitrogen was maintained by adjusting the outlet pressure of these vessels. Various gauges monitored the pressure and liquid level of the cryostat for proper operation. There were three mechanisms of pressure relief. The first was a controlled pneumatic feedback system that monitored the pressure in

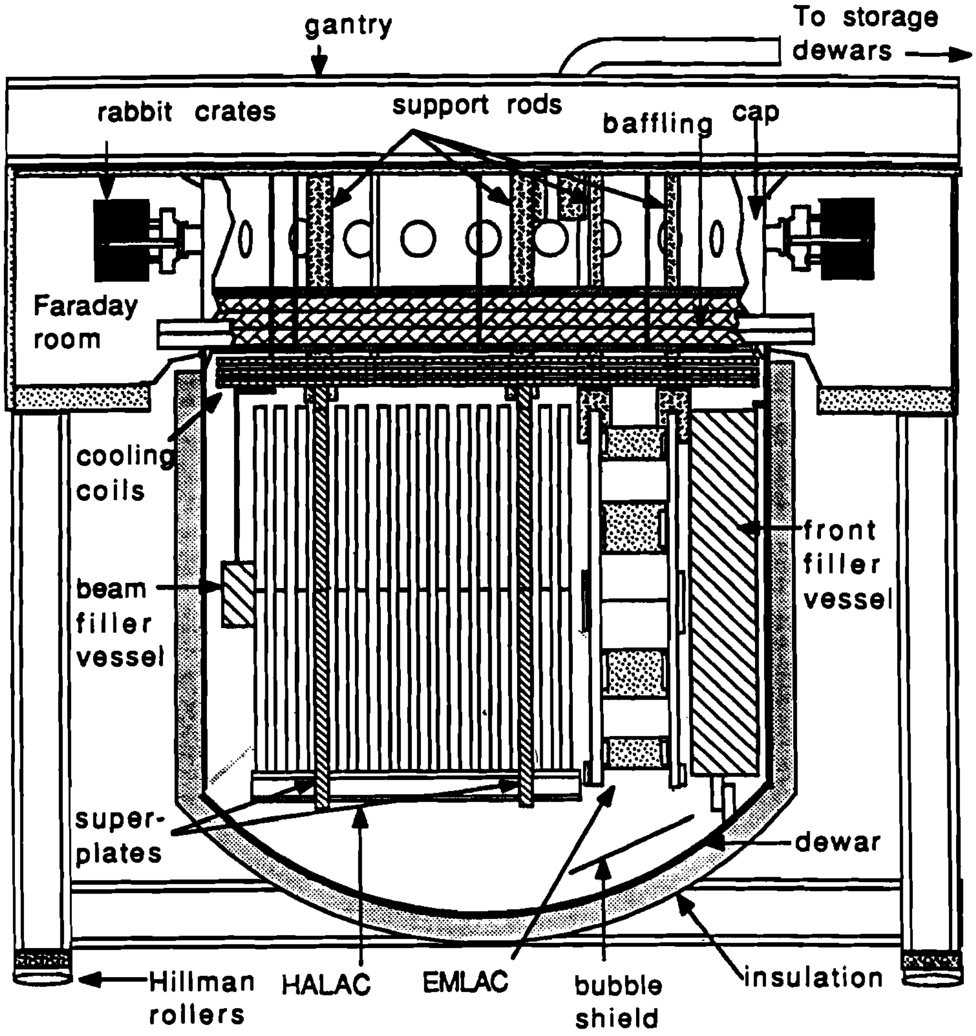

Figure 11: The Liquid Argon Calorimeters, Cryostat and Gantry.

the LAC. It was only designed for small gas flow. The second was a diaphragm relief valve. The third was a rupture disk. The secondary and tertiary relief mechanisms were designed for a rapid release of overpressure. The first and second mechanisms were recoverable. They were designed to close after the pressure became normal. The third measure had no recovery option. The calorimeters were brought to near liquid argon temperatures by introducing argon gas in spurts and allowing convection cooling. Liquid was introduced into the system after the calorimeters were near liquid argon temperature. The process began by lowering the pressure in the LAC vessel and raising the pressure in the storage dewar. The midline of the LAC was about even with the storage dewar so this pressure difference was required to completely fill the LAC.

Electromagnetic Shower Detector.

The electromagnetic calorimeter, EMLAC, was made up of 66 layers of 2 *mm* lead sheets interleaved with 66 layers of 1.6 *mm* double clad G-10 boards. This may be seen in a previous figure 9. The lead served as the high voltage cathode and the readout boards were the anode. The gap between the lead and readout boards was 2.5 *mm* and was filled with liquid argon during operation. The readout boards were double copper clad G-10 with the same pattern on both sides. There were two patterns of boards, R-boards and Φ-boards. The R-boards had strips of a constant radius of 5.5 *mm* cut in them making concentric circles. The Φ-boards had two sections of a constant angle cut into them. The separation of sections was made at R=40cm from the beam, defined as inner and outer Φ. The inner Φ-board had an azimuthal angle of 16.4 mrad and the outer Φ had an azimuthal angle of 8.2 mrad. The inner and outer Φ sections were read out separately. The R and Φ layers alternate in the calorimeter.¶For the coordinate system described above, with the target at the origin, the size of the individual radial cuts grew in depth, Z along the beam, such that they always subtended the same solid angle. This effect was called focusing. Reconstructed showers from target produced particles should have the same radius in the electrical front and back of the calorimeter. Reconstructed showers from particles produced elsewhere would have an unusual ratio of radii front to back. The ratio of radius front to radius back was called directionality and was expected to be unity. This focusing effect may be seen in figure 12. The EMLAC was 30 radiation lengths in depth. The energy resolution $\frac{\sigma}{E}$

71 cm in depths

~~28~~ 27.8 rad length

was measured to be $\frac{\sigma}{E} \approx \frac{21\%}{\sqrt{E}}$. This will be discussed in more detail in the chapter on analysis. The position resolution was found to be better than 1 mm, and was calculated to be able to resolve π^0 up to 250 GeV/c.

Figure 12: An example of focusing of the Electromagnetic Calorimeter.

2.7. OVERVIEW OF HADRON LAC.

The Hadron calorimeter had 53 cells. Each cell consisted of a detector plane with $\frac{1}{8}$ inch effective argon gap and a 1 inch steel plate. The detector planes, called cookies, were a laminate of $\frac{1}{32}$ inch single and double copper clad G-10 interleaved with strips of $\frac{1}{8}$ inch G-10. Triangular pad readout was used to collect the deposited charge. An illustration of the cookie pattern may be seen in figure 13. The triangles grow proportional to z coordinate of the detector plane in size from a height of 4.4 inches to a height of 5.5 inches to focus on the target. This was analogous to the focusing described in the EMLAC section. It was also sometimes called towering.[*] The calorimeter was separated into two sections. The front section was the first 14 planes and associated steel plates. The back section was the remaining 39 planes and steel plates. The total number of absorption lengths in the Hadron calorimeter, HADLAC, was 9.6. The HADLAC was expected to have an energy resolution $\frac{\sigma}{E}$ of $\frac{\sigma}{E} \approx \frac{80\%}{\sqrt{E}}$ where E is in GeV/c. Due to electronic noise and techniques described later the actual resolution was found to be $\frac{\sigma}{E} \approx \frac{180\%}{\sqrt{E}}$.

Cookie Description.

The detector planes or cookies were made up of 7 layers glued together. The cookie was divided into two halves when cut in z. The back half was a conjugate of the front half. The assembly figure of one half of detector plane is shown in figure 14. The read out patterns were the rows of equilateral triangles read out at the edges. The read out board was made up of $\frac{1}{32}$ inch thick single clad G-10. The high voltage planes were made up of $\frac{1}{32}$ inch thick G-10, copper clad on both sides. The entire plane was made up of either 3 or 4 individual planes. The size

---

[*] During the focusing process some of the triangles fell off the edge of the detector planes due to the size limitations of the calorimeter.

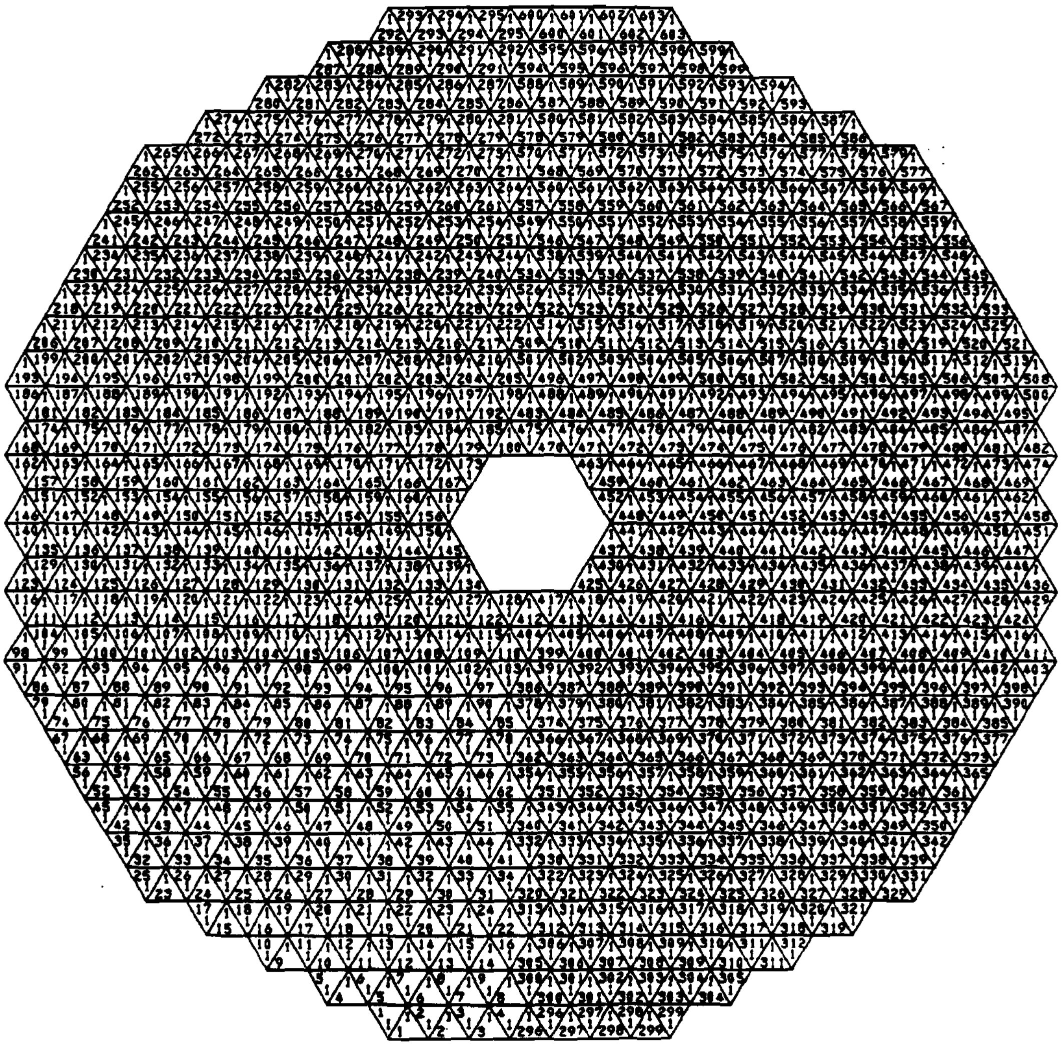

Figure 13: A view of the triangle pattern tessellating the Cookies.

of these planes was roughly 12 feet by 4 feet.[†] The outer perimeter was cut to the shape of an octagon. The G-10 strips were the spacers to obtain constant argon gaps of $\frac{1}{8}$ inch between the read out pads and high voltage boards. These spacers also give the rigidity to the detector

---

[†] The size of the planes was governed principally by the size of the G-10 that we could get in one sheet. The maximum size we were able to get was 144 x 48 inches. The second parameter that governed the size was determined by how well the active region could be covered.

plane. The front and back halves were glued together with support ribs in between them. The support ribs were tied together with two $\frac{1}{8}$ thick stainless steel header bars at the top of the detector plane.

one word?

Figure 14: One half of a detector plane, upstream.

Cookie Assembly.

- Preparation of Boards.

The read out and high voltage boards were prepared on a device specially manufactured by Fermilab for our use. A Gerber computer driven pen/photo plotter with a 16 by 5 foot bed was modified to accept a high speed, 20-60,000 r.p.m., routing head in place of the pens. We used $\frac{1}{8}$ inch diameter drilling and contouring bits and 32 to 40 mil diameter routing bits to produce our holes and patterns.[*] The high voltage boards were simple by comparison to the read out boards. A $\frac{1}{32}$ inch thick double clad G-10 board was used. The first step was routing a gap of $\frac{1}{2}$ inch of copper around the contour of the board. The gap was to prevent the high voltage from arcing to ground on the back side of the board. The second step was to drill two or four locating holes and to cut the board to shape around the outer contour of the routing. ¶ Three steps were used to make a pad board. A $\frac{1}{32}$ inch thick single clad G-10 board was used. The first step was to rout $\frac{1}{4}$ inch gap around the contour. This gave a better edge once the board was contoured or cut out. The second step was to rout the pattern on the board. The third step was drilling the locating holes, holes for the ejector tabs and holes for the rivets for the shorting stubs. The ejector tabs were to hold the readout card edge connectors. The shorting stubs were backplates of gold plated copper that provided a ground to the cookie for the readout cables. The card edge connections that were milled into the pad boards were too thin to be used with standard card edge connectors. There was also the problem of having the underside grounded for the conjugate connections on the connector. This problem was fixed by using $\frac{1}{32}$ inch thick copper shorting stubs that were punched to size shown in figure 15. These were gold plated with 10 microinches of gold over 150 microinches of Nickel.[†]

---

[*] Tapes were generated by a program written on Fermilab's Cyber 875 by Professor M. Glaubman of Northeastern University. Three types of pad boards, single clad, and High Voltage boards, double clad were produced. At cookie number 38 through 41 four types of pad boards and three types of High voltage boards were produced. After cookie 41 four types of each were produced. Two sets were produced in each case. This made up the front and back halves of the cookies.

✓ Capital letters

[†] Cost prevented us from using more gold plating.

These pieces were attached to the pad boards with gold plated brass eyelets.

Figure 15: Shorting stub and placement on cookie card edge.

The card edge connections themselves were also gold plated. The plating system consisted of a high current D.C. power supply, a flat wand that had gold plated thickly on one side, and a solution of gold cyanide. A cotton sleeve was placed over the wand, and this entire wand assembly was dipped into the plating solution and then wiped onto the connections. The pad and high voltage boards were then cleaned using a pneumatic sander with Scotch-Brite pad and water to remove rough edges and corrosion. The final rinse was ethyl alcohol.

- Glue.

The glue used was an epoxy made up of resin DER332 and catalyst V40, equivalent to V140.[★] The ratio of mixing by volume was roughly 1:1.[†] We used two additives in the glue. The first was glass beads having a size between 200 and 230 standard mesh sieve. These beads determined the minimum gap between glued parts. This also allowed us to control the spread of a bead of glue. The mix was 250 grams of glass beads per liter of glue resin. The second additive was Cab-O-Sil, fused silica.[‡] The mix on this was 50 grams of Cab-O-Sil per liter of glue resin. The glue was dispensed on strips and ribs by an automatic device. This glue machine had a linear drive track for moving a strip or rib of G-10 horizontally. As the strip/rib was moving a bead of glue was dispensed. The amount of glue dispensed was a constant volume per unit length.[§] This was achieved by connecting the horizontal drive to the plungers on the glue tubes through a variable speed transmission. ¶We found that there were many dissolved gasses in the glue. We feared that the gasses might cause outgassing problems later. To aid in outgassing, the glue components were stored in separate pressure vessels mounted on the glue machine body. These vessels were fitted with agitators to mix and keep in suspension the additives to the glue. The vessels were agitated and evacuated by vacuum pump at least 16 hours prior to gluing. The storage vessels were connected to the cylinders used to dispense the glue

---

[★] V40 and V140 are slightly different grades by different manufacturers of the same catalyst.

[†] Initially a polyurethane glue was chosen for its low Young's modulus. This glue was later found to contaminate the liquid argon.

[‡] This is a thixotropic agent used widely in industry in epoxies and milk shakes.

[§] see appendix, The Glue Machine, David Williams of Northeastern University.

by tubes. These tubes were connected to three way valves. The second passage of the tubes away from the plungers was connected to a static mixer. The static mixer was a tube of stainless steel that contained plastic spirals that enhanced turbulent flow. The mixed glue went through reinforced tygon tubing to nozzles. The tubing went through a pneumatic valve which operated like a guillotine to kink the tubing tightly, and stop the flow of glue. The entire assembly may be seen in figure 16.[¶]

- G-10.

G-10 is an industry code name for a specific type of glass epoxy laminate. We purchased sheets of G-10 in bare $\frac{1}{8}$ inch thickness, and single and double copper clad $\frac{1}{32}$ inch thick. All the sheets measured 144 or greater by 48 or greater inches when trimmed. Trimmed meant that the rough edges from the processing were removed. Special requests were made on shipping to prevent breakage and insure cleanliness. Requests were also made in production to use Kevlar instead of mold release during manufacture since the mold release stayed on the boards and was difficult to remove during cleansing. The $\frac{1}{8}$ inch thick sheets were cut into one inch ribs and varying sized strips by a diamond saw by a firm contracted by Fermilab. The $\frac{1}{8}$ inch strips and ribs were cut to length locally. The strips were notched on both ends for the purpose of locating during the gluing process. The ribs were first cut to 144 inches. The ribs had an $\frac{1}{8}$ inch diameter hole drilled in them at the top. At the bottom a notch or V was cut. This $\frac{1}{8}$ inch hole at the top was fastened into the header assembly. The header assembly was a eighth inch thick by 0.75 inch wide by 96 inches long steel strip that was precision machined to locate

---

[¶] Some problems occurred in this system. The glue was compressible. This caused the valves to spurt glue when opened. The trolley system for the strips and ribs would easily jam or slip causing glue blobs. The V40 component of the glue solidified at room temperature. If this component was not heated for a long enough time crystalline chunks would clog the delivery system.

Figure 16: The Glue machine assembly showing important aspects.

the top of the cookie. The bottom of the rib was placed into a comb whose arrow matched the notch cut into the rib. This comb would locate the bottom of the ribs and prevent sideways motion during the gluing process.

- Assembly Procedure of a Detector Plane.

The cookies were assembled on a bedplate of cast iron. The bedplate had an aluminum plate, called the mother plate bolted to it in the shape of a cookie. The bedplate had locating holes in it to locate each plane relative to the others. It also had a device to hold the headers, described previously, in place during gluing. Attached to the sides were scales with aluminum blocks in the shape of arrows clamped to them. The aluminum arrows on the bedplate were set to the required position for a particular strip. The arrows on the east and west would then fit into the V-notch, mentioned previously, on the strip and locate it. They also served to hold it in place during gluing. After assembly was complete a plate similar to the mother plate was brought into place. This plate, called the father plate, was suspended from a rolling frame that would bolt to the bedplate. Air bags between the father plate and the rolling frame were inflated to seven p.s.i. to press the cookie. The process of laying down the glue and G-10 took about 2-3 hours. The press was left inflated for 12 or more hours.

- H. V. Testing.

After gluing, each cookie was tested in air with high voltage. The maximum voltage a cookie was taken to was 4.0 K.V. The minimum voltage for passing was 2.5 K.V. No cookies measured below 3.0 K.V. during testing on the table. High voltage problems were usually caused by dust in the argon gaps. This was rectified by passing a strong flow of dry Nitrogen gas through the gap. The high voltage boards were individually tested to 4.0 K.V in air. The breakdown of the G-10 used was found experimentally to be $8.0K.V. \pm 500V$

- Pad Capacitance and Continuity Testing.

Each pad board underwent a series of tests that were computer driven. A RABBIT crate interfaced to an IBM PC was used. The card designed and built by the Particle and Instrumentation Group, PIG, at FNAL was a multiplexed ADC interface. The card had two functions; it could measure resistance between two points or capacitance

awk

between a point and ground. Resistance was measured by passing a current through a known resistance and multiplexing to the measured points. The voltage drop across the known resistance and the unknown resistor was converted and stored to disk files. The capacitance measurement was a triggered process. A trigger pulse caused the point of measurement to be charged and then drained through a known resistor. A sample voltage was taken at two points in time, using a timer circuit and two sample and hold circuits. This allowed a rate of discharge to be calculated. The output of each sample hold and circuit was fed into an op-amp and the difference was converted. The conversion was done with a 16 bit ADC in the EWE. The EWE is described later in the LAC electronics section. The measurement point was determined by the computer controlled multiplexor. There were three tests done. A weight was placed on the pad board to make it flat against the ground plane. Then capacitance tests were run on each of the pads sequentially. The next test checked for pad to pad shorts. The final test shorted all the pads together and checked for continuity through the lines. This final test was called the braid test. After a series of trials and errors it was found that the best way to short all the pads together was to use tinned copper braids filled with shot to give them weight. While these tests were redundant, it was generally felt that each test might find some problems that would not be found in another. This proved to be true in one instance where a hairline short across the read out line passed the capacitance and resistance tests but failed the braid test. After the cookie was fully assembled the capacitance and resistance tests were repeated. Problems were found to be dirt or dust. Cleaning of the card edge connections or blowing out the channel with nitrogen usually solved the problem. Occasionally, a short that could not be solved by any of the above methods was burnt out by means of a high voltage capacitive discharge.

Description of Steel.

The steel for the hadron calorimeter ~~acts~~ acted as an absorber or nuclear interaction region for incoming hadrons. The steel was also a skeleton for the hadron calorimeter. The entire package of steel and cookies was called a HADPACK. Two steel plates, two bottom I-beams, and top Support plates formed a solid box structure as seen in figure 9. These two steel plates were called super plates. The two I-beams were 106 inches long and were bolted to the super plates at mounting holes. The super plates support the entire weight of the HADPACK. The force is transmitted through the super plates to the the clevis and support rods. The support rods were suspended from the gantry. Each I-Beams supported 50 other mechanically passive steel plates, dubbed Zorba plates as shown in figure 18. Every other Zorba plate supports a pair of Cookies. All steel plates were cut in the shape of an octagon, like the Cookies. The beam hole ~~is~~ was a circle of radius equal to twice the height of a triangle at the position in z measured relative to the target and tower~~s~~ed like the triangles as seen in figure :

not capitalized before

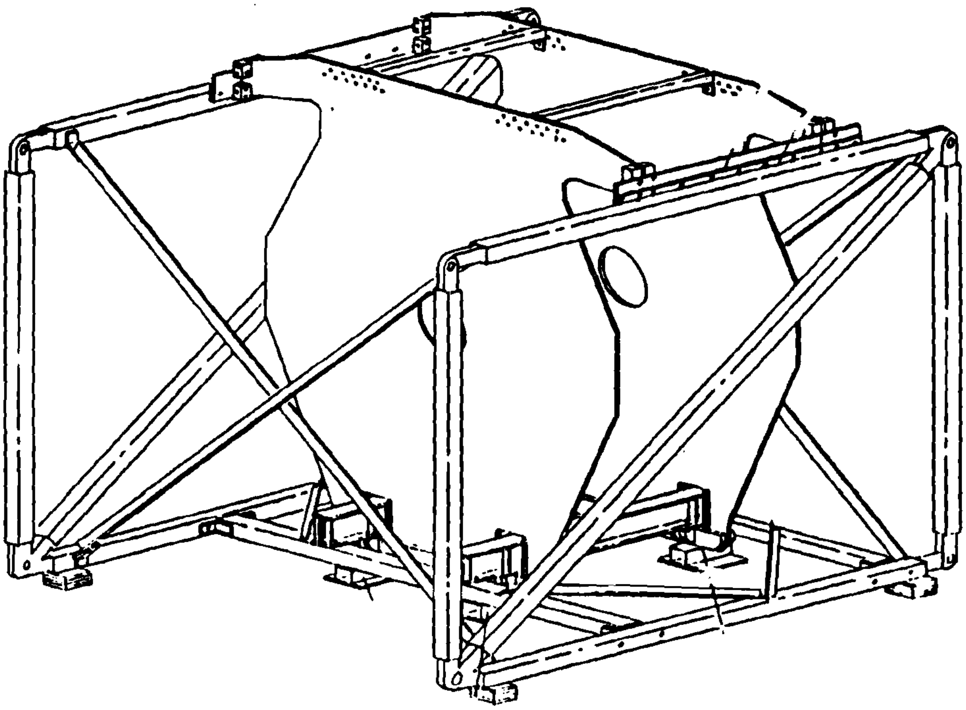

Figure 9: Hadron steel frame.

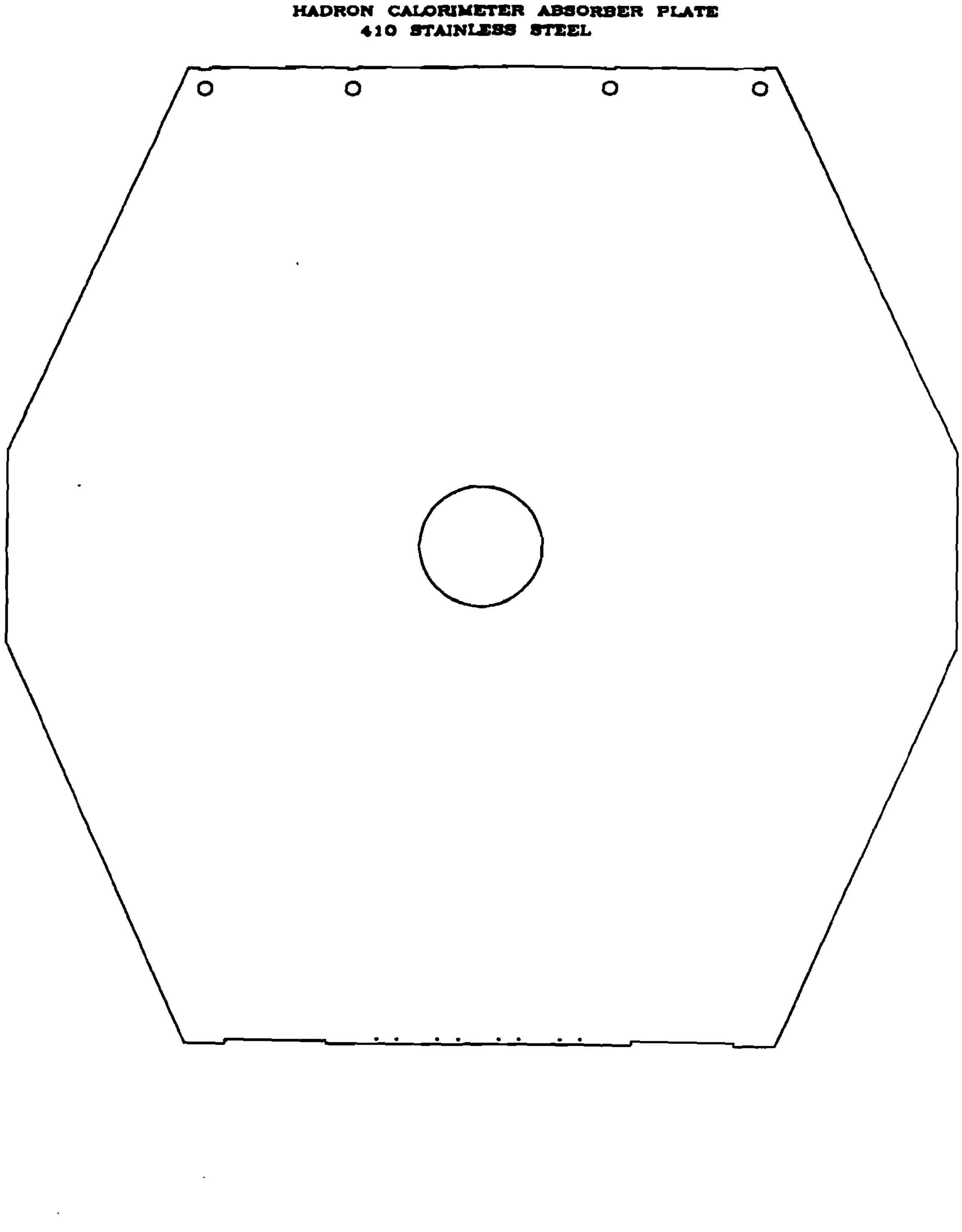

Figure 19: Passive Absorber Plate.

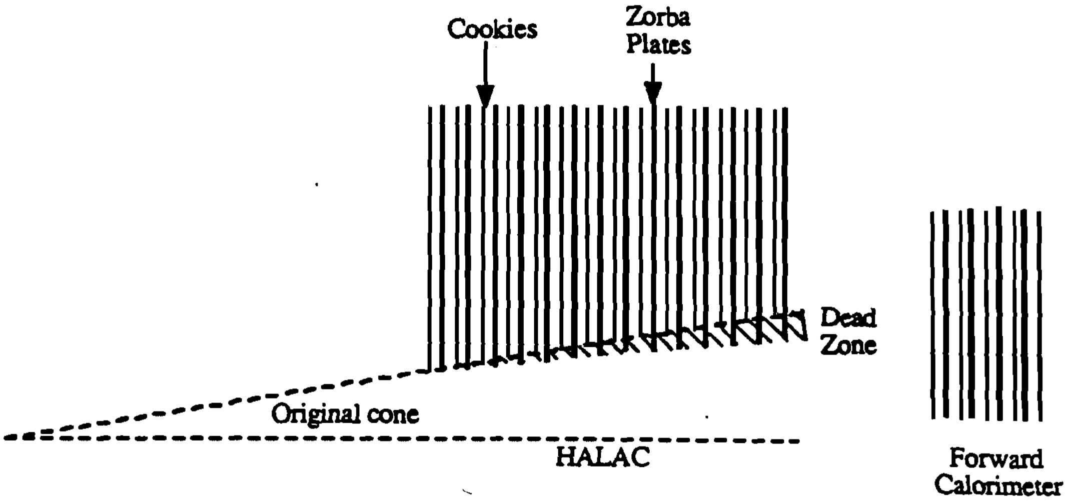

Figure : Example of beam hole focusing in cookie and steel.

Absorbers	Actual Diameter	Proposed Diameter
1-4	17.156	17.280
5-8	17.250	17.627
9-12	17.344	17.973
13-16	17.438	18.320
17-20	17.531	18.667
21-24	17.625	19.013
25-28	17.718	19.360
29-32	17.813	19.707
33-36	17.906	20.053
37-40	18.000	20.400
41-44	18.094	20.747
45-48	18.188	21.093
49-52	18.281	21.440

Table 2

The steel was designed to reside at 381.0 inches from the target. The hole started with a diameter of $17\frac{5}{32}$ inches and incremented $\frac{3}{32}$ inches modulo 4 in plate number. The beam hole was meant to tower with the cookies. The proposed value did not equal the accepted value for reasons of miscommunication. This did however lead to an uninstrumented region between the hole diameter and the beginning of the cookie. This correspond~~s~~ed to the angular region from ± 19.0 mr to ± 22.2 mr. This region shadow~~s~~ed the forward calorimeter and degrad~~es~~ed the energy and position resolution in this region. The entire *HADPACK* weighed approximately 200 tons.

- Super Plates.

The super plates were made of 304 steel, a low carbon high nickel content steel that had been used extensively in cryogenic applications. The nickel in the steel added to its plasticity at low temperatures. Most cryogenic vessels use this type of steel. There were 2 *super plates.* One can be seen in figure 20.

- 410 Stainless Absorber.

The remaining 50 Absorber plates were made of 410 steel, a low grade stainless which contain~~s~~ed a high carbon content and barely fell into the category of stainless steel. The absorber plate had to support its own weight and the weight of two cookies. Each of the absorber plates rested on the I-beams. The horizontal motion of the Zorba plates was prevented by the use of sway bars. The sway bar and steel assembly can be seen in figure 21. These bars extended out like arms to the sides of the box structure formed by the super plates and top frame rails. Along the inside of the top frame rails were two $\frac{3}{4}$ inch diameter threaded stainless steel rods. These rods ~~have~~ had two nuts for every Absorber plate. These serve a double function. The first and major function was to support the Zorba plates from above so that the stack would not topple forward or backward. The second function was to provide some stiffness and straighten the warpage of the plates. Each sway bar had two half moon cut outs of half cross section thickness. Two nuts on either side of each of the two fix points formed a short lever arm. The forces needed to straighten the plates ~~is~~ was small at room temperature, about 10-20 pounds at the center line.

These bars were mounted to the top of every absorber plate with Barrel nuts. They were connected to rods fixed to arms on the two *super Plates.* Any lateral motion ~~is~~ was transmitted along these rods.

- Support I-Beams

The support I-beams were 106 inches in length. They were fabricated

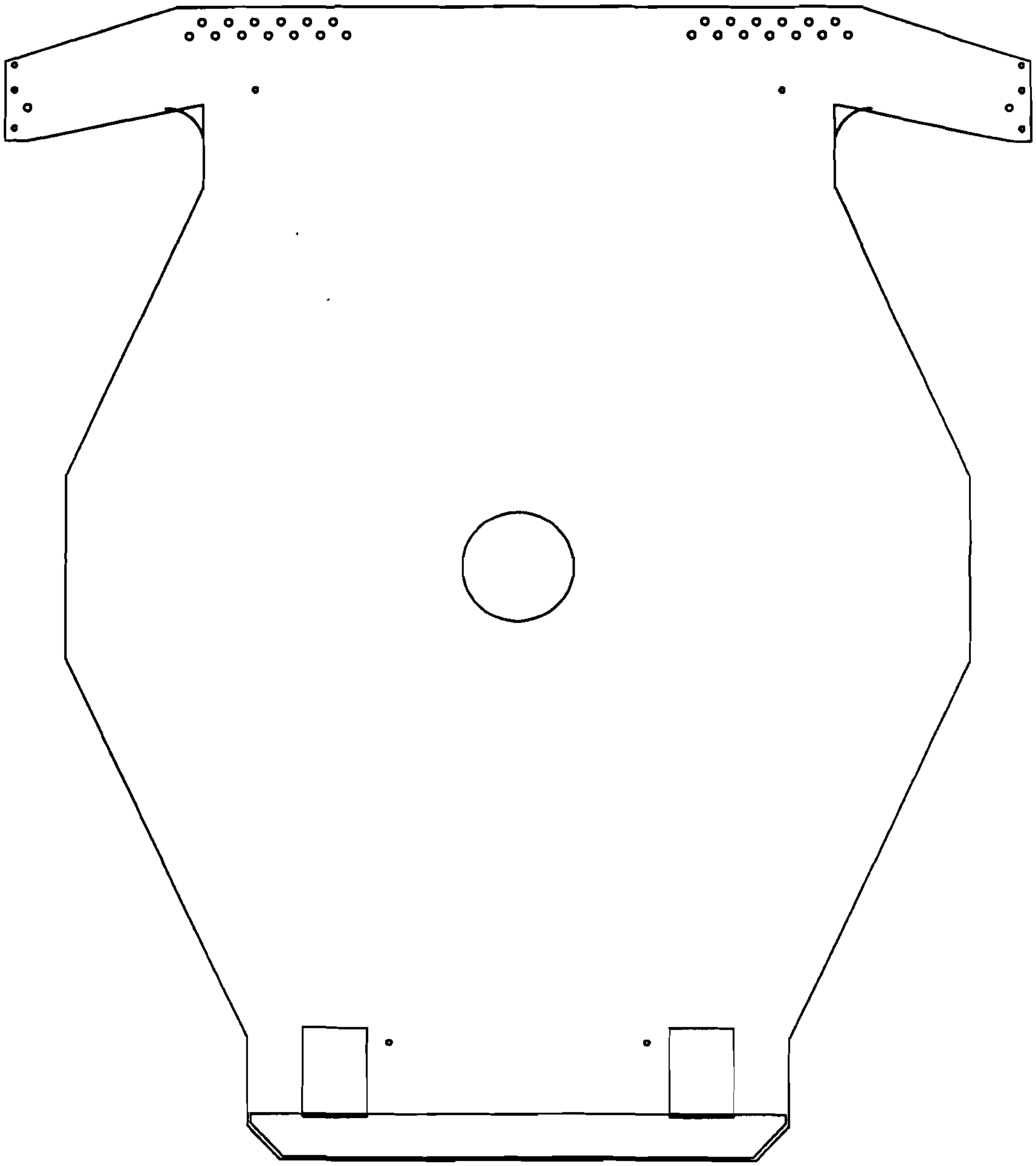

Figure 20: Super plate.

Figure 21: Sway bar and its installation on a typical steel absorber.

from sheets of 316L stainless steel. They were heavily re-enforced at the super plates and at the ends. A drawing may be seen in figure 22.

- Suspension System

The suspension system consisted of two sections of 4.5 inch diameter 316L stainless steel rods. As mentioned before the tops of these rods terminated above two box beams that were integral to the gantry structure.

Figure 22: A drawing of the Hadron Support I-Beams.

They passed through the cover of the cryostat and had flexible stainless steel bellows around them. The bellows served as a gas seal and allowed normal flexing of the rods under load. A coupling much like a turnbuckle connected the upper rods described with the lower rods connected to the Clevis. The coupling provided a means for fine adjustment in Y of the entire hadron calorimeter structure. The coupling was located just above the PVC insulation separating the gas and liquid phases.

AWK

[illegible] need picture why capital

- Clevis.

The clevis to fit the super plates were much as any clevis. The difference lies in the load bearing surface of the pin. To minimize the stress and meet the criteria necessary to achieve the proper load bearing surface thirteen 1 inch stainless steel pins were used. The clevis-super plate engagement is shown in figure 23. Each of the four clevis weighed 500 lbs.

Figure 23: Clevis and Super Plate.

- Installation of Support Clevis.

The lower rods were threaded into the clevis on the ground. Alcohol was used as a lubricant. To keep the rod and clevis lined up v-blocks with rollers were used to support the rods. The assembly was place on a die table under the gantry. The die table in turn rested on top of a hydraulic lift. The lift brought the clevis up to the desired position and the die table did the fine upward positioning. The couplings were already on the upper rods. Thread lengths were measured so that we could tell the engagement by measuring the visible thread. After the clevis were threaded each was carefully surveyed into position based on a calculation of deflection and contraction of the individual components to achieve a nominal beam height. This survey was repeated three times to insure accuracy.

Preparation of Steel Plates.

- Pre-clean and Stack.

The fifty 410 stainless plates were placed in order for cleaning and installation. During the restacking each plate was examined for gross defects and cleaned. The cleaning was done with a very coarse Scotch-Brite buffing pad and acetone.

- Burr removal. Sandpaper was used along the edges and around holes to remove any burrs that might harm personal or Cookies.

✓ capital?

- Copper fin Holes. Holes were drilled in the bottom of the plates for copper fins. The copper fins will be discussed later under cool down procedures. Their main purpose ~~is~~ was to aid in the heat removal from the steel.
- Oil removal. Oil was removed from each plate with a soap and water bath. We purchased a soap called "Micro Soap" from VWR Scientific for it's its ease of rinsing. It seemed to leave less residue, soap film, than other soaps. This solution in water was put onto the

plate in a horizontal position. The plate was then scrubbed using a Pneumatic sander with Scotch-Brite pads.

- Rack Cleaning. After both sides of each plate were cleaned with micro soap the plate was put into a vertical position in a rack.
- Acid Etch. Once in the rack a concentrated, 15 Molar, solution of Oxalic acid was used to remove any oxides left on the plate. The plate was then rinsed with distilled water and scrubbed with Scotch-Brite pads as necessary.
- Ethanol Rinse. The final cleaning was done with 200 proof Ethyl Alcohol. This was applied and wiped off with Kaydry wipes. We hoped to remove any remaining organic compounds this way.
- Sway bar installation. The final work done on a steel plate before lifting into place was the installation of the Sway bars. These bars were 1 inch by 2 inches and were well machined. They mated ← with the steel plates in four well machined spots to insure accurate measurement in the y direction. The edge of the steel plates were plasma cut and only machined in 6 small spots to lower cost., ~~T~~the four previously mentioned spots and the two spots where the plates rest on the I-beams. Threaded lifting eyes went through the sway bar, through accurately machined spacers, and into barrel nuts in the steel as shown in figure 24 .

? A spreader bar was attached to the lifting eyes to lift the steel into place.

<u>The Lift.</u>

Figure 24: Barrel Nuts in Absorber plates.

- Copper Fin and Heater installation. The steel was lifted high enough off the ground to install the 158 copper fins. The fins were installed with four nuts and bolts, and belville washers to maintain force. A steel bar .25 inch thick by 2 inches by 48 inches was placed over the steel as a washer and to prevent the steel from walking off the I-beams. A heater was also installed on the copper to aid in outgassing and heat up in the event that we had to fix something fast.

- Cookie Installation The cookies were taken one at a time from their storage bags and placed on a specially manufactured table. This table enabled us to bring the cookie from a vertical to horizontal position and vice versa in a controlled manner. When the cookie was in the horizontal position final checks were made. The Ejector/Fastener ears were installed at each card edge connection. These were installed to ensure that the cables had good mechanical support. A last minute electrical check of high voltage wiring was done. Mylar was installed to electrically isolate the cookie ground from the steel/gantry ground. It was felt that grounding at one known point minimized the noise. The cookie was brought again into an upright position and a spacer equal to the thickness of a steel plate and twice the thickness of the cookie-steel gap was put over the cookie. Then a second cookie was placed on this sandwich. The horizontal procedure was repeated for the second cookie. Then the high voltage wires were installed, and the final support mechanism. The support mechanism was tied to a spreader bar and tilted vertical. The cookie pair and spreader were lifted with the overhead crane and slid between the steel. At halfway point we stopped to cutout the beam hole for the filler vessel.
- Cookie Support System.

The cookie suspension is shown in figure 25.

At the gap between ribs a plate called the Tongue plate was placed through the slot between the Headers. It protruded from the bottom side enough to attach two $\frac{1}{8}$ inch by $\frac{3}{4}$ inch aluminum plates on either side, called Cheek plates. The Cheek plates were fastened into place with clevis pins. The top of the Cheek plates had a hole to accept $\frac{1}{2}$ inch diameter steel rod. The steel rod was attached to a T piece. This T piece made of aluminum was designed to mount two Cookies at once on

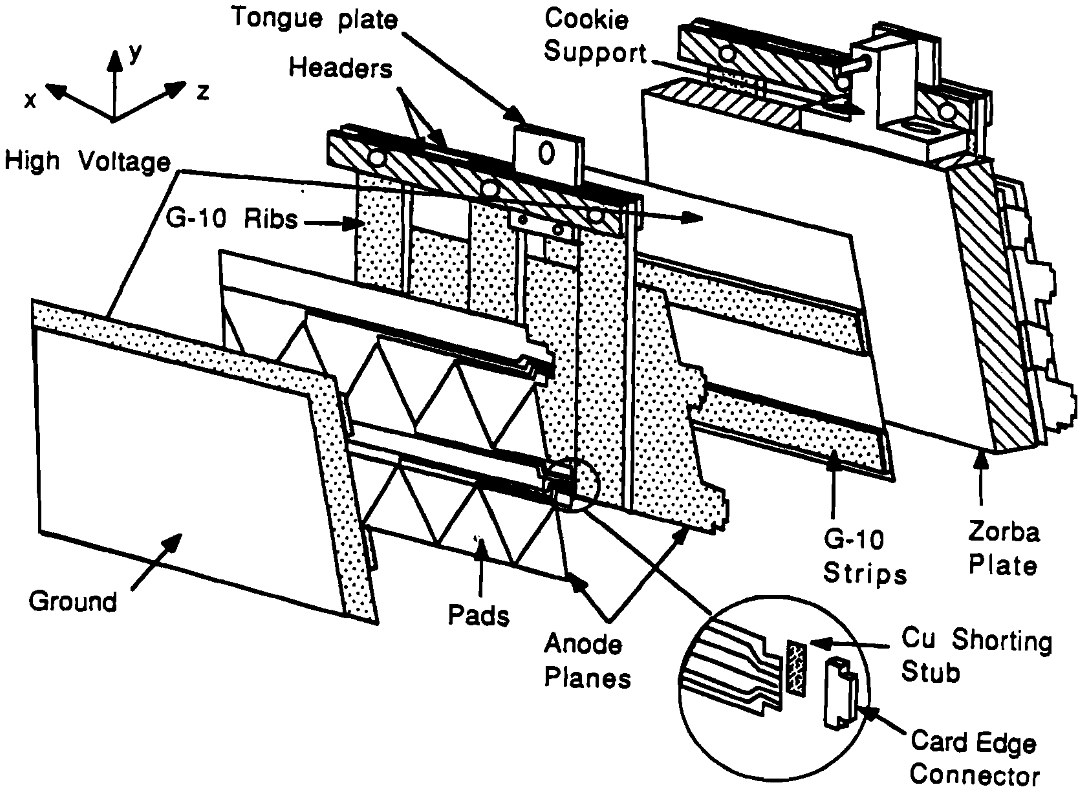

Figure 25: Cookie Suspension showing cheek and tongue plates in the header.

an Absorber plate. The Cookies hung on either side of the steel plate. This made up an arrangement where every other steel plate supported two cookies. This alleviated the problem of mounting the cookies at the ends of the calorimeter and near the Super plates. The T pieces were slotted to permit adjustment in X. Adjustment in Y was done using the mounting screws and nuts under the T piece. Adjustment in Z was done by moving the tongue plate on the steel pins.

<u>Survey.</u>

- Cookie Support Y position.

The cookie support system as explained earlier ~~is~~ was based on the vertical ribs of the cookie terminating in the header. There were two possible support locations on the left and right sides of the steel header. These locations were staggered to not interfere with each other. A device called a Tongue plate, described previously, was placed at these locations. The height of the cookies was determined by this total support system. Based on nominal values a calculated height was determined by surveying the top of the sway bars. Shim was installed to bring the support system to this nominal value. After all the cookies were installed they were surveyed using the locating pin holes. A G-10 Target was devised to aid in the survey. This measurement was done from both sides of the cookie. The survey enabled us to tabulate the x,y displacements of each cookie and rotations.

- Position in X. The position in x was adjusted by moving the support system from above in x. This moved the cookies in pairs. If the pair were skewed relative to each other little could be done. The x offsets were minimized for the pair and only for the blatant offsets.
- Position of Y. This again was only adjusted for those that were blatantly off. This was achieved by slightly elevating the cookies by their headers and installing shims between the header and support.
- Daisy Chain Installation.

The milling of the pattern on the pad boards terminate~~s~~ed in card edge connection. This card edge connection ~~is~~ was an industry standard 100 mil wide strips on a 100 mil pitch. Then number of connections on an edge was equal to the number of pads +1. The largest connector used ~~is~~ was a 60 pin, 30 pad. Each cable for daisy chaining the pads together ~~is~~ was made symmetrically so that it may be used for both the front and back half of the cookie. The Hadron calorimeter use~~s~~d mass terminated card edge connectors on a ribbon cable. This cable daisy chain~~s~~ed the towers together in groups. The groups corresponded to the rows of the cookies. The chain ~~is then~~ terminated on the patch board. The patchboard reconfigure~~s~~d the output to match the read out cables. During this reconfiguration the signals were ordered such that all pads in a row were read out consecutively. The card edge connector had the pads were read out starting from the center pin. The center pin was a dummy. All up pads were read out starting from the center and going up on a board. All down pads were read out starting from the center and going down as seen if figure 26 . AWK

- Patchboard Installation. Cookie read out and ~~Patchboard~~ Interface. AWK The patchboard was designed to rerout the cookie daisy chain cables into the 16 channel configuration needed for the Gore cables.*

2.8. THE READ OUT ELECTRONICS FOR THE LAC.

RABBIT System and MX read out. This section describes the read out of the LAC. Both the hadron and electromagnetic calorimeters were towered in two sections. This tower is made by an electrical .OR. of all sensitive areas that were geometrically focused on the target 9 M away. The electromagnetic calorimeter use~~s~~d strings made up of thin tinned copper braid with small friction fit connector~~s~~ soldered ? on. Each string represent~~s~~ed one channel or tower. There were 6000 such strings. The read out cables were specially made for our experiment by the W. L. Gore Co. in Phoenix, Arizona. The cables ~~can~~ could be treated as transmission lines with a characteristic impedance. These cables were flat and carr~~y~~ied groups of 18 signal lines. Due to the usage of these cables the middle two signal lines

---

* W. L. Gore Trademark.

Figure 26: Read out on cookie to connectors.

were held at ground.[†] The impedance of the cables was selected to match the input impedance of the amplifiers. The input impedance of the amplifiers ~~was~~ were designed to give a fast risetime. The input impedance of the amplifiers ~~is~~ was 12 ohms. A tower with capacitance of ten nanoFarads, nF, limit~~s~~ed the risetime of the signal to 120 nanoseconds.[‡] When ordering the

---

[†] See E706 memo # 157, D.D. SKOW "FEED for RABBIT".

[‡] The characteristics of the first set of cables made for the EM calorimeter were miscalculated

cables for the Hadron calorimete~~r a~~ sample was made reducing the width of the cental conductors by 2 and increasing the overall gap between the conductor and the shield relative to the cables for the electromagnetic calorimeter. The result was a cable of lower inductance and capacitance and impedance between $12 - 16\Omega$. F~~f~~igure 27 shows the Hadron cable design.

Figure 27: Gore read out cables.

---

by a factor of two. These cables were found to have twice the expected inductance.

you ha[illegible] this in [illegible] past tense.

The RABBIT system. The RABBIT or Redundant Analog Bus Based Information Transfer system is a FERMILAB standard bus for particle physics experiments.* Each crate has a dual bus, named Top and Bottom, with both analog and digital lines. Each bus has its own controller called EWE. The EWEs for the crate sit in the two left most slots. The EWEs have a 16 bit ADC that can digitize a signal multiplexed from the backplane in 20μ second. Additionally, the EWE has an analog adder and threshold circuit for pedestal correction and zero suppression.† Each EWE can address 64 devices each with 64 subaddresses. The rabbit system may be seen in figure 28.

The signal from the crate enters the EWE from the backplane and is added to the output of a Digital to Analog Converter, DAC. This DAC is called the pedestal DAC. The pedestal DAC adjusts each channel such that they read roughly the same value when no signal is present. The resulting signal may be tested to see if it exceeds some threshold. The threshold here was meant as a method of hardware zero suppression or data sparsification. The pedestal adjusted signal was attenuated by a threshold DAC and put into a set of comparator with a mutual constant offset. If the attenuated signal exceeded the constant offset in a positive or negative direction then a bit was set in the status register. This procedure was called test over threshold, TOT. The digitized value was the pedestal adjusted signal. The last card in the crate is a BAT or Before After Timer. It generates the timing for the sample hold circuits within the crate as well as providing calibration and monitoring voltages, and terminating the backplane. The EWEs were in turn controlled by the MX. The MX is a custom designed emitter coupled logic, ECL, list processor with some arithmatic capabilities. There were a maximum 8 EWEs allowed per MX bus. We ran with 6 EWES per MX bus in all

---

★ FERMILAB PN-52 "RABBIT System Specifications", T.F. Droege, K.J. Turner, T.K. Ohska

† FERMILAB PN 95

Figure 28: The Rabbit System and EWEs.

but the back of the hadron calorimeter. The MX is essentially a smart "sequencer." The MX is made up of program, data and event memories, a sequencer, an Arithmatic Logic Unit, ALU, and two interfaces for communications. Communications were done between the EWEs and MX, and a UNIBOX and MX. The UNIBOX was an interface to a Digital Equipment Corporation PDP 11/45. The data memories contained information about each channel addressed by a EWE. This information, determined at the begin of run, was made up of pedestal DAC setting, threshold DAC setting, and a coded map word for offline processing. The event memories buffered up to three events during readout. At the start of each run the MX programs were downloaded and run. The precise order in which the tasks were executed is covered in the section on data aquisition.

The Amplifier and Trigger Modules. Each amplifier card had 16 channels on it and occupied one slot in a RABBIT crate. Each of the 16 channels was a charge amplifier whose signal was delayed by 800 milliseconds and fed to a charge to voltage converter. The delay circuit was to allow time for the trigger to be formed. The charge going into the delay was fanned out and amplified again to a fast out on the front panel. This fast out was used in the trigger and will be discussed later. The last stage of the amplifier fed a set of sample hold circuits. The sample hold for every channel was simultaneously triggered by the BAT in the RABBIT crate. A successful physics trigger would sample the signal immediately and again at a fixed and controllable time later. These signals were called the before and after. This was done to avoid a pileup of signals in the argon if the decay time of charge collection was exceeded. The signals from each of the before and after sample hold circuits was put onto the RABBIT analog bus in a programmable fashion. During readout the before signal was subtracted from the after to remove any shifts or drift in the system. Every four channels were serially added and the resulting signal triggered a common stop Time to Voltage Converter, TVC. There were two TVC circuits per four channels. A master and slave TVC combination allowed a two hit capability in the event that a channel was multiply occupied before readout. The TVC was a RC circuit with sample holds triggered on the before pulse mentioned above.[⋆]

[⋆] See D. Skow thesis for details. or E706 memo # 157

3. Data Aquisition and Trigger.

3.1. COMPUTER SYSTEMS.

The E706 data acquisition system consisted of a multilayered computer network; ~~at~~ A the top level of the Data Aquisition system was a Digital Equipment Corporation, DEC, Microvax II series computer. This μVAX was used as a control and tape writing machine. Below it in the chain were four DEC PDP-11 series mini-computers. Each major element of the apparatus ~~is~~ was controlled and read out by a separate DEC PDP-11. The subsystems were Planes, consisting of the Silicon Detectors, and Multiwire Proportional chambers, LAC, consisting of the Hadron and Electromagnetic Shower counters, FCAL, the forward calorimeter, and MUON, consisting of the muon multiwire chambers. All the PDPs except the LAC PDP-11 read data through serial and parallel CAMAC crates. The LAC PDP-11 involved one more level, the MX processors which were discussed previously in chapter 2. A schematic of the entire system may be seen in figure 29.

The μVAX ran a multilevel program called VAXOnline, that was provided by the Fermilab computing department. VAXOnline involved four major processes. These were Global Menu, which directed the user to the other attached processes, Output, which controlled and spooled output to magnetic tape or disk, Run Control, which was the user interface to the system. Run control also sent commands to the front end systems, ie. the four PDP-11 computers acquiring the data. The final process was event builder which took the data, concatenated it and parsed it to the other processes. A fraction of the data was sent to a DEC VAX 780 computer where online data analysis and full event reconstruction took place. Several programs were run to monitor the apparatus. The Planes monitor showed plane multiplicity on an event by event basis. The trigger monitor reconstructed the trigger from CAMAC data and

✓ capitals

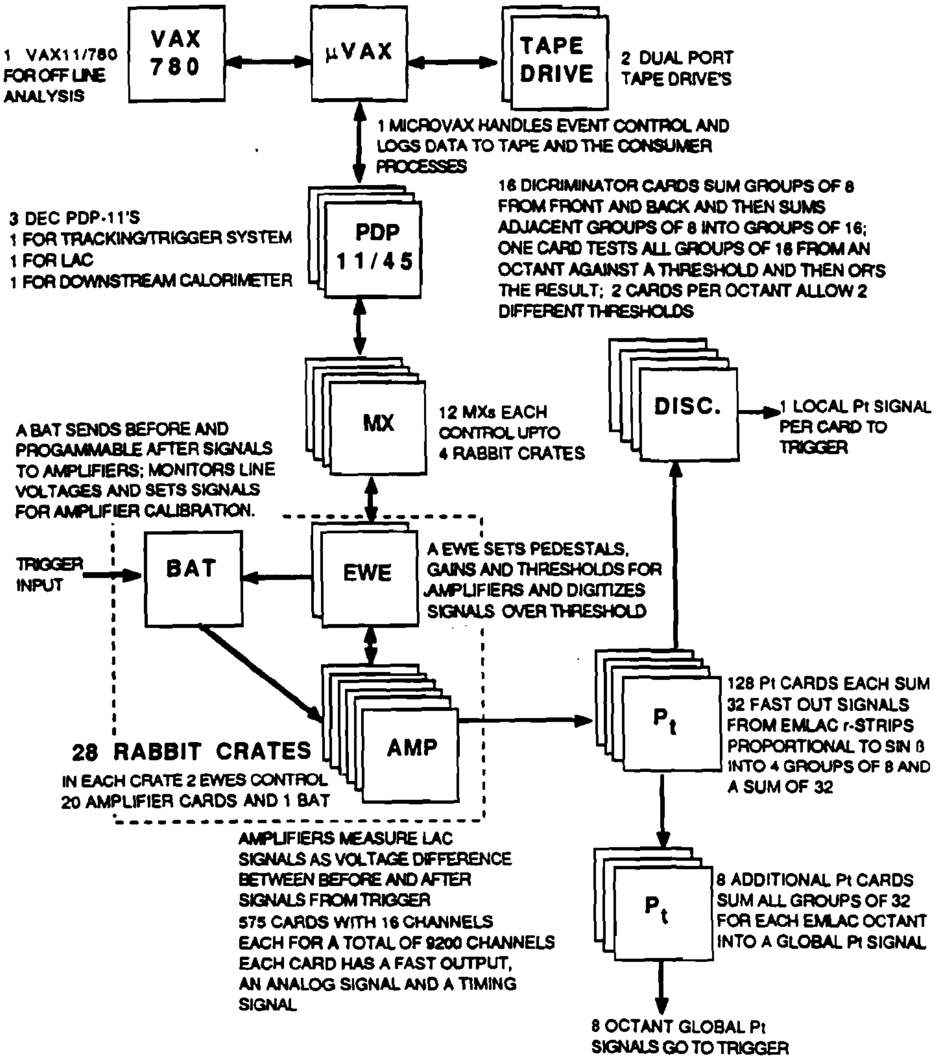

Figure 29: The E706 data acquisition system showing the μVAX , PDP-11's and MX's.

displayed the results and monitored for inconsistencies. A scalar Monitor showed all scalars that were read out during the spill. An event monitor showed event size in each separate computer. A monitor looking? at the time history, stored in the same way as the forward calorimeter displayed data from various devices as a function of accelerator clock buckets. This what? monitored data from the Cerenkov ring and antiring, the veto wall elements~~,~~ and, beam and hole counters. AWK

3.2. RUN MONITORING AND COLD START TASKS.

During the data acquisition period monitor tasks were usually run at the beginning of a run. A run was defined as a block of data identified by a run number, during which no parameters were varied. A run ended with either a change in parameters or with the end of a 6250 bpi magnetic tape. Occasionally, every 3 to 4 runs, a cold start task was run on each of the subdevices. The cold start task both initialized data in the hardware and recorded pedestals for ADC channels and gains for amplifiers. The planes cold start task downloaded a bit map into the electronic latches. This map controlled the assignment of a physical wire to a number for readout. There ~~are~~ were a series of runs where a problem exists for this particular operation.

LAC Pedestal and Gains Monitoring.

AWK There were several possible LAC cold starts were varied. A typical cold start done frequently during a 8 hour data shift was called a pedestal task. Additionally, at the end or beginning of each shift a gains task was run in conjunction with the pedestal task. The object of the pedestal task was to get pedestal offset for each and every channel of the electronics. The EWE, as described in the hardware section, was able to offset the measured value using the pedestal DAC. The combined value would be compared with the Test Over Threshold DAC, TOT DAC.

$$|Channel\ Value - Pedestal\ DAC\ Value| \overset{?}{\geq} TOT\ DAC \tag{3.1}$$

If equation (3.1) was satisfied then a bit is set in the status register and a software controlled decision may be made to digitize the result or not. We choose not to digitize when equation (3.1)was not satisfied. This increased readout speed and reduced the number of channels to write to tape. It thus becomes important to set the pedestal and TOT DACs correctly. The pedestals were not subtracted by the hardware before digitizing. Pedestal subtraction was done in offline reconstruction. This required storing the pedestal values in a database. The pedestal task preformed a software trigger to sample and hold every channel in the crate. Each channel was digitized 16 times and averaged; the average value was stored. The TOT or Zero suppression window was set to be a constant for each entire EWE. We wanted to have the pedestal DAC to offset the signal such that the TOT window was symmetrically centered on the pedestal value. The Pedestal DAC setting was varied little by little to find the upper and lower limits to the zero suppression window. The middle was calculated and the pedestal DAC readjusted to place the channel in the middle of the window. This new pedestal DAC setting was stored. After completing the pedestal task on every channel in an MX the values were transferred to a database on the data acquisition VAX. The process was called update. See G. Ballochi for details. A gain task was done by injecting charge on each channel. The reference value was generated and fanned out by the BAT. A software trigger caused the process to begin and the channel to be sampled. The resulting sample was digitized and stored. This process was repeated some 32 times to compute and store an average value. The injection charge was varied and the process repeated. A fit was made of ADC value vs charge injection, this became the gain. Every channel for amplifiers and TVC were calibrated in this manner. This acted as a monitor of the performance of the electronics and as a correction to the energy in the reconstruction. The MX kept track of TOT and Pedestal DAC settings for every channel. During event read out the DACs were loaded with the settings of the channel addressed before the channel was tested.

3.3. LAC EVENT READOUT.

The sequence of events to reading out the crates are as follows. A trigger is received. The first channel of the first crate of the first, top or bottom, bus is addressed and the pedestal and TOT DACs are set with values from the MX memory.[*] If the channel satisfied TOT a start convert signal was issued, and the MX moved onto the next EWE in the address chain. If TOT was not satisfied then the next channel was polled until TOT was satisfied and start ADC conversion signal was given. The MX did not wait for the conversion to finish in the EWE, rather it went on to the next crate and so on until it returned to the original EWE when it tested on conversion done signal. We did not use the RABBIT redundant feature as it was planned. We connected half of the 20 available read out slots in a crate to the top EWE bus and the remaining half to the bottom EWE bus. This however, enabled us to cut our conversion time in half by having two ADC's per crate. Since we ran this process asynchronously it had a tendency to cause a great deal of noise in the crate. In the future a synchronous system will be used to eliminate this noise. Each MX would read out its list of crates as described above until it exhausted the readout list held in it's memory. The MX would then set a done bit. When done was received from all MXs, the PDP-11/45 would start to read out the from the MX and ship the data to the concatenating μ-VAX. The PDP would also read out an event scaler to be used in the event header. This header had the event number and time stamp in it.[†]

---

[*] The registers referred to here are documented in the hardware chapter under LAC Electronics, Also see D.D. Skow Thesis.

[†] see G. Alverson software note E706 Event Formats.

3.4. TRIGGER DEFINITION.

The trigger system was set up to allow a variety of triggers from the apparatus. Each of the triggers was appropriately identified in the data stream. The triggers were, BEAM, interaction, local $P_T \bullet$ Global_Low, local $P_T \bullet$ Global_Hi, and Muon. Each of these triggers will be discussed with the exception of the Muon triggers. The symbol $\bullet$ represents a logical AND and the symbol $+$ represents a logical OR. The trigger was formed in two sections, a pretrigger, and the final trigger. This was necessary because of the long time required to define the photon trigger. All the electronics required a signal to latch the results sooner than the final trigger could be formed. This also allowed us to use a multiple trigger definition. About 800 ns was required to form the photon trigger. During this time all information about the potential event had to be held in the electronics. The pretrigger was a fast signal indicating that energy deposited in an octant of the EMLAC exceeded a threshold in coincidence with LIVE_INT1, which is described below. When a pretrigger occurred, the PWC/SSD latches were strobed to hold the hit wire locations, the before pulse was sent to the LAC BATS to sample the LAC signal, the clock on the FCAL was stopped. If a final trigger was not generated, all of the above conditions were cleared and the apparatus was ready for another pretrigger.

Interaction Definition.

The first part of the trigger definition was called LIVE_INT1.

LIVE_INT1 formed the basis for the secondary muon and photon triggers. INT indicated a beam particle was present, and there was a signal in one of the four interaction counters. LIVE_INT1 built on this by demanding that there were no particles present in the previous 3 time slices, buckets, and no particles came in the next three buckets. The forming of LIVE_INT1 may be seen in figure 30.

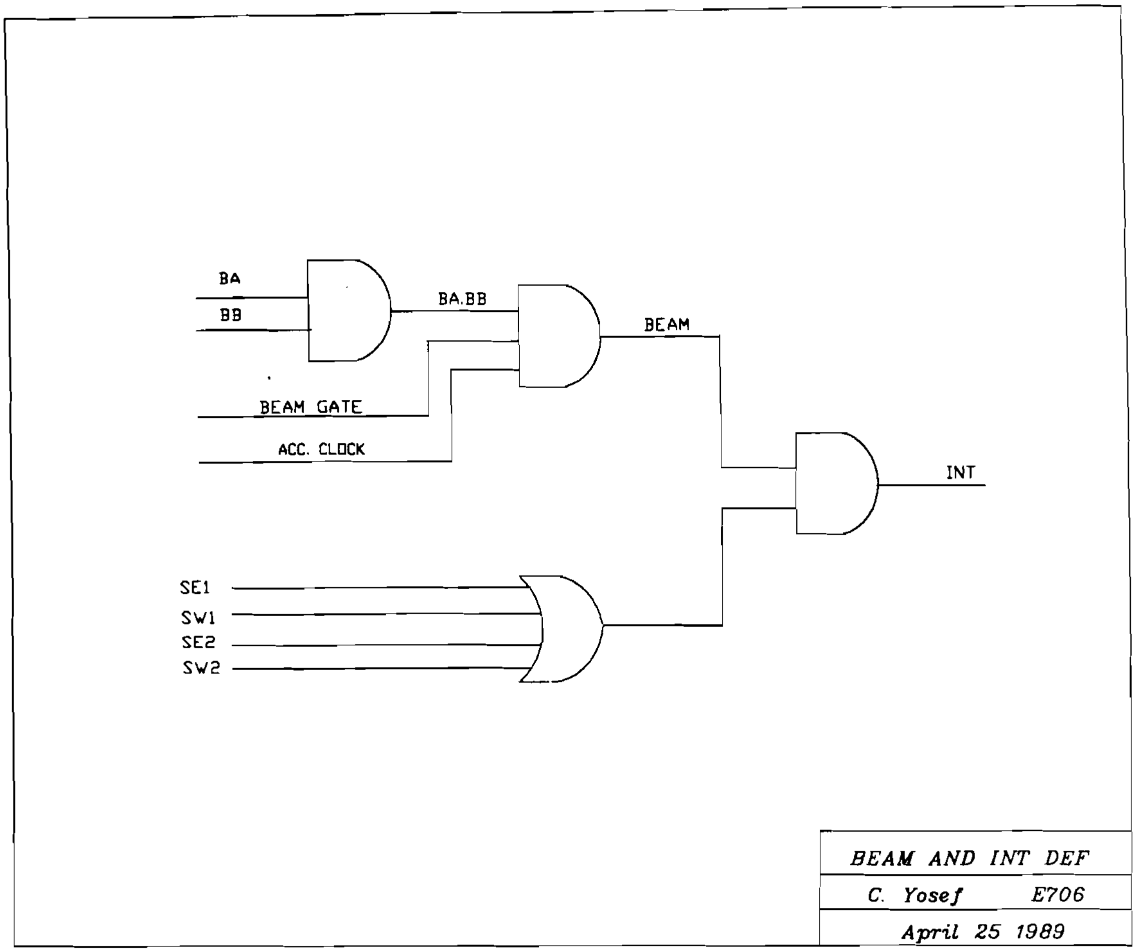

Figure 30: Trigger Logic showing INT and LIVE_INT1.

LIVE_INT1 was first formed by making a BEAM logic signal. Two overlapping scintillators 1 inch square called BA and BB were at nominal beam height. They were also aligned in a one inch diameter hole in a 5 inch square scintillator called BH. BA and BB were put in coincidence with BEAM_GATE to form BEAM. BEAM_GATE was a signal provided by the accelerator to indicate the possibility of live beam in the current accelerator bucket. Four counters, called SE1, SW1, SE2, and SW2 East and West , upstream and downstream of the magnet OR'ed together formed a simple interaction definition. The location of these counters is shown in figure 31.

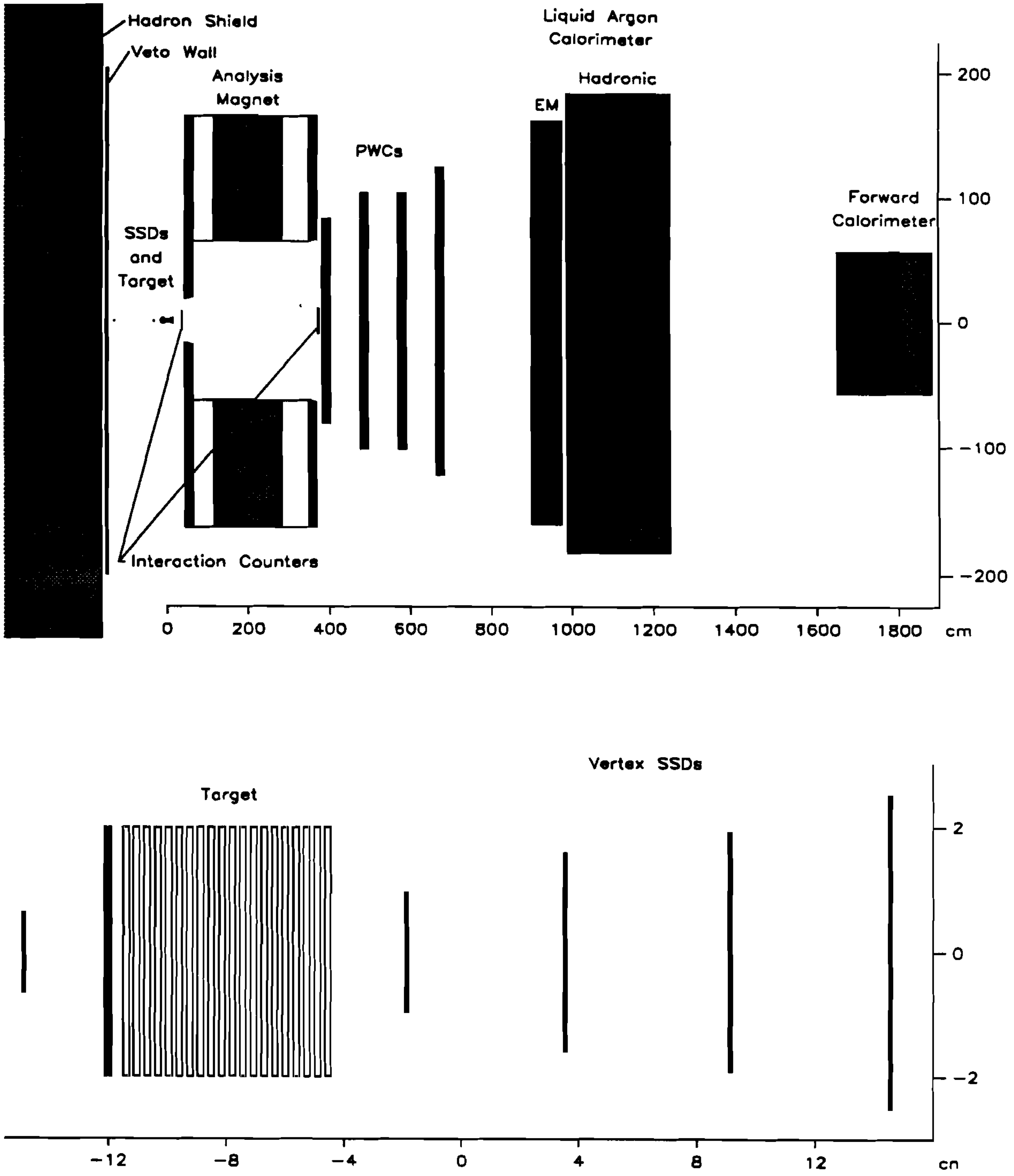

Figure 31: Location of Veto wall, Beam and Interaction Counters.

This signal AND'ed with BEAM formed a signal called INT. That is,

$$\mathbf{BEAM = BA \bullet BB \bullet BEAM\_GATE}$$

and

$$\mathbf{INT = (SE1 + SW1 + SE2 + SW2) \bullet BEAM}$$

INT was fanned out 7 ways, each of the seven channels were delayed by a different amount and then all seven signals were recombined in coincidence-anticoincidence circuits. The purpose of this was to pick out interactions for which there were no interactions within 3 buckets preceeding or in the 3 buckets following the trigger interaction. Number the buckets 1 through 7, where 1 is the earliest and 7 the latest, and 4 is the bucket of interest and using obvious notation where overbar means anti-coincidence we have:

$$\mathrm{CLEAN\_EARLY} = \overline{\mathrm{Bucket1}} \bullet \overline{\mathrm{Bucket2}} \bullet \overline{\mathrm{Bucket3}} \bullet \mathrm{Bucket4}$$

and

$$CLEAN\_LATE = \overline{Bucket5} \bullet \overline{Bucket6} \bullet \overline{Bucket7} \bullet Bucket4$$

and finally

$$LIVE\_INT1 = CLEAN\_EARLY \bullet CLEAN\_LATE \bullet$$

$$\overline{BH} \bullet CMPTR\_READY \bullet BEAM$$

The pretrigger was formed by taking the interaction definition in anticoincidence with the veto wall and anticoincidence with SCRKILL. SCRKILL was a signal designed to prevent a coherent noise that might trigger the LAC system. Quite small signals since 2048 signals were amplified and summed together. The veto wall was described earlier. It consisted of two segmented walls of scintillator directly after the hadron absorbing steel pile. The signals were ORed by wall segments and ANDed between walls. The pretrigger definition follows.

$$VETO\_WALL = VETO\_WALL1 \bullet VETO\_WALL2 \qquad (3.2)$$

$$PRETRIGGER = \overline{VETO\_WALL} \bullet \overline{SCRKILL} \bullet LIVE\_INT1 \bullet LAC$$

The formation of the pretrigger can be seen in figure 32.

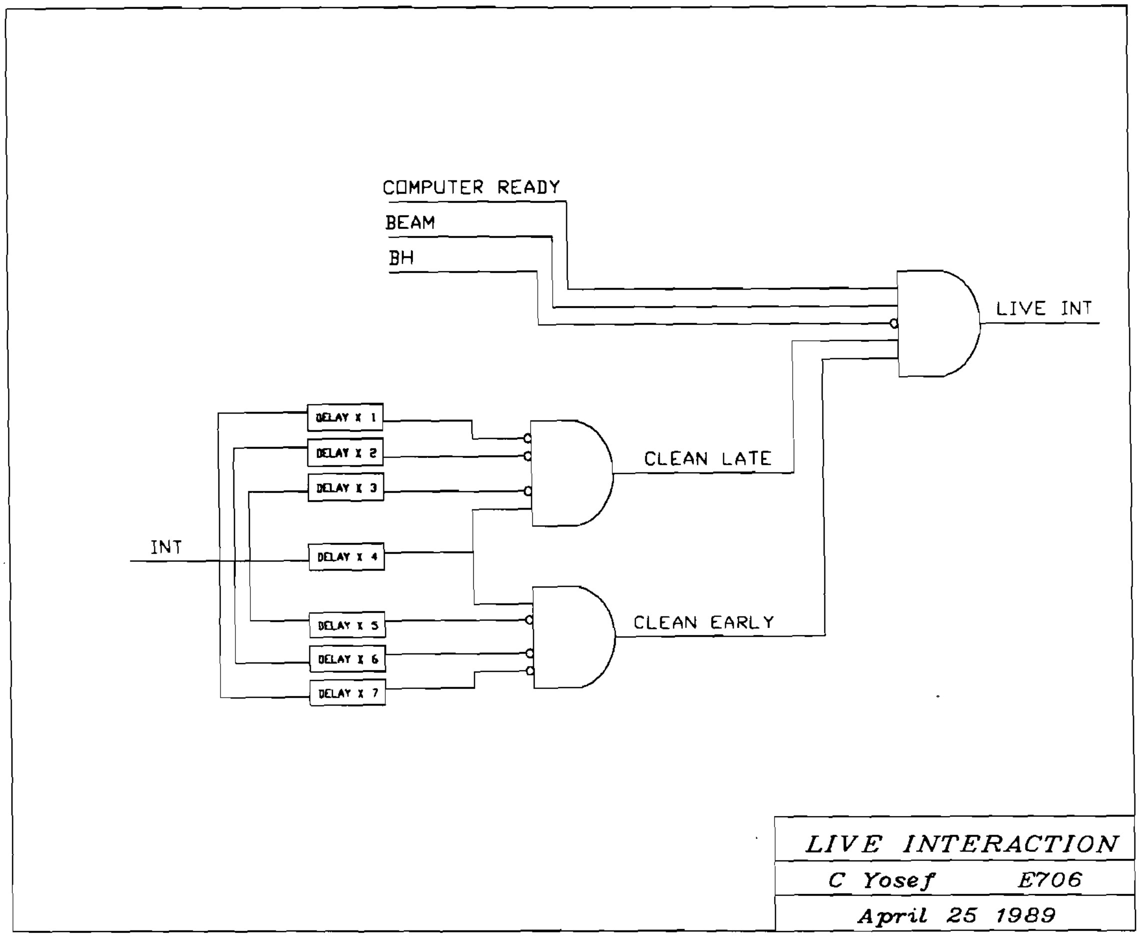

Figure 32: The formation of the pretrigger.

When there were no other triggers present, the BEAM and INT each prescaled, divided, by a factor of 10 were used as both a pre-trigger and final trigger.

3.5. SINGLE PHOTON TRIGGERS.

The various LAC triggers involved different methods of detecting local deposition of transverse momentum. The triggers were Local• Global_Low, Local• Global_High and Single Local. Each trigger element was broken down into octants. This was done because of the electrical separation between octants. The Global_Low and Global_High differ only in threshold setting and Global_Low essentially included the range spanned by the set Global_High.

The Global Trigger.

A feature of the LACAMP described earlier was the 800 ns delay line. The fast out of the LACAMP was formed by chopping the amplified signal to 180 ns. This signal was used to form the secondary trigger. The R-channels of the photon calorimeter were used exclusively to form a local deposition of transverse energy trigger. An estimate of transverse momentum was generated by a weighted sum of the charge deposited in these channels. P_T is defined as

$$P_T = E_\gamma sin\theta \tag{3.3}$$

where theta is the laboratory angle between the beam axis and the photon direction. The angle for each R strip is calculated by

$$sin\theta = \frac{R_i}{\sqrt{R_i^2 + D_T^2}}$$

where R_i is the radial distance to the i th R strip, and D_T is the distance to the target. The modules which did the weighted sum were called the P_T modules. They were computer controlled, located in a RABBIT crate, and worked in the following manner. The front and back segments of the same r channel were summed and a sum of four channels was put through a 8 bit DAC. This DAC acted as a computer controlled attenuator which was proportioned to $\sin\theta$. The P_T trigger modules were placed on every radial channel of the photon calorimeter. Each P_T module could handle 32 input channels. The modules summed two adjacent channels and put the sum through a multiplying DAC. The DAC was used as a computer controlled attenuator. Four DAC outputs were summed to produce a sum of eight input channels. This sum of eight was output to the front panel. Another a sum of 32 was formed by summing four groups of eight and outputted to the front panel. A box pictorial showing the operation of the P_T summing module can be seen in figure 33.

The DAC settings were calculated from the Radial location and set to the sine of the angle formed with the target. This gave a P_T weight for every two channels. The discriminated summed output became the Global_Hi and Global_Lo triggers, the name indicating a high or low discriminator threshold.

$$P_{T\ Global} = \Sigma p_t \tag{3.4}$$

The Local Trigger.

The LAC single local trigger was added during the run to enhance the single photon sample. The single local trigger was a local deposition of high transverse momentum energy. The trigger was formed using the local discriminator module shown in figure 34.

The sum of eight output from the P_T module was sent to the local discriminator module and front and back channels were summed, and discriminated. These individual front/back sums of eight were then

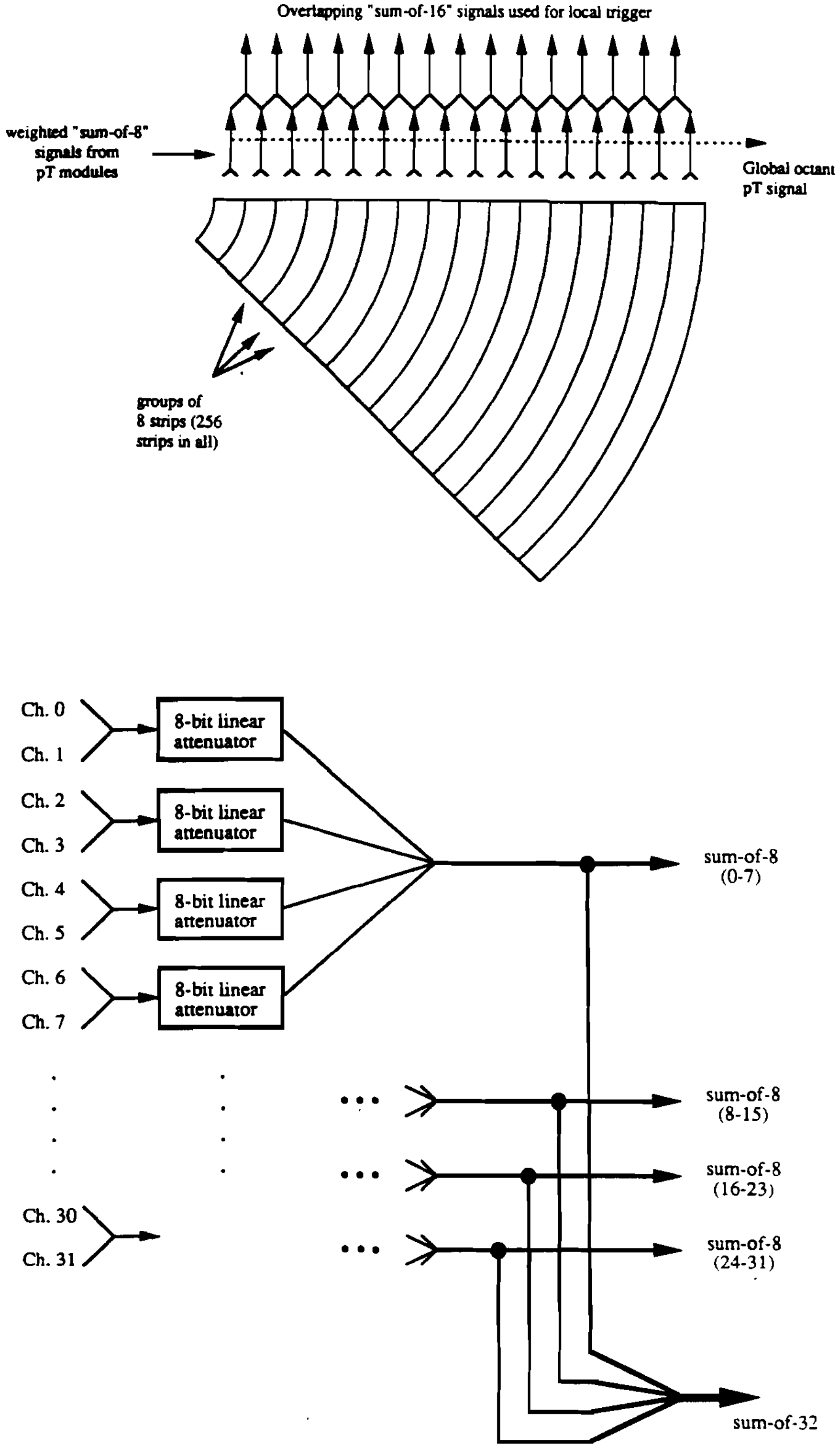

Figure 33: The E706 P_T Summing Module.

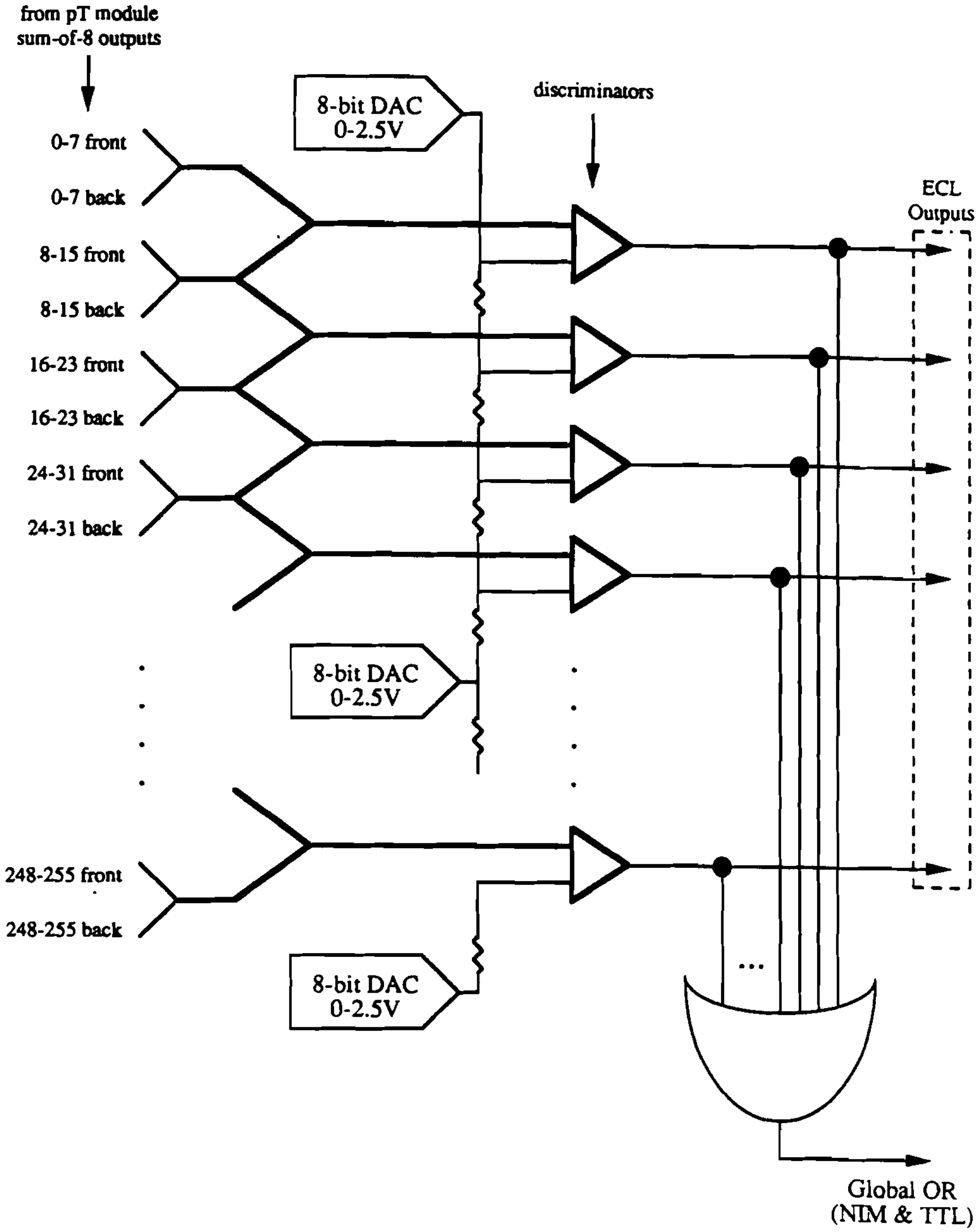

Figure 34: E706 Local Discriminator Module.

summed in an overlapping manner with adjacent sums of eight and discriminated. The discriminator value was adjusted though a series of computer controlled 8 bit DACs. Each of the overlapping groups of 8 channels were wire ORed to become the local trigger.

The Image Charge Problem.

The electromagnetic calorimeter had an image charge problem which was caused by charge collected in one region due to a shower depleting the surrounding regions within a quadrant. This was due to inductance in feeding the high voltage to the lead plates. The resulting effect was that wrong polarity voltages were observed at the fast-outs of amplifiers near a shower as seen in figure 35. These wring polarity signals caused the P_T summing modules to be ineffective. All the P_T modules were modified at the beginning of the run to only accept correct sign signals.

This image charge still affected the overall performance of the trigger by reducing the signal seen by the electronics. The detector was segmented electronically to reduce on the wrong sign signal detracting from the actual signal. As stated above sums were formed on the inner and outer boundary of the photon detector. The boundary was defined to be the cut along the inner and outer ϕ boundary. Additionally, the trigger was divided up into sections in the radial direction. The outer sixteen of the 256 radial, R, channels were disconnected for most of the data sample taken here. This region was where the image charge was the most intense.

3.6. SCALERS.

Each of the Trigger quantities was counted/scaled and the scalers were read out once per spill. This enabled us to monitor as an online and offline process how well the trigger was actually functioning. The

Figure 35: The Image charge seen on the fastouts of the LACAMP.

scaled values also allowed us to normalize our cross sections. These will be discussed further in the analysis chapter.

3.7. INITAL TESTS OF THE LAC.

After the LAC vessel was full of liquid argon many tests were done to see if the equipment was working as expected. Initially, before the LAC was filled and also during filling, pulsing studies were done to test the integrity of the system. The electromagnetic calorimeter pulser had such bad electrical characteristics that it was used only for continuity. The hadronic calorimeter pulser had excellent electrical characteristic. It was used to test the before-after timing in the readout system and to verify the changes of the system during cooldown. A plot of a typical output can be seen in figure 36. The change in pulse height vs channel number is caused by the readout lines under the G-10 strips which maintain the argon gap. This variation in gain is an artifact of the pulsing system and was not present in the real data. The test pulse was applied to the H.V. and Ground sides of a H.V. board. Capacitive coupling is used to couple the pulse to the readout pads. The readout lines under the strips, which has a dielectric constant 5 times that of liquid argon, contribute a major fraction of the total capacitive pickup. Pads near the center of a cookie had a longer readout lead and higher capacitance. Pads near the edge had almost no lead. This effect was taken into account for the gain measurement of the amplifiers. As mentioned previously, the amplifier gain task was accomplished by injecting charge on the input of the amplifier. Some of this charge was shared by the detector and transmission line. The desired goal was to measure how much charge propagated through the charge amplifier. This was corrected offline by modeling the combined amplifier, transmission line, and detector system. The overall correction was on the order of 1-2 %.

The Hadron Calorimeter Pulser.

The Hadron Calorimeter was divided longitudinally,into four physical

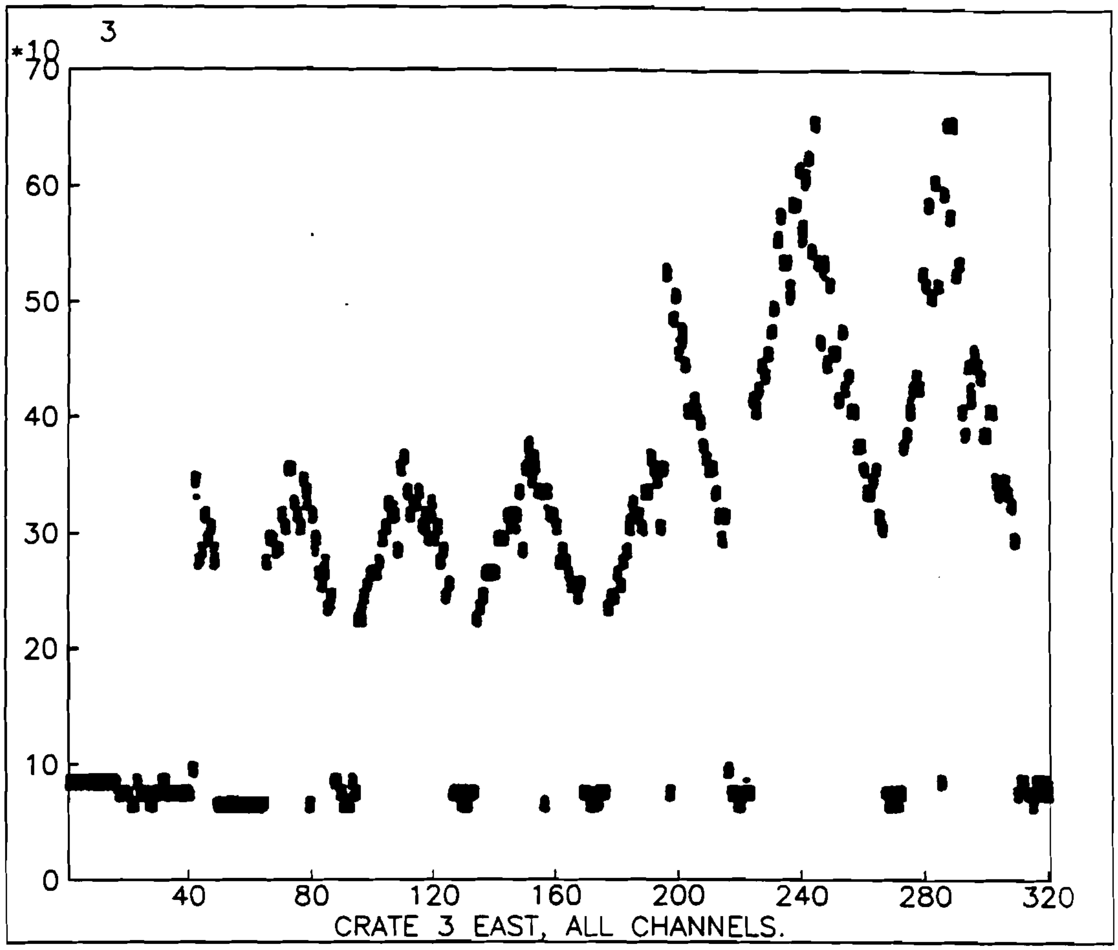

Figure 36: Pulse Height vs Channel number in back section of Hadronic LAC.

sections, numbered, JS = 1,2,3,4. Of these four sections,JS=1 was electrically isolated from the other three, and was composed of cookies numbered 1 through 14 inclusive and comprised the front section of the calorimeter. The remaining three sections, JS=2,3,4, were daisy chained together to make up the back of the hadron calorimeter. As the calorimeter deepened along the beam some of the pads and rows 'fell off the edge' of the cookies. This can be seen in figure . The Outlined pads fall off the edge going from cookie 15 to 53. This is detailed in table three.

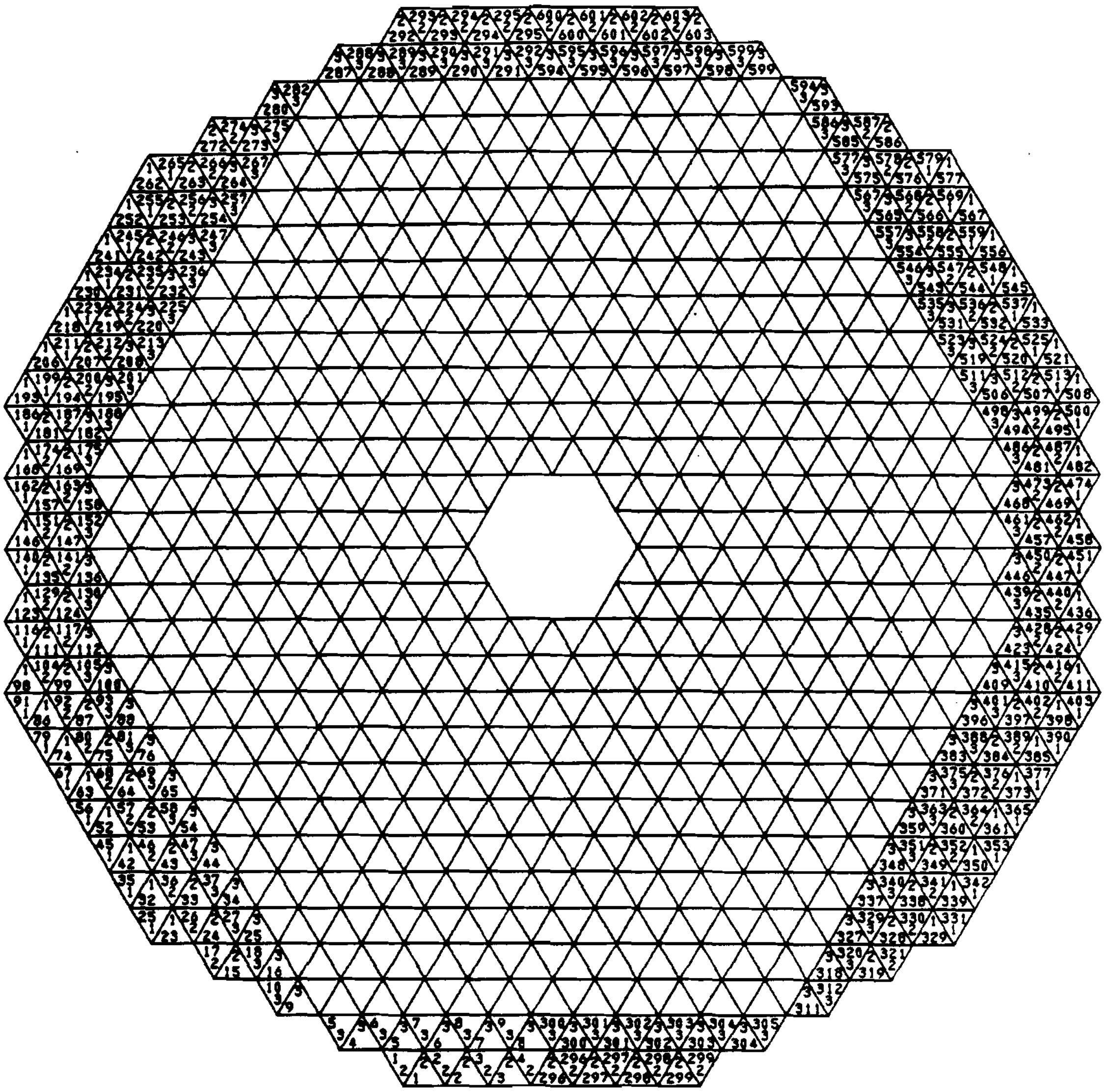

Figure 37: Pads falling off edge of cookie.

Cookies 10 and 53 were pulsed, 10 for the front electronics and 53 for the back. Some of the pads do not end up pulsed, because of the geometric focusing of the pads. These towers were at the edge of the calorimeter and did not pose a problem. The numbering from the front to the back was such that pads in a tower are given the same cookie address in the front and back. The pulsing was divided up between High voltage planes on the cookies. Cookie 10 had three planes in front and three in back. Each section of the high voltage plane covered approximately one third of the cookie. Each third carried either even or odd rows depending if it is on the front or back of the cookie. Cookie 53 had four planes on front and back, planes, 1 and 3, each covered one third area, and plane 4, and 2, covered the remaining space. The tables following document this process.

JS section	Cookies	Rows Covered	Section	Remarks
1	1-14	1-30	Front	
2	15-27	1-30	Back	Missing some pads.
3	27-40	2-29	Back	-
4	41-53	2-28	Back	-

Table 3

Front Pulser cable	Rows covered
1	22,24,26,28,30
2	21,23,25,27,29
3	12,14,16,18,20
4	11,13,15,17,19
5	2,4,6,8,10
6	1,3,5,7,9

Table 4

Back Pulser	Rows Covered
1	3,5,7,9
2	4,6,8,10
3	12,14
4	11,13,15
5	16,18,20
6	17,19
7	21,23,25,27
8	22,24,26,28

Table 5

Row	Pins on cookie	Back Left		Back Right	
		Card	Amp	Card	Amp
3	15	2	16	3	6
3	19	3	1	3	7
4	25	3	5	3	8
4	23	3	3	3	9
4	19	3	2	3	10
4	17	3	4	3	11
5	17	4	14	4	7
5	19	5	1	4	8
5	23	5	2	4	9
5	25	4	15	4	10
6	25	5	5	4	11
6	23	5	4	4	12
6	19	5	3	4	13
6	17	5	6	4	14
7	27	7	5	7	13
7	25	7	7	7	14
7	21	7	6	7	15
7	19	7	4	8	1

Table 6

Row	Pins on cookie	Back Left		Back Right	
		Card	Amp	Card	Amp
8	27	8	11	8	2
8	25	8	9	8	3
8	21	8	8	8	4
8	19	8	10	8	5
9	29	9	14	10	9
9	27	9	15	10	10
9	23	9	16	10	11
9	21	9	13	10	12
10	29	10	4	10	12
10	27	10	2	10	13
10	23	10	1	10	14
10	21	10	3	10	15
11	29	12	11	13	8
11	27	12	13	13	9
11	23	12	10	13	10
11	21	12	11	13	11
12	35	13	1	13	12
12	33	12	14	13	13
12	29	12	13	13	14
12	27	12	15	13	15

Table 7

Row	Pins on cookie	Back Left		Back Right	
		Card	Amp	Card	Amp
13	33	15	11	16	11
13	29	15	12	16	12
13	27	15	10	16	13
14	27	15	15	16	13
14	23	15	14	16	14
14	21	15	13	16	15
15	25	18	7	19	6
15	21	18	8	19	7
15	19	18	6	19	8
16	25	18	10	19	9
16	21	18	9	19	10
16	19	18	11	19	11
17	27	21	2	22	1
17	23	21	3	22	2
17	21	21	1	22	3
18	33	21	5	22	3
18	29	21	4	22	4
18	27	21	6	22	5

Table 8

Row	Pins on cookie	Back Left		Back Right	
		Card	Amp	Card	Amp
19	35	23	15	25	2
19	33	24	2	25	3
19	29	24	3	25	4
19	27	24	4	25	5
20	29	24	6	25	6
20	27	24	4	25	7
20	23	24	5	25	8
20	21	24	7	25	9
21	29	26	13	28	1
21	27	26	15	28	2
21	23	26	14	28	3
21	21	26	16	28	4
22	29	27	3	28	5
22	27	27	1	28	6
22	23	27	2	28	7
22	21	27	4	28	8
23	27	29	6	30	12
23	25	29	8	30	13
23	21	29	9	30	14
23	19	29	7	30	15

Table 9

Row	Pins on cookie	Back Left		Back Right	
		Card	Amp	Card	Amp
24	27	29	12	30	15
24	25	29	10	31	0
24	21	29	11	31	1
24	19	29	13	31	2
25	25	31	11	33	3
25	23	31	13	33	4
25	19	31	14	33	5
25	17	31	12	33	6
26	17	32	2	33	7
26	19	31	16	33	8
26	23	31	15	33	9
26	25	32	1	33	10
27	25	33	12	35	6
27	23	33	14	35	7
27	29	33	15	35	8
27	17	33	13	35	9
28	15	34	15	35	10
28	19	35	1	35	11

Table 10

3.8. BEAM IN THE LAC.

After verification of the electronics and the timing of the trigger, a simple beam trigger was implemented to test the LAC. This trigger consisted of a scintillator placed on the front face of the LAC in the expected beam position. Although these tests were mainly analyzed online, a few short tapes of data were written. Most of our time was spent in understanding one problem in the hadronic readout. Crate boundries seemed to have a noise source of unknown type. Much later it was found to be that the before-after sample window had been set too wide, and the computer hash was included in the sample. That is, the before-after window allowed the noise generated from the readout system to propagate through the delay line and appear in the after sample and hold circuit. Effectively, the noise of the readout was included. The MX readout computer introduced a substantial noise in the LAC electronics, as did the trigger. It was this noise that was sampled in the wide window.

3.9. ENERGY AND POSITION IN THE LAC.

At two times during the run, a beam of known energy was put into the LAC for calibration purposes. The first was a quick calibration done in December with both electrons and hadrons. The second was done in February during the last two days of the run. The second calibration was done systematically hitting the LAC at various positions and energies. During the second calibration we turned the zero suppression off in the area under calibration. This was not always successful for various reasons, and seriously degraded the results of the calibration data.[★]

Energy Monitoring during Data Aquisition.

The energy in the LAC was also monitored in a variety of ways during data taking.

[★] For details on calibration and results see W.E. DeSoi Thesis, University of Rochester.

1. Through the use of γ converted in the target producing e^+e^- pairs. For a fraction of the π° decay photons, either one or both would pair convert before the PWC planes. These would leave tracks in the PWC system that were reconstructed; they also deposited their entire energy in the EMLAC. This provided a measure of $\frac{Energy}{Momentum}$ that enabled us to calibrate the LAC and measure LAC and reconstruction efficiency.
2. Through the monitoring of π° and η mass. The π° and η mass were 134.96 and 548.8 MeV/c respectively. The $\gamma\gamma$ decay mode deposited the entire energy of the decay in the LAC. The reconstructed mass was and width was monitored to see that the response across the face of the calorimeter was uniform.

3.10. LAC RESOLUTION.

The energy scale and resolution of the LAC are measured using the calibration data.† For the Electromagnetic calorimeter the energy deposited in the two views, R and ϕ, were used to determine the energy resolution, coherent and incoherent noise. More on this subject is presented in the analysis chapter.

---

† For details, see W. DeSoi thesis. U. of Rochester

4. Reconstruction Software for Spectrometer.

The data from the VAX was written to tape in a compact form which was using a library of routines called FSLIB.[*] The raw, unprocessed data tapes were referred to as FSP tapes. These FSP tapes were analyzed on the Fermilab Advanced Computer Project, ACP, multi-CPU processor. The analysis program called MAGIC with it's sub pieces, apparatus reconstructors, were run on each node/cpu. Only those pieces of the program that the Author worked on or that relate to the analysis reported here are discussed.

4.1. PHYSICS ANALYSIS

Roughly 1500 6250 bpi data tapes were written in the 1987-88 run. These were all processed using the E706 reconstructor, called MAGIC, on the ACP, Advanced Computer Project, facility. During the first pass of processing all useful variables for understanding the operation of the software and hardware were written to tape. Subsequent processing reduced the data set size by stripping off all but useful physics quantities. The details of this process follows in the paragraphs below. The flow of the offline reconstruction is controlled by a program called MAGIC.[†] MAGIC is a steering routine, controlling all the reconstructors. At the first stage reconstruction each hardware device was treated as a separate device. It is during the second and subsequent stages that analysis is combined between apparatus. MAGIC itself is controlled by the user through a set of control cards.[‡] The reconstructors that are called by magic are PLREC to reconstruct charged track momentum vectors, EMREC to reconstruct showers in the electromagnetic Calorimeter, HCREC

---

[*] VAX Online System User's Guide, Data Acquisition Software Group, Fermilab Computing Department. Fermilab PN 252.0 , VAX Online Programmer's Guide, IBID, Fermilab PN 253.0

[†] **E706 MAGIC Guide** E706 memo 139 and updates, G. Alverson and E. Pothier

[‡] E706 software note, no number, G. Alverson, magic$ root:[doc]CCARD.DOC on the Meson west Physics cluster.

to reconstruct showers in the hadron calorimeter, FCREC to reconstruct showers in the forward calorimeter, MUREC for tracks in the downstream E672 Muon system. This discussion here will mainly concentrate on EMREC.[§]

4.2. MAGIC

Code Management MAGIC is maintained by a CERN computer software package called PATCHY, a code management system. PATCHY allows internal switches for machine specific computer code. It also has a method of managing global variables, FORTRAN common blocks, and compile time definitions so that all users has access to these variables and definitions. Each of the reconstructors exists as a patchy input file. An input file for PATCHY is referred to as a CARD file. A compact form is available but not used since CARD files were easy to read. At any given time all of these individual pieces would be processed and linked together to form a library and standard executable program. Users of the program would link their own user code to the MAGIC library of routines.

Data structure MAGIC uses several other CERN software packages. The main one is ZEBRA,[¶] a dynamic memory management package. Structures were defined to hold all of the raw data and physics quantities. These structures were defined throughout the program and could easily be written to tape. ZEBRA provided a method through which machine independent format tapes could be written. The data structure was subdivided into banks, each could have either a linear or parallel structure for the details see the ZEBRA manual. Each bank contained raw data in a specific apparatus, unpacked data, or reconstructed physics quantities

---

[§] A more complete discussion can be found in the thesis J.P. Mansour.

[¶] R. Brun, M. Goossens, and J. Zoll, ZEBRA, CERN document DD/EE/85-6, CERN program library number Q100, unpublished or run constants such as pedestals and spatial alignment values. Internal checks were done to see that the structure did not become corrupted at various stages in the program. ZEBRA provided a disciplined storage method that was dynamic and whose output was interchangeable. It also provided consistency checks of the data during processing and on write out and read in from storage.

Event Flow Event flow was controlled by MAGIC. MAGIC in turn provided user entry points into the program for the viewing of event structure. As a stand alone program MAGIC would take a raw data tape and produce an intermediate output tape. This output tape contained the reconstructed data generated with the set of user parameters specified at run time. While reconstructor order was under user control, the event processing generally remained roughly the same. An entire event was read from tape and put into a input ZEBRA bank. The overall/global event information was stripped off and put into common blocks. This was information included event number, number of data words, which apparatus was on and writing data, etc. Then an unpacker was called for each apparatus. The unpacker would take data from the raw data bank , sort it, preform some simple consistency checks, assign spatial location, and in the case of the LAC provide gain and pedestal corrections and an energy scale.

The LAC Unpacker The LAC unpacker checked to see if the order in which the data was written to tape matched the expected order of the data aquisition program. As it was read, in the data was sorted by strip value, spatial location, and by detector. The hadron calorimeter and electromagnetic calorimeter had different geometries and hence used different data banks. The data was organized in increasing strip number order and placed in a sparse array of temporary storage. During this time the data was counted to estimate the storage space needed for the final banks. Additionally, the bank containing the gains for each of the LAC channels was checked for dead strips. If a dead strip was found within ±1 of an active strip and the dead strip was not read out, a flag was put into the array as a marker for the reconstruction program. Banks were constructed of the correct size from the data count. The data was then taken from the sparse array and put into a parallel data structure. This structure was one long array list for the hadron calorimeter, and consisted of five parallel banks. The banks were; address, energy front, energy back, TDC front, TDC back. To use or not use the hadron calorimeter TDC banks was an option under user control. The charge collected was so small that most of the time, the TDCs were not triggered. The TDC data were not used at all for this set of data. The electromagnetic data structure was broken up according to view. The views were R-Left, R-Right, ϕ inner , ϕ outer. Each view had 5 parallel data banks: strip number, energy front, energy back, Σ energy front back, TDC front, TDC back. As mentioned earlier there were two TDC's for every channel. The TDC word in the bank was packed into a long integer. The low order 16 bits were the master TDC and the high order 16 bits were the slave. When that data was moved from the sparse array into the data banks a pedestal was subtracted and the result was multiplied by a gain and conversion constant. The Pedestal was an electric zero offset that varied from channel to channel. As mentioned before, during the run these pedestals were measured and written to data disk. The channel gains were also stored in a similar manner. The conversion was:

$$E_i = AG_i(N_i - N_{0i}) \tag{4.1}$$

where

- E_i was the energy in strip i;
- A was the conversion from from ADC counts to GeV/c ;
- G_i was the measured gain for amplifier attached to strip i;

- N_i was the measured ADC value for charge collected;
- N_{0i} was the measured pedestal offset in ADC counts.

4.3. THE ELECTROMAGNETIC RECONSTRUCTOR, EMREC

EMREC was the reconstructor for the electromagnetic detector. As mentioned before the electromagnetic detector was patterned to collect charge in a radial coordinate system. EMREC tried to reconstruct the photon or electron energy from the readout of the showers generated in the LAC. To accurately predict the energy and resolve multiple particle showers, a parametrized shape was fitted to each peak. The reconstructed values were then stored in the physics banks. EMREC dealt with showers in terms of four views per quadrant, R-Left, R-right, ϕ inner, and ϕ outer. The R left and right correspond to the octants within a quadrant and were segmented symmetrically at $\phi = 45°$. The inner/outer ϕ boundary was at R = 40 cm, where the ϕ segmentation changes from $\frac{\pi}{192}$ to $\frac{\pi}{384}$ radians per strip. Electrically the EMLAC is read out in front and back sections. These sections were summed to remove the effect of shower origin on the shower shape in the reconstructor. The reconstruction proceeds in four steps. Groups of channels were formed, separately by view, such that the initial or seed strip satisfied a software threshold for group formation. A parametrized shower shape was fit to each group found in every view, the final fit was called a gamma. The gammas are then correlated between views to form photons. Finally, the reconstructed photons were given a time from the TVC values of their constituent strips.⋆

<u>Group Reconstruction</u> Groups were considered collections of strips terminated on either side by no strip energy. Two photons depositing energy in overlaping strips were not resolved at this level. Groups could

---

⋆ Reference, J.P. Mansour Thesis, Chapter on Electromagnetic Reconstruction.

be separated by dead channels. The unpacker informed the the group algorithm of known dead strips. The dead strip was filled in with an average of surrounding energy and the group search continued. At the group level front and back strips were treated separately, since adding in the back might degrade the front peaks. A group consisted of the following

1. At least 3 strips, only 2 in the outer ϕ view, above threshold
2. Total group energy $>$ 750 MeV/c .
3. Average strip energy$>$ 150 MeV/c .
4. Maximum strip energy $>$ 750 MeV/c .

Peak Finding The group was stored and the process was iterated until each view is exhausted. Each group was individually searched for peaks by measuring the slope between strips making up the group. Dips in pulse height either side of a local maximum constituted a peak. For R views the radial position is calculated in front and projected to the back. If a peak is found near the projected position then the directionality is calculated.

$$D_{peak} = \frac{R_{front}}{R_{back}} \tag{4.2}$$

For particles originating at the target D_peak should be one. Muons and particles traveling parallel to the beam will have D_peak different from one. The directionality is not calculated for the ϕ views since they yield no such information. Construction of gammas was done by fitting a parametrized shower shape to the peaks within a group. Radial position is given by

$$R_i = 20.2233 + i_r \times 0.5455cm \tag{4.3}$$

where R_i is the strip position and i_r is the strip number. Azimuthal position is given by

$$\Phi_i = (i_\phi - 1) \times 0.0164 + (quad - 1) \times \frac{\pi}{2} \tag{4.4}$$

where Φ_i is the Azimuthal angle of the strip and i_ϕ is the strip number.

Correlation into Photons The gammas were correlated between views to form photons. Due to the construction of the calorimeter, a photon would deposit roughly equal charge/energy in both views. The algorithm worked by matching gammas of equivalent $\frac{E_{front}}{E_{total}}$ ratio.

Matching speed was increased by requiring that inner ϕ gammas compare with R-view gammas of radius less than 40cm and outer ϕ with $R > 40$cm. Problems arose at all boundaries of the views because the program had difficulty in cases where the energy was shared between four regions.

Photon Time Time of photons was measured by looking at TVC values of the individual strips that made up the photon. Part of EMREC groups TVC values that are geometrically close and within $3\sigma(45)$ns of each other. These are stored in arrays/banks and later matched with gamma pairs to give an overall photon time.[⋆]

4.4. THE PLANES RECONSTRUCTOR, PLREC

A cut described in the analysis section requires a vertex in the tracking system, this a short discussion. The downstream, MWPC, and upstream, SSD, systems are treated in a similar manner. They each have views, 4 for the MWPC X, Y, U, V and 2 for the SSD X,Y. Two dimensional tracks, called view tracks, were made up from hits in each view. The view tracks are then matched between views to form three dimensional space tracks. The term hit describes a wire or strip in a view that

---

[⋆] E. Prebys, E706 internal note, Does Anyone Care What Time It is?

contains sufficient charge to fire the readout latch. This charge may have been deposited from a charged particle or amplifier noise.

View Tracks Each view of the SSD and MWPC system was treated the same. There were four planes per view numbered from 1, the most upstream, to 4, the most downstream. Planes 1 and 4 were selected as seed planes. One hit was selected in each seed plane; a line through these hits defined a search region ±1.5 wire spacings wide. IF 2 hits, one per plane, were found in the search region, including the search planes, a least squares fit to a straight line was made. If the χ^2 was too high, one of the hits was dropped and another fit was tried. An acceptable value of χ^2 results in a so called view track being recorded in a track list. This process was continued until all pairs of hits in the seed planes were used. To alleviate the problems of inefficient wires and random loss, a second search was made. Planes 2 and 3 were used as the seed planes and planes 1 and 4 as search planes and the process was repeated. Only combinations not previously satisfying the 4 hit requirement were accepted. Every track found in each case for all 4 MWPC ,and 2 SSD views were stored. After view track construction, all 4 hit tracks were compared. The 4 hit track of best χ^2 of all 4 hit tracks sharing 3 or 4 hits was kept while others are dropped. Those 3 hit tracks sharing 2 or 3 hits with 4 hit tracks were dropped.

Space Tracks A similar algorithm was used to find space tracks, first taking X and Y view tracks and searching for U,V view tracks and then the reverse. The seed views were projected onto the search tracks and search tracks within ±1.5 wire spacing were considered. The following cuts apply,

1. Search views contributed at least 2 hits per view.
2. Seed views contributed at least 6 hits total.
3. The final space track hits exceeded 13.

After space tracks were constructed, those tracks sharing 6 or more hits were discriminated by χ^2 and hit quantity.

SSD Clustering SSD strips were clustered into single strips for high multiplicity events. This eased the load on the view reconstruction by reducing the number of possible combinations.

Magnet Linking between SSD and MWPC The analysing magnet bent in the X plane, and tracks were treated as point bending at an effective center of the magnet. Each MWPC track was projected to this center and SSD tracks were searched for a match. The radial difference in projections was called the projection difference and was minimized. The absolute difference in slope was called the bend angle, and with the parametrization of the magnetic field allowed a momentum to be calculated for the track.[⋆]

Vertex Finding Vertex formation was done on a view basis in the SSD system. If there were more than four 4 hit tracks linked with PWC tracks, only these tracks were used, and if there were not enough linked 4 hit tracks, the next choices were unlinked 4 hit tracks followed by linked three hit tracks. Insufficient number of tracks satisfying this criteria aborted the vertex finding routine. The tracks were used to solve a set of simultaneous equations in X, Y, and Z. Both views were used in this method. The result became the vertex.

4.5. SECONDARY PROCESSING

The secondary tape written by MAGIC underwent a process in which it was split into separate data streams according to hardware and software trigger types. Using the split stream data, which is slightly compressed, an individual user could quickly obtain high statistics about specific physics event topologies. The LAC streams, totaling 5, contained

---

[⋆] E706 internal note, Upstream, Downstream, F. Lobkowicz and L. DeBarbaro only LAC triggers and data were stripped of all but physics results and written to a machine specific fortran unformatted file. The analysis of this thesis was produced from one of these streams of data. These files were indexed by run number. The files were grouped by run number as seen in the table below.

Set	Run number	Triggers	Beam Polarity	Target	LTB
A	2852-3036	786,171	-	CuBe	3.3945×10^{10}
B	2588-2670	439,851	+	CuBe	-
C	2387-2586	1,224,950	+	CuBe	6.7652×10^{10}
D	2062-2382	1,242,178	-	Be	7.5598×10^{10}
E	1728-2007	1,508,174	+	Be	7.0210×10^{10}
F	1672-1719	160,885	+	C	-

Table 11

4.6. MONTE CARLO

The monte carlo program for the experiment was maintained in a fashion similar to MAGIC. The output simulated a raw data tape and could easily be read by MAGIC. The overall package used was GEANT[†] which is a overall simulation package made up of several smaller packages including ZEBRA. Embedded within it are other monte carlo packages for simulation of different detector elements, such as GESHA, for simulation of hadronic showers and EGS for electromagnetic showers. The Calorimeters were studied individually to generate parametrization of showers rather than use a full generation for each shower. The entire apparatus is entered in any detail desired and particles entering will be subjected to all physics processes. any level of the detectors may be turned on or off.

[†] CERN program Library AAAA 000, R. Brun, F. Bruyant, M. Maire, A.C. McPherson, P. Zanarini

5. Analysis of Results

The compressed free format binary data summary tapes were processed in sets,groups of runs seen, as mentioned in the previous chapter. This format provided a quick easy way to view the data. Further processing produced a N-dimensional array or Ntuple which was viewed and manipulated by PAW.* PAW allowed interactive manipulation of the data at high speed. Cuts were implemented in this processing to weed out bad events and reduce the data set. The effects of various cuts may be seen in table the table below.

order	Cut Type	Events Cut
1	Veto Wall	40-60%
2	Vertex	5-12%
3	Uncorr.	1-3%
4	Fiducial	19%
5	Octant	75%

Table 12 The data were searched for the $\gamma\gamma$ decay modes of the π^0 , and η neutral mesons. The $\gamma\gamma$ branching ratios for the two mesons are $98.798 \pm 0.032\%$ and $38.9 \pm 0.34\%$ respectively. The π^0 and η were identified by calculating the invariant mass of all $\gamma\gamma$ pairs. The invariant mass is given by

$$m^2 = 2 \times E_i E_j (1.0 - cos\theta_{ij}) \tag{5.1}$$

with the errors given by

$$\frac{\Delta m}{m} = \frac{1}{2}\sqrt{\left(\frac{\Delta E_i}{E_i}\right)^2 - \left(\frac{\Delta E_j}{E_j}\right)^2 + \left(\frac{E_i E_j}{m^2} - 1.0\right)\Delta\theta^2} \tag{5.2}$$

where E_i and E_j are the energies of the photons and θ_{ij} is the opening

---

⋆ PAW, Physics Analysis Workstation, R. Brun et al. Cern Program Library Document Q121, and accompanying documents.

angle between the photons. A mass distribution for the region between 0. and 1. GeV/c^2 is seen in figure 38.

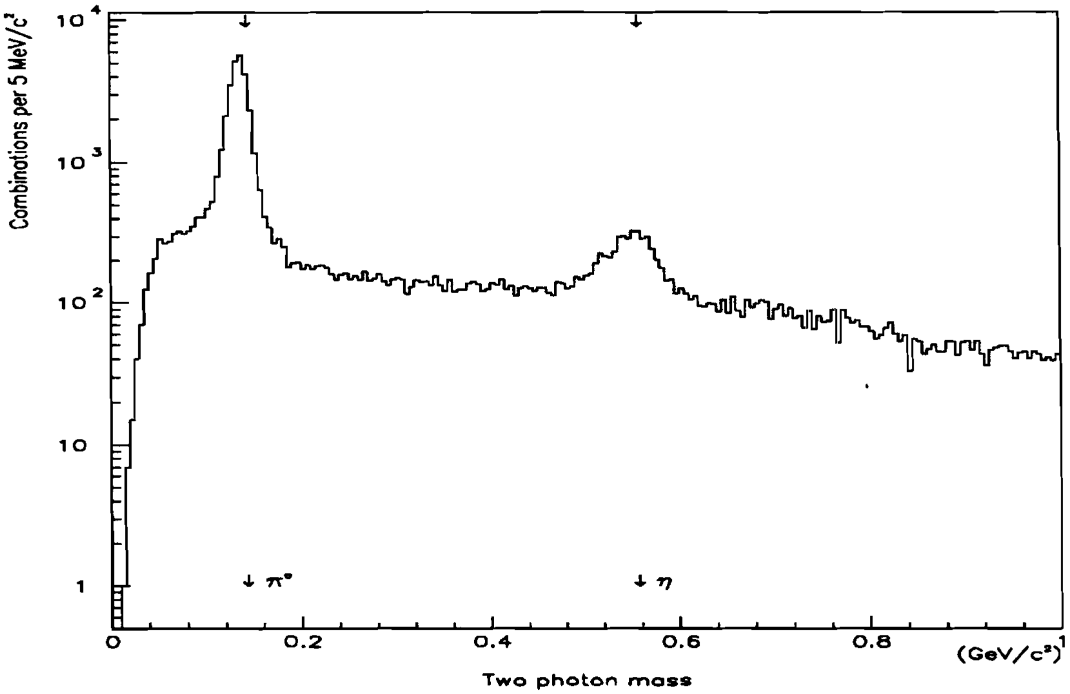

Figure 38: $\gamma\gamma$ mass distribution in $5 MeV/c^2$ bins from 0 to 1 GeV/c^2

It is seen from the equation (5.2) above that good mass definition is dependent on the energy and position resolutions. As stated before offline calibration was done using π^0 photon conversions in the target. These electrons and other calibration data indicate that the intrinsic resolution varys from $\frac{10\%}{\sqrt(E)}$ to $\frac{14\%}{\sqrt(E)}$ across the face of the calorimeter. Additionally, the energy scale calibration varies across the face of the calorimeter. Using π^0 and η decay photons we find an effective resolution of $\frac{20\%}{\sqrt(E)}$ due to the variations mentioned above. This value of $\frac{20\%}{\sqrt(E)}$ is consistent with the width of the η mass plot. The energy resolution and η width may be seen in figure 39. The plot of energy resolution is fit by

$$\sigma^2 = [M \times EGeV/c]^2 + C^2 \tag{5.3}$$

where M is the energy resolution and C is the constant noise term.* This equation shows the energy resolution as function of incident photon energy. The values for this fit are $M^2 = 0.04805$, and $b^2 = 0.167$. The value for M is an idication of the energy resolution and b is the incoherent noise in the system. This gives an energy resoulution of $\frac{22\%}{\sqrt(E)}$. This is a bit large due to averaging over all runs and data sets.

The variations of energy scale as a function of position may be seen in figure 40. The data shows a dip at radius = 40cm where the reconstruction program is known to have problems. This effect has been parametrized and slightly removed. In addition, there are thought to be electronic problems at this boundary as well.

5.1. MONTE CARLO STUDIES

All of the measurements made by the apparatus were biased by its physical characteristics. Thus any measurement made must be corrected for by the physical limitations of the apparatus. An analytic solution to some of the corrections was feasible while it was not for others. Those corrections which were not suitable to analytic solution were trigger, reconstruction and acceptance corrections. The monte carlo simulation

---

⋆ Calorimetry in High Energy Physics, C. Fabjan, and Fluctuations in Calorimetry Measurements, U. Amaldi to be found in Experimental Techniques in High Energy Physics, T. Ferbel Editor, Addison-Wesley Publishing Co., 1987, ISBN 0-201-11487-9

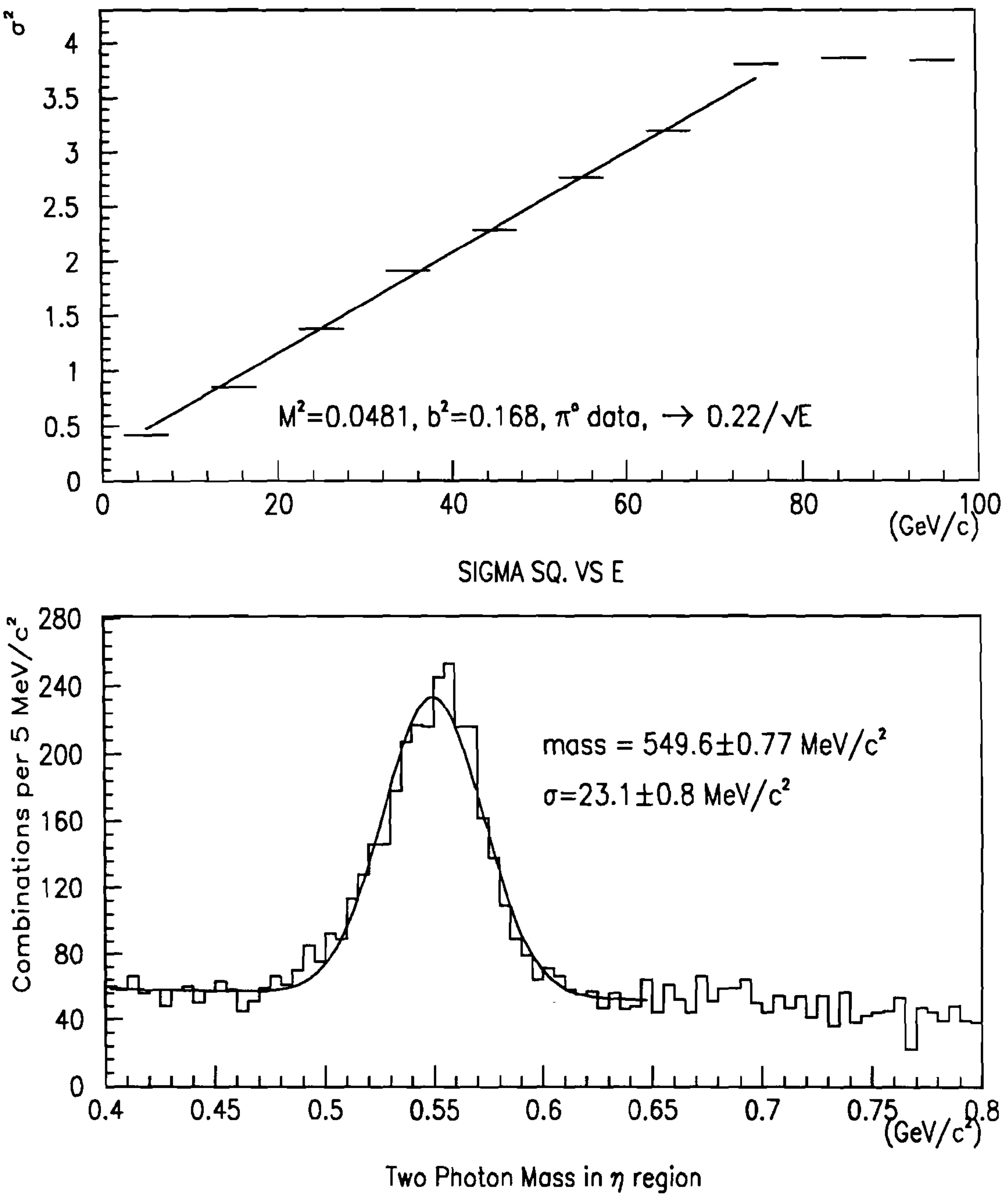

Figure (5.3): A) Energy resolution of the LAC, B) Fit to Two photon mass of η

of the apparatus allowed calculation of the correction factors as a function of transverse momentum and rapidity. The process of generating a geometric and trigger acceptance correction for π^0 or η events, involved generation of a file containing particles generated on a fixed grid of P_T and rapidity. The P_T of the generated particles was varied from 4.0 GeV/c to 8.0 GeV/c in steps of 500 MeV/c and from -1. to 1. in rapidity in steps of 0.2. These events were output to a file using a GEANT routine. The E706 version of GEANT program MCE706 was run on the file decaying the π^0 or η randomly in asymmetry and azimuth. The resulting photons were put through the simulation of the full E706 spectrometer/calorimeter and their final energy in the electromagnetic calorimeter was stored in strip values to be read by MAGIC. The original values were also stored along with particle type etc. MAGIC was run on the GEANT output stream to produce reconstructed photons. These photons were combined to see if they passed the cuts to make the original particle. The cuts used will be described in detail in this chapter.

Geometric and Reconstruction Effects. A monte Carlo simulation was used to determine the reconstruction efficiency and the geometrical acceptance of the calorimeter for π^0 and η. Additionally, the single photon background from π^0 and η particles was calculated for use in the determination of the direct photon signal. A count was kept of generated, detected, and reconstructed particles.

The ratio $\frac{DetectedParticles}{GeneratedParticle}$ gave the geometric acceptance correction.

The ratio $\frac{ReconstructedParticles}{DetectedParticle}$ gave the reconstruction efficiency correction.

The ratio $\frac{ReconstructedParticles}{GeneratedParticles}$ gave the overall geometric and reconstruction acceptance correction.

Separate corrections were determined for π^0 and η particles and may be seen in The results are shown in tabular form below. It was found that near the beam hole a finer segmentation in rapidity was necessary due to the rapid falloff of acceptance.

P_T in GeV/c →										
Y	3.5	4.0	4.5	5.0	5.5	6.0	6.5	7.0	7.5	8.0	8.5
-1.0	.2348	.4072	.4908	.5583	.6196	.6310	.6836	.7168	.7284	.7551	.7532
-0.8	.6611	.6104	.6468	.6903	.7256	.7224	.7123	.7763	.7490	.7383	.7857
-0.6	.7206	.6291	.6566	.6822	.7103	.6997	.7373	.7434	.7360	.7387	.7500
-0.4	.5207	.6005	.6086	.6771	.6734	.7106	.7031	.7201	.7531	.8080	.7460
-0.2	.3869	.5678	.5965	.6587	.6743	.7090	.7100	.7133	.7168	.7080	.7170
0.0	.9948	.5854	.6622	.6595	.6671	.6667	.6905	.6896	.7005	.7000	.7500
0.2	.3570	.5584	.5857	.6056	.6594	.6453	.6213	.6487	.6779	.6580	.7030
0.4	.2740	.4780	.5197	.5628	.5604	.6127	.6489	.6343	.6767	.6560	.6940
0.6	.0247	.0313	.0296	.0361	.0693	.0622	.0733	.0844	.0906	.1150	.0960

Table 13

P_T in GeV/c →									
Y	3.5	4.0	4.5	5.0	5.5	6.0	6.5	7.0	7.5
-1.0	.0176	.0179	.0181	.0180	.0179	.0179	.0172	.0165	.0164
-0.8	.0249	.0178	.0174	0.0169	.0163	.0161	.0162	.0150	.0158
-0.6	.0243	.0175	.0176	.0170	0.0162	.0167	.0159	.0159	.0164
-0.4	.0222	.0178	.0179	.0172	.0172	.0166	.0164	.0162	.0159
-0.2	.0208	.0182	.0180	.0173	.0172	.0166	.0168	.0166	.0166
.0	.0051	.0181	.0172	.0173	.0172	.0174	.0168	.0168	.0167
.2	.0210	.0179	.0179	.0179	.0175	.0175	.0175	.0175	.0171
.4	.0186	.0179	.0184	.0184	.0181	.0179	.0174	.0177	.0173
.6	.0070	.0063	.0061	.0068	.0093	.0089	.0095	.0010	.0011

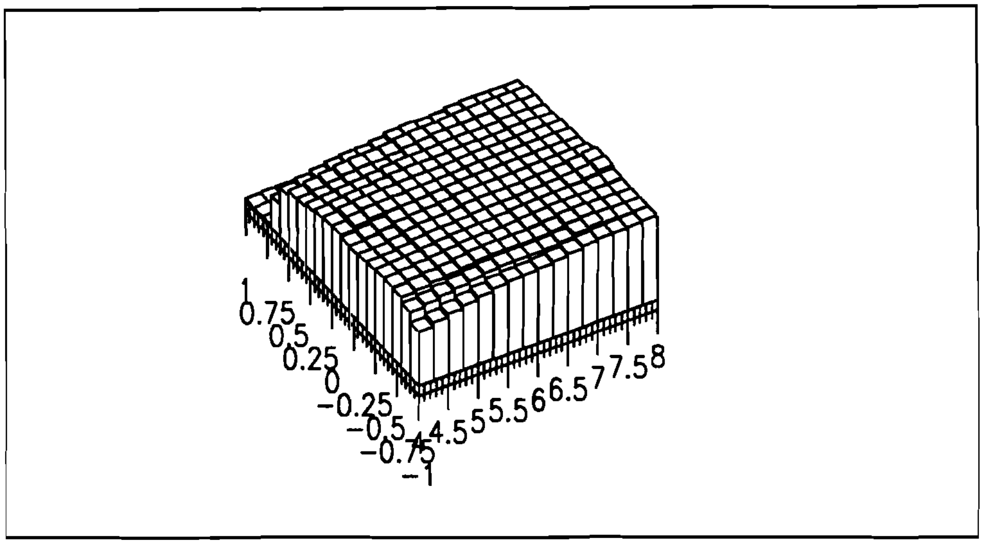

acceta.for

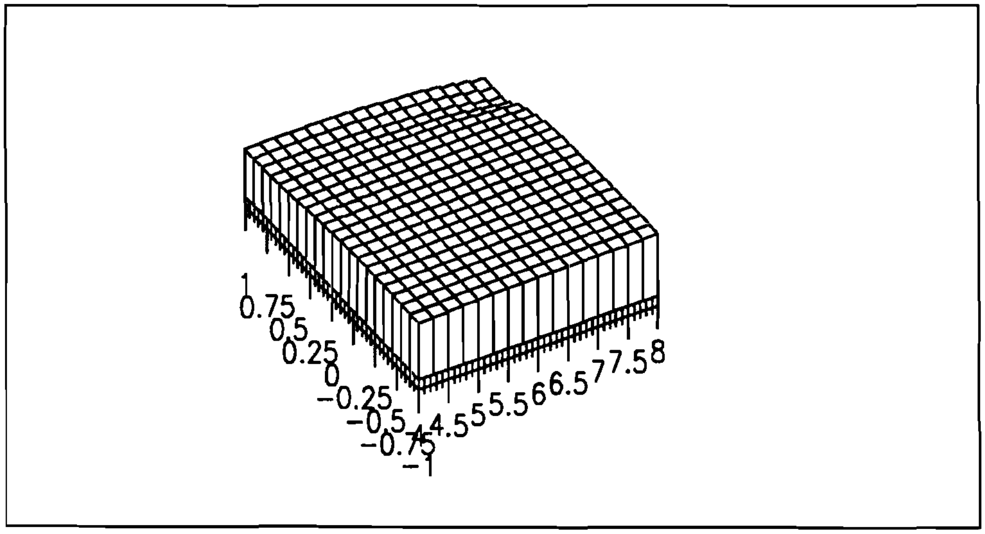

accpi0.for

Figure 41: Acceptance corrections for a) π^0 and b) η particles as a function of rapidity and P_T

Table 14

P_T in GeV/c →											
Y	3.5	4.0	4.5	5.0	5.5	6.0	6.5	7.0	7.5	8.0	8.5
0.2	.6970	.6200	.5673	.6551	.6909	.6776	.7255	.7268	.7211	.7050	.6712
0.3	.5166	.5673	.5730	.5737	.5864	.6107	.6276	.5901	.5740	.5687	.6500
0.4	.3372	.5796	.5799	.6287	.6340	.6801	.6825	.6730	.6684	.7111	.6883
0.5	.3010	.4799	.5426	.5934	.6050	.6420	.6146	.6724	.6425	-	-
0.6	.2337	.3629	.4183	.4644	.4803	.5611	.5539	.5811	.5981	-	-
0.7	.1154	.1460	.2413	.2137	.3068	.3225	.3891	.3903	.4205	-	-
0.8	.0211	.0320	.0551	.0543	.0485	.0761	.0664	.0800	.0900	-	-

Table 15

P_T in GeV/c →									
Y	3.5	4.0	4.5	5.0	5.5	6.0	6.5	7.0	7.5
.2	.0400	.0245	.0254	.0255	.0236	.0244	.0233	.0229	.0230
.3	.0400	.0245	.0254	.0255	.0236	.0244	.0233	.0229	.0230
.4	.0400	.0245	.0254	.0255	.0236	.0244	.0233	.0229	.0230
.5	.0204	.0191	.0209	.0183	.0175	.0185	.0182	.0181	.0222
.6	.0178	.0181	.0207	.0178	.0184	.0241	.0174	.0179	.0243
.7	.0176	.0182	.0253	.0172	.0180	.0252	.0175	.0180	.0256

Table 16

Trigger Acceptance.

The trigger acceptance was calculated in a methods Similar to the geometric acceptance. The difference from the acceptance calculation was in the reconstruction phase. The reconstruction program for the trigger acceptance contained a parametrization of the trigger as a function of P_T . This parametrization returned an event or not based on the software model of the trigger. The trigger was modeled by measuring the trigger turn on in octants other than the trigger octant in real data. During data taking the analog trigger value for each octant was logged to tape as well as the state of the trigger. The trigger threshold was modeled by reconstructing the photons in each octant and measuring the analog trigger value in the same octant. The reconstruction program used in determining the trigger corrections had all of these thresholds within it. Photon decay products smeared by the detector resolution were tested against the trigger threshold as a function of their position. A count of triggered vs non-triggered was kept. This count was divided up into the three electrical regions as discussed in chapter 3, as well as by octant. A fit was made to this data to determine the threshold for trigger turn on and it's width. The data from the fits consisted of a threshold and a gaussian width. The determination of the trigger corrections in the analysis program consisted of a Heavyside function convoluted with a gaussian. The offset of the Heavyside function was the threshold, the gaussian provided the width needed. The functional form was;

$$P(x) = \frac{1}{\sqrt{2\pi}\sigma} \int_{-\infty}^{\infty} dx' \theta(x + x' - a) e^{-\frac{x'^2}{2\sigma^2}} \tag{5.4}$$

where a represents the trigger threshold and σ the width of turn on. A curve of trigger efficiency will be presented below.

5.2. CUTS ON THE DATA.

Various cuts were placed on the data to reduce the sample to a region where the variables involved were reasonably well understood. This section will discuss those cuts.

P_T cut. A P_T cut of 4.0 GeV/c was placed on all data presented for cross sections. Figure 42 shows the trigger efficiency as a function of P_T for a specific octant in the electromagnetic calorimeter. The threshold in the trigger can be clearly seen. The trigger did not reach it's full efficiency until a P_T of 4.0 GeV/c for runs with run number greater than 2904. Runs less than run 2904 had a much higher trigger threshold and the trigger did not become fully efficient until 5.0 GeV/c P_T . The trigger corrections become quite large and unreliable below this cutoff of 4.0 GeV/c .

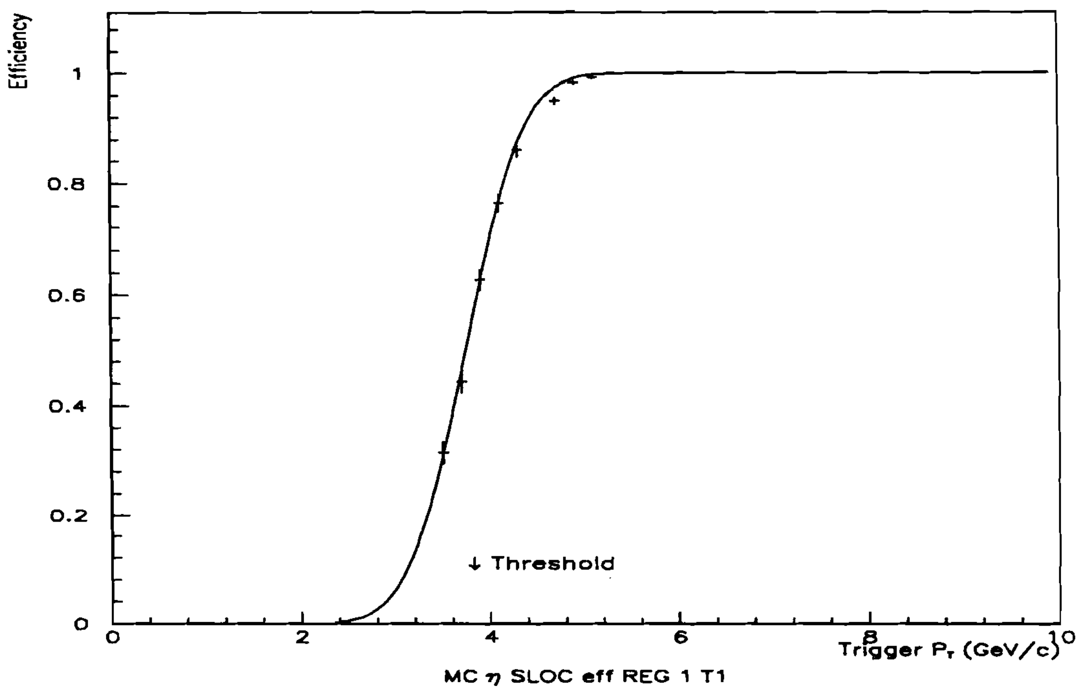

Figure 42: Trigger efficiency as a function of P_T , a pointer to the trigger turn on is shown.

Rapidity distribution and Acceptance. Figure 43 shows rapidity as a function of radius at E706 incident momentum, the arrows mark the boundaries of the calorimeter. This plot shows clearly that the physical device extends to ±1 units of rapidity in the center of mass system.

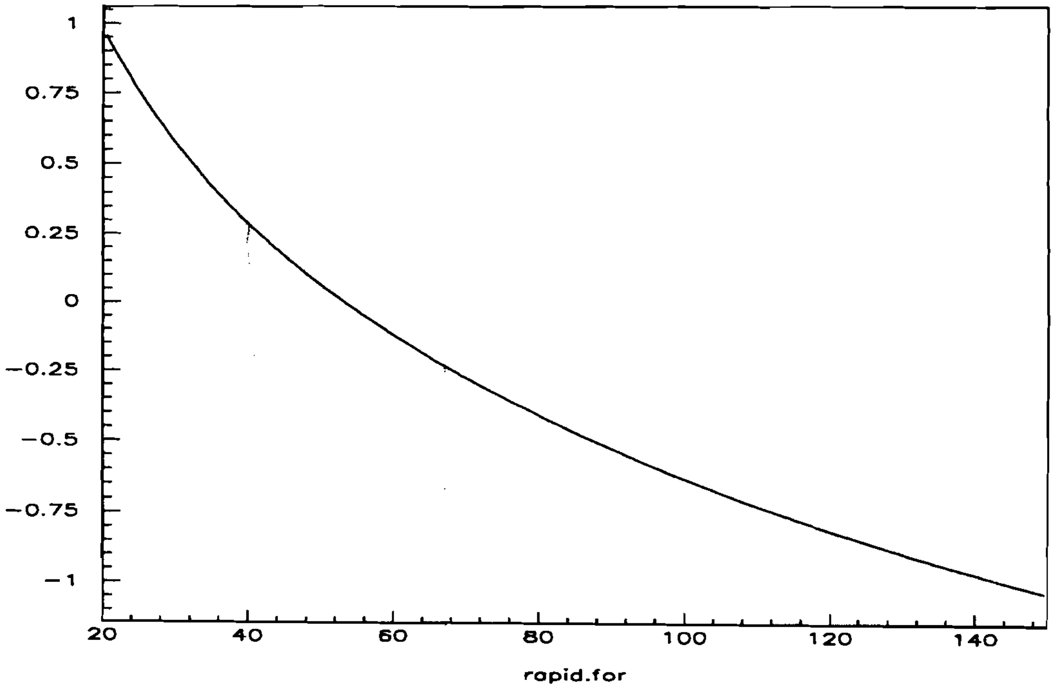

Figure 43: Rapidity as a function of radius at $\sqrt{s} = 31.7$ GeV/c .

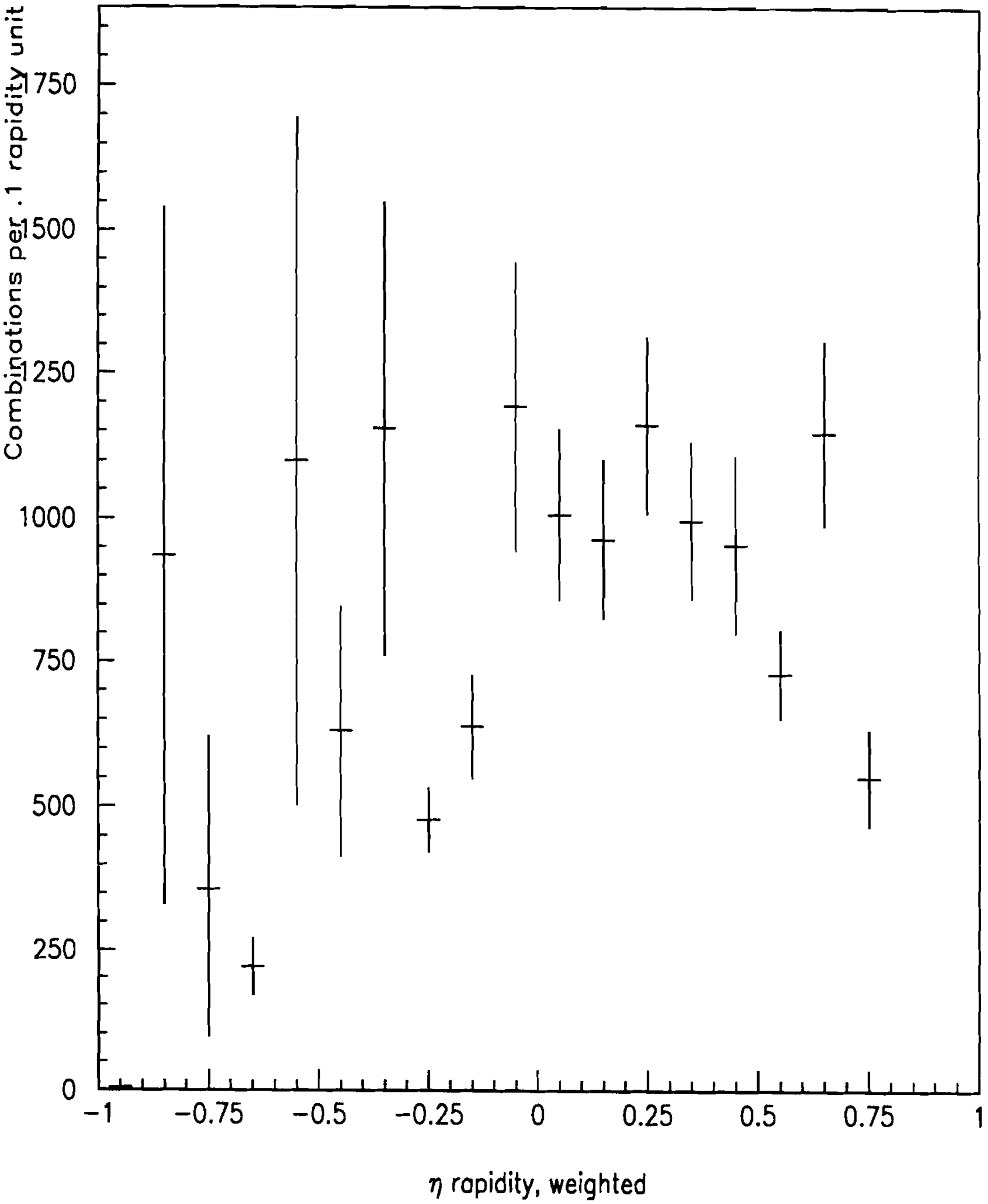

Figure 44: Rapidity distribution for η.

Figure 44 shows that rapidity distribution for the η falls a substantial amount before ±1 unit of rapidity. This is due to the opening angle between the decay photons of the η. One photon may reside within the detector volume while the other misses. These missed pairs contribute to the direct photon background. It can be seen from the generated and real data that a cut of ±0.7 units of rapidity in the center of mass does not significantly reduce the data set, but does keep us away from the boundaries. The inner and outer edge of the detector are known to have special problems due to both the reconstructor and the electronics.

Background Subtraction and Asymmetry.

The π° and η decay into two equal energy photons with an opening angle of 180° in the rest system of the parent particle. The transformation into the lab system results in an energy asymmetry. This asymmetry is defined to be

$$Asymmetry = \frac{|E_{\gamma 1} - E_{\gamma 2}|}{|E_{\gamma 1} + E_{\gamma 2}|} \tag{5.5}$$

This asymmetry distribution is expected to be flat since the η or π° decay photon angles should be isotropic in the rest system. The background to the η or π° must be removed from the production data. This was achieved by fitting a linear background under using the sideband mass region and estimating the background under the mass curve. The sideband region was defined to be a region either side of the defined mass range. The mass range for the data presented was

$$\eta\ mass\ region 0.45 \leq mass \leq 0.65 \tag{5.6}$$

$$\eta\ sidebands 0.35 < mass < 0.45\ .or.\ 0.65 < mass < 0.75 \tag{5.7}$$

This enabled the background subtraction to be simplified because the sum of the sideband region equals the mass region. Figure 45 shows the validity of this method.

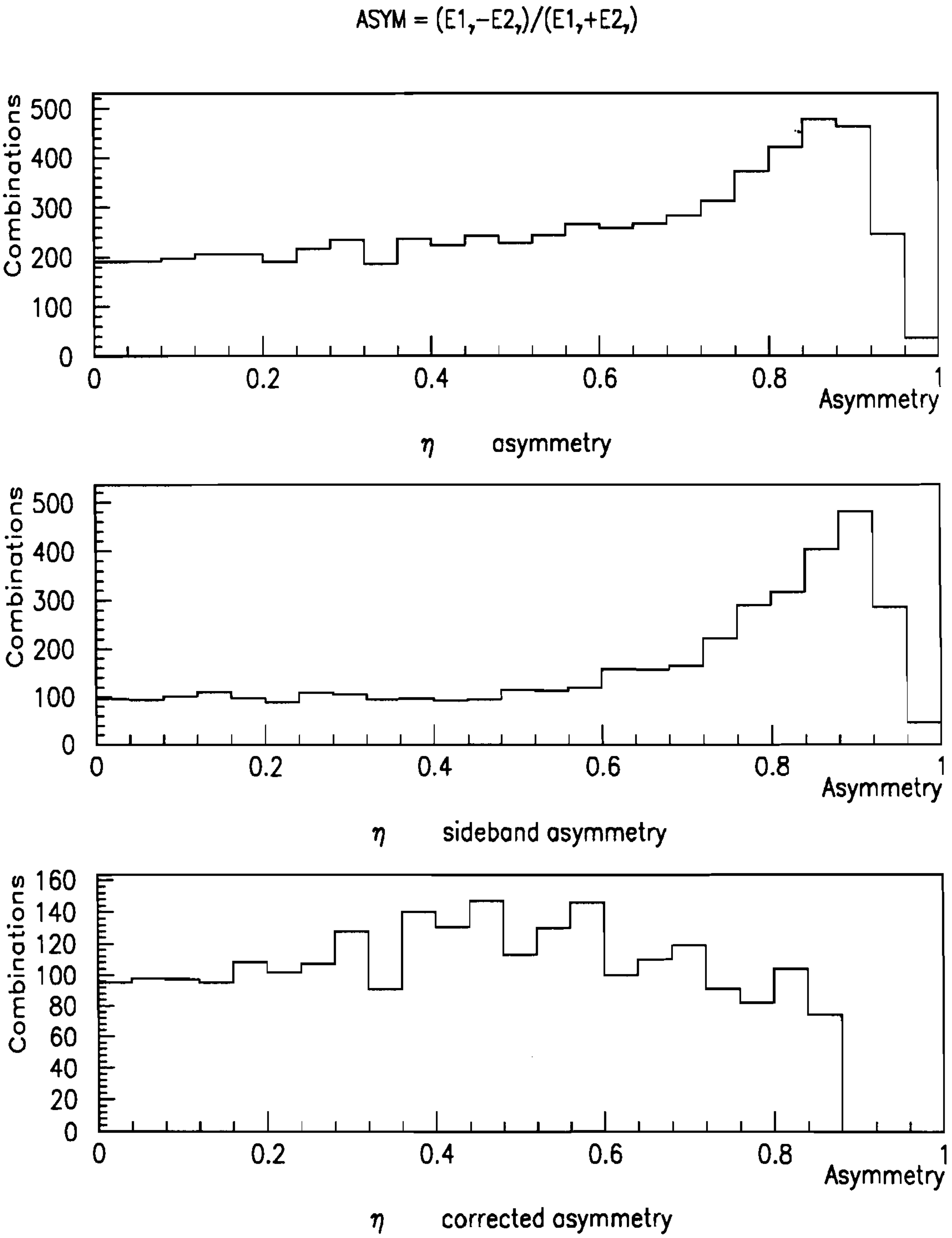

Figure 45: Asymmetry of η decays A) Mass region, B) Sideband regions, and C) Sideband subtracted.

These set of figures show the asymmetry for the η mass region, the sideband region and the result of the subtraction of the two. Figure 46 shows the monte carlo distribution overlayed on the real data with background subtracted. The energy asymmetry was chosen to test this background subtraction process since it is believed to be a variable independent of physics quantities to be measured. An Asymmetry cut of 0.75 is made to reject accidental combinations made with a muon and a low energy photon, or a single photon and a low energy photon. The rapidity distribution starts to fall rapidly around .75 as can be seen in figure 46.

Beam and Target Cuts.

The data presented here includes only the majority particle in the beam, protons for positive polarity beam, and π^- for negative polarity beam. A vertex cut was made to isolate the target type. Figure 47 indicates our ability to localize the interaction to one target cell. For the purposes of this analysis, the beryllium target was chosen, since the other target used had insufficient statistics in the η mass region.

Cuts on Veto wall.

A cut was made on the .OR. of the veto wall signals. The effect of this cut may be seen in figure 48. Studies by J.P.Mansour[⋆] showed that most of the contributions from the veto wall were out of time events, and presumed to be muons.

Sumary of Cuts.

To get a clean sample of η particles we have issued the following cuts;

- no hit in the veto wall.
- majority particle in cerenkov counter.

[⋆] See J.P. Mansour thesis chapter on analysis.

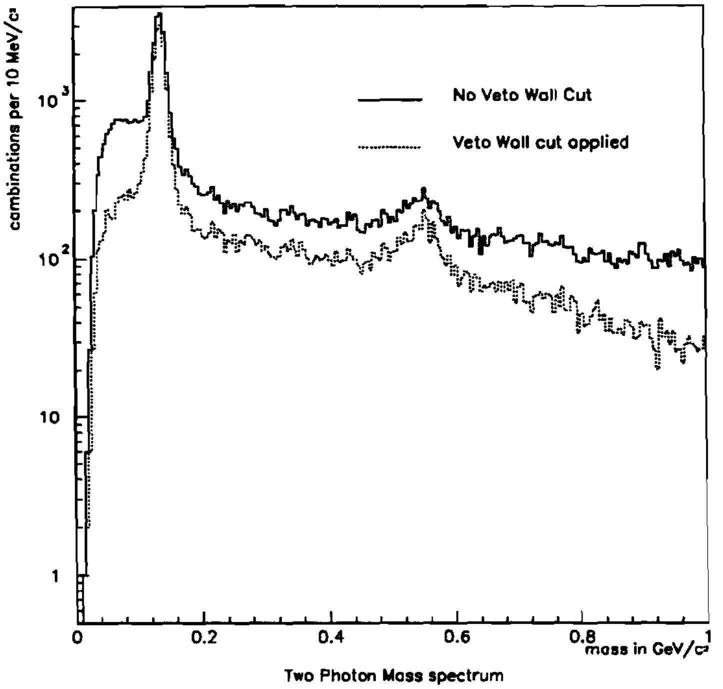

Figure 48: The effect of the veto wall cut on diphoton mass distributions.

- single local trigger.
- particle exceeds a pt of 4.0 GeV/c
- Energy asymmetry less than 0.75
- Rapidity less than 0.7 and greater than -0.7 in C.M.S.
- The vertex is within the beryllium target volume.
- the two photon mass falls in the η mass range.

Figure 49 shows the effect of these cuts on the data sample.

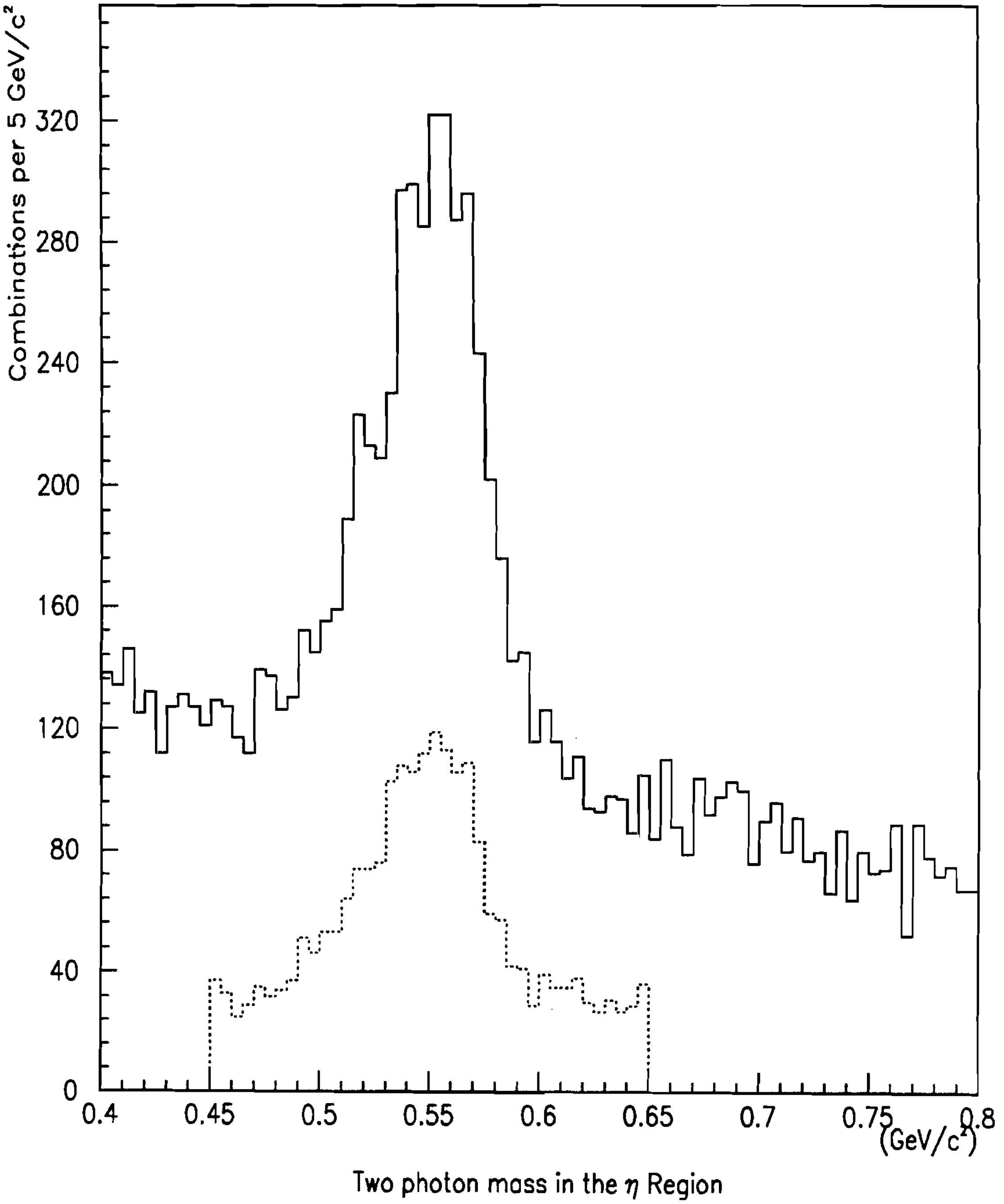

Figure 49: Two photon mass spectrum in the η region before and after cuts.

5.3. COUNTED QUANTITIES, OR SCALERS.

During the course of the data aquisition, every signal thought to be of importance was counted by a scaler. The scalers used were CAMAC based and read out at the end of every spill. A list of scalers can be seen in the table below with typical quantities.

Scaler Reference	Value	Scaler Reference	Value
1 BCDIFF1	$0.20502E+09$	17 $D23 \bullet \overline{V2}$	$0.86705E+07$
2 BCDIFF2	$0.38489E+08$	18 $D6 \bullet \overline{V2}$	0.69361E+06
3 BCDIFF3	• 0.22750E+09	19 $D5 \bullet \overline{V2}$	0.42930E+07
4 BCDIFF4	0.19076E+09	20 $D4 \bullet \overline{V2}$	0.15270E+08
5 BCDIFF5	0.24042E+09	21 D23	0.92737E+07
6 BCDIFF6	0.10759E+09	22 D6	0.74058E+06
7 BCANTI1	0.24162E+09	23 BCSCNT1• 2	0.92284E+09
8 BCANTI2	0.50802E+08	24	0.00000E+00
9 BCANTI3	0.15627E+09	25 VWALL OR	0.13967E+10
10 BCANTI4	0.53395E+08	26 VW(1• 2)	0.62765E+09
11 BCANTI5	0.13256E+09	27 VWALL1 OR	0.10342E+10
12 BCANTI6	0.20339E+09	28 VWALL2 OR	0.99023E+09
13 BCSCNT1	0.30419E+09	29 VW(1• 2) QUW	0.22872E+09
14 BCSCNT2	0.18669E+09	30 VW(1• 2) QUE	0.18401E+09
15 BA.BB.BHB	0.66810E+08	31 VW(1• 2) QDW	0.16618E+09
16	0.00000E+00	32 VW(1• 2) QDE	0.56100E+08

Table 17

Scalers 1 through 6 were the differential ring beam chrenkov photomultipliers. Scalers 7 through 12 were the differential anti-ring beam chrenkov photomultipliers. These identified light from the minority and majority particles respectively. Scalers 13 and 14 represented beam scintillators before and after the cerenkov counter. Scaler 15, E706 beam definition, without prescaling. Scalers 17 through 22 were values for various logical combinations of the Cerenkov signals. Scalers 25 through 32 represent various quantities about the veto wall.

Scaler Reference	Value	Scaler Reference	Value
33 BA	0.12250E+10	49 SE2+SW2	0.10558E+09
34 BB	0.97653E+09	50 INT	0.18107E+09
35 BEAM	0.96646E+09	51 LIVE_INT1	0.71184E+08
36 LIVE_BEAM1	0.75999E+09	52 INT1	0.11435E+09
37 LIVE_BEAM	0.60059E+09	53 LATE_INT	0.59696E+07
38 BEAM.BHB	0.76101E+09	54 EARLY_INT	0.52958E+07
39 LIVE_BM.BHB	0.47299E+09	55 LIVE_CLINT	0.10254E+09
40 BH	0.55070E+09	56 LIVE_INT	0.11060E+09
41 LIVE_(PSBM.CLIN)	0.36800E+03	57 LIVE_BINT	0.76988E+08
42 SE1	0.23377E+09	58 SE1.AND.SW1	0.10885E+09
43 SW1	0.13295E+09	59 SE2.AND.SW2	0.91969E+08
44 SE2	0.12587E+09	60 TRIGGERS	0.77820E+04
45 SW2	0.18545E+09	61 CLN PRESCLBM/INT	0.11360E+04
46 SE1+SE2	0.16425E+09	62 PRESCALED BEAM	0.42900E+03
47 SW1+SW2	0.11221E+09	63 PRESCALED INT	0.80000E+03
48 SE1+SW1	0.16375E+09	64 NC	0.00000E+00

Table 18 Scalers 33 through 40 were scaled quantities related to the formation of the E706 beam definition. Scalers 41 through 59 were scaled values of the various stages of beam target interaction definition.

Scaler Reference	Value	Scaler Reference	Value
65 LACPRETRIG1	0.33756E+06	81 LIVE INT1	0.71184E+08
66 LACPRETRIG2	0.33756E+06	82 GATED INT1	0.70673E+08
67 LACPRETRIG3	0.33756E+06	83 G*VW	0.23114E+08
68 LACPRETRIG4	0.33756E+06	84 G*SK	0.81477E+07
69 PRESCALED TRIGGER 1	0.51900E+03	85 G*SK+VW	0.28563E+08
70 PRETRIG_OR1	0.34441E+06	86 G*SK+EP1+VW	0.28611E+08
71 672_PRETRIG	0.63630E+04	87 G*SK+EP2+VW	0.28582E+08
72 NO PRETRIG	0.70268E+08	88 G*SK+EP3+VW	0.28608E+08
73 LACPRESCLPT1	0.33756E+06	89 G*SK+EP4+VW	0.28615E+08
74 LACPRESCLPT2	0.33756E+06	90 G*SK+EP5+VW	0.28603E+08
75 LACPRESCLPT3	0.33756E+06	91 G*SK+EP6+VW	0.28584E+08
76 LACPRESCLPT4	0.33756E+06	92 G*SK+EP7+VW	0.28573E+08
77 PRESCALED TRIGGER 2	0.51900E+03	93 G*SK+EP8+VW	0.28576E+08
78 PRETRIG_OR2	0.34441E+06	94	0.00000E+00
79 PRS672PTG	0.63630E+04	95 PRESCALED BEAM	0.44955E+06
80 PRESC_NOPTG	0.70268E+08	96 PRESCALED INT	0.80000E+03

Table 19 Scalers 65 through 68 and 73 through 76 scaled the exact same value, the pretrigger for the E706 spectrometer/calorimeter. Scalers 70, 78 and 72, 80 represent the .OR. of all pretriggers and the number of times no pretrigger was formed. Scalers 71, 79 were the number of times E672 sent E706 pretrigger information. Scalers 69, 77 were the number of LAC triggers taken. Scaler values 83 through 93 represent the various stages of veto in the final trigger, (G)ated Interaction, (SK) scrkill, (EPx) deposition of early transverse momentum, energy left over from the last event, and (VW) Veto Wall, muons were present in both veto walls.

Scaler Reference	Value	Scaler Reference	Value
97 Cerenk press.	0.24579E+02	113 NC	0.23238E+02
98 NC	0.24190E+02	114 NC	0.22796E+02
99 NC	0.22559E+02	115 NC	0.21282E+02
100 NC	0.22750E+02	116 NC	0.23570E+02
101 NC	0.22715E+02	117 NC	0.21226E+02
102 NC	0.22010E+02	118 NC	0.22322E+02
103 NC	0.18774E+02	119 NC	0.21206E+02
104 NC	0.16325E+02	120 NC	0.24068E+02
105 NC	0.15394E+02	121 NC	0.11170E+02
106 NC	0.12410E+02	122 NC	0.21441E+02
107 NC	0.82979E+01	123 NC	0.21221E+02
108 NC	0.57460E+01	124 NC	0.19358E+02
109 NC	0.35873E+01	125 NC	0.19441E+02
110 NC	0.00000E+00	126 NC	0.15123E+02
111 NC	0.00000E+00	127 NC	0.86398E+01
112 NC	0.00000E+00	128 NC	0.11795E+01

Table 20

Scaler Reference	Value	Scaler Reference	Value
129 PWC1X THRESH	0.23238E+02	145 GAS FLOW ARGON	0.15049E+04
130 PWC1Y THRESH	0.22796E+02	146 GAS FLOW AR-FREON	0.70330E+00
131 PWC1U THRESH	0.21282E+02	147 GAS FLOW ISOBUT	0.17488E+04
132 PWC1V THRESH	0.23570E+02	148 ALCOHOL TEMP.	0.85470E-01
133 PWC2X THRESH	0.21226E+02	149 NC	0.61538E+00
134 PWC2Y THRESH	0.22322E+02	150 NC	0.00000E+00
135 PWC2U THRESH	0.21206E+02	151 NC	0.17543E+04
136 PWC2V THRESH	0.24068E+02	152 NC	0.00000E+00
137 PWC3X THRESH	0.11170E+02	153 NC	0.17548E+04
138 PWC3Y THRESH	0.21441E+02	154 NC	0.00000E+00
139 PWC3U THRESH	0.21221E+02	155 NC	0.20179E+03
140 PWC3V THRESH	0.19358E+02	156 NC	0.00000E+00
141 PWC4X THRESH	0.19441E+02	157 NC	0.49482E+03
142 PWC4Y THRESH	0.15123E+02	158 NC	0.21219E+03
143 PWC4U THRESH	0.86398E+01	159 NC	0.16823E+03
144 PWC4V THRESH	0.11795E+01	160 NC	0.33930E+03

Table 21

Scaler Reference	Value	Scaler Reference	Value
161 OCT1 PRETRIGGER	0.20263E+06	177 LOCAL*GBL LO 1	0.75000E+02
162 OCT2 PRETRIGGER	0.86890E+05	178 LOCAL*GBL LO 2	0.76000E+02
163 OCT3 PRETRIGGER	0.68892E+05	179 LOCAL*GBL LO 3	0.11400E+03
164 OCT4 PRETRIGGER	0.13894E+06	180 LOCAL*GBL LO 4	0.11200E+03
165 OCT5 PRETRIGGER	0.11143E+06	181 LOCAL*GBL LO 5	0.14500E+03
166 OCT6 PRETRIGGER	0.99673E+05	182 LOCAL*GBL LO 6	0.96000E+02
167 OCT7 PRETRIGGER	0.35694E+05	183 LOCAL*GBL LO 7	0.57000E+02
168 OCT8 PRETRIGGER	0.88865E+05	184 LOCAL*GBL LO 8	0.25900E+03
169 LOCAL*GBL HI 1	0.15900E+03	185 LOCAL*GLOBAL HI TRIG	0.22170E+04
170 LOCAL*GBL HI 2	0.19300E+03	186 LOCAL*GLOBAL LO TRIG	0.93000E+03
171 LOCAL*GBL HI 3	0.39100E+03	187 SINGLE LOCAL TRIGGER	0.37850E+04
172 LOCAL*GBL HI 4	0.20000E+03	188 TWO GAMMA TRIG.	0.30100E+03
173 LOCAL*GBL HI 5	0.25000E+03	189 672 TRIGGER	0.63630E+04
174 LOCAL*GBL HI 6	0.20000E+03	190 PRESCALED BEAM TRIG	0.18200E+03
175 LOCAL*GBL HI 7	0.98000E+02	191 PRESCALED INT TRIG	0.33700E+03
176 LOCAL*GBL HI 8	0.73500E+03	192	0.00000E+00

Table 22 All quantities here correspond to the various levels and forms of the final LAC and other triggers.

Scaler Reference	Value	Scaler Reference	Value
1 LIVE_BM.BHB	3224134.0	4 PL_LOADS	344411.0
2 LIVE_INT1	4074739.0	5 PL CLEARS	344432.0
3 NUMBER SPILLS	22.0	6 PL READS	7782.0

Table 23 PL_READS were the number of times data was written to tape in a run.

Scaler Reference	Value	Scaler Reference	Value
1 TRIGGER DEAD FR.	0.40484	4 NEGATIVE K FRACTION	0.12978
2 COMPUTR LIVE FR.	0.62144	5 LIVE TIME FRACTION	0.33854
3 LIVE_CLINT/LIVE_INT	0.92711	6 LIVE INT1 CHECK	1.00722
4 INTERACTION RATE	0.16277	7 TRIGGER RATE	0.16453
5 BEAM.BHB/BEAM	0.78742	8	0.00000

Table 24 Each of the spill scalers was read and cleared at the end of a spill. The Run scalers accumulated quantities for an entire data run. The data was written to tape and accumulated during processing of the data. For unknown reasons many of the data tapes did not have the end of spill marker and the data for the last spill of the tape run. This gives rise to uncertainty in the overall normalization of the data. An estimate of the value in the data was given by the ratio of the number of events on tape to the number of events processed at the last spill scaler. A variety of cross correlation checks were done on scalers to sort out bad runs. Quantities scaled in two different scalers were found to have the same in value within 1 to 2 parts per 100,000. The live interaction 1 signal sent to the faraday room had transmission problems. It double pulsed and was sometimes lost. The value scaled in the faraday room always differed by 0.1% and sometimes up to 10

5.4. CROSS SECTION.

The π^0 or η cross section as a function of P_T is given by

$$E\frac{d^3\sigma}{d^3p} = \frac{N_\eta}{N_{beam}N_{scat}} \times \frac{1}{2\pi\Delta P_T \Delta Y P_T} \tag{5.8}$$

- N_η was the number of η particles reconstructed.
- N_{beam} was the number of beam incident particles.
- N_{scat} was the number of scattering centers.
- ΔP_T was the size of the P_T bin.
- ΔY was the rapidity interval integrated over. The expression $\frac{1}{2\pi\Delta P_T \Delta Y P_T}$ normalizes the cross section to an element of phase space.

The apparatus did not record all η's produced but only sample. The actual sample must be corrected for by the operation of the apparatus. The number of η particles detected as a function of P_T was corrected for by the monte carlo results for geometric and trigger acceptance. This section will discuss the other corrections to the cross section calculation. The number of beam particles, N_{beam}, that could have cause a trigger is discussed below and labeled live triggerable beam. The number of scattering centers is a function of the density and length of the target material. The number of η particles produced is a function of trigger, geometric and reconstruction acceptance and was discussed earlier. all of these corrections are shown below.

Beam and Target Type →				
Correction	$\pi^{\pm}$ on Be	$\pi^{\pm}$ on Cu	p on Be	p on Cu
missing octant	Function of Run and P_T			
Geometric Acceptance	Function of Run and P_T			
Trigger Acceptance	Function of Run and P_T			
Target Conversions	Function of Reconstructed Vertex Position.			
Double Beam Occupancy	0.98			
Asymmetry < 0.75	1.333			
π^{0} $0.11 < mass < 0.16$	1.04			
η $0.45 < mass < 0.65$	1.04			
$\gamma\gamma$ conversions after target	1.069			
Veto Wall and UNC_EN	1.176			
absorbtion before target	1.010			
Density (gm/cm^3)	1.848	8.96	1.848	8.96
Atomic Number	9	29	9	29
Beam Absorbtion	1.043	1.004	1.056	1.005
Cerenkov contamination	1.014	1.014	1.06	1.06
Vertex efficiency	1.0019+0.0079*Reconstructed Vertex Position			

Table 25 The corrections to the data are justified above and elsewhere, veto wall uncorrelated energy, and vertex effieciecy can be found in the thesis of J.P. Mansour, chernkov contamination can be found in the thesis of A. Lanaro.

Beam Normalization.

The total beam particle count was corrected for the time the apparatus was not able to take data. The corrected or live triggerable beam was used as the number of beam particles that could have produced an interaction. Each of the quantities discussed below were counted or scaled as part of the trigger definitions as discussed in the previous chapter. That is each time a part of the trigger was satisfied, it was counted. The first part of the trigger was the definition of a clean interaction; there were no other particles within $\pm 60ns$ of the interacting beam particle. This introduced some dead time.

$$Clean\ Interaction\ Correction = \left(\frac{Live\_Clean\_Interaction}{Live\_Interaction_{LH}}\right) \tag{5.9}$$

Where LH indicated a quantity that was scaled in the latch house as opposed to the faraday room, FR. This was the fraction of time the apparatus could have a clean interaction verses any interaction. This signal was transmitted to the LAC trigger with some loss. This loss is corrected by,

$$Trigger\ Transmission\ losses = \frac{Live\_Interaction_{FR}}{Live\_Interaction_{LH}} \tag{5.10}$$

The pretrigger mechanism was not instantaneous. The fraction of time spent "thinking" about a pretrigger is given by

$$Pretrigger\ dead\ time = \frac{(Pretrigger + NoPretrigger)}{Live\_Interaction_{FR}} \tag{5.11}$$

Certain signals could fake a trigger and were effective vetos, the fraction of dead time introduced by the veto aggregate was given by

$$Veto\ dead\ time = \frac{(1.0 - GINT1 \bullet (VW \bullet SCRK \bullet Early\_P_T))}{Gated\_Interaction} \tag{5.12}$$

where VW was the logical .AND. of the veto walls, SCRK was the ambient coherent noise that could have caused a trigger, and Early P_T was a veto on energy deposited by an event before the pretrigger. The last correction was called the missing spill correction. The data aquisition system did not write the final spill scaler to tape when a data tape was finished. This was corrected on a run by run basis by dividing the total number of triggered events by the number of triggered events seen at the last recorded spill scaler. Multiplying all theses corrections by the beam definition gave the result of live triggerable beam, used in normalization.

$$L.T.B. = Live\_Beam \bullet BHB(Corrections) \tag{5.13}$$

A plot of all corrections as a function of run number/time may be seen in figure 50.

6. Results of Analysis.

This chapter will deal with the final results for the η cross section as a function of P_T. The previous chapter dealt with the analysis of the results and how the data was filtered and corrected for. The cuts that were chosen cleaned the data and provided a clean sample of η particles. Similar analysis was made for π° data.[8] This chapter primarily comments on the production of η particles for majority beam particle on beryllium target. The statistics were too small, 0-6 events, to make any useful comments about production from copper targets or from K^- or π^+.

6.1. η CROSS SECTION ON BERYLLIUM.

All of the cross section plots presented were produced in the same manner with different data input. The sample for clean η and π° particles was produced from the following list of cuts.

- cut on veto wall,
- for objects above P_T of 4 GeV/c ,
- Cerenkov majority tagged,
- reconstructed vertex in beryllium,
- asymmetry less than 0.75,
- absolute value of rapidity less than 0.7,
- was produced in a single local trigger,
- $0.45 < Mass < 0.65$
- Sideband Mass $0.35 < Mass < 0.45 .OR. 0.65 < Mass < 0.75$ and has been integrated over rapidity.

Positive polarity beam.

The cross section per nucleon for proton on beryllium is shown in figure 51.

Negative polarity beam.

The cross section for proton on nucleon is shown in figure 52.

6.2. η TO π^0 RATIO.

Figure 53 shows the production ratio of η to π^0 as a function of P_T for π^- beam particles.

6.3. SUMMARY.

Tables representing the cross sections computed are given below. The η to π^0 production ratio for π^- beam particles averages to 0.47 ± 0.2 and for proton beam 0.85 ± 0.2. The η to π^0 production ratio agrees to the published values 0.4-0.55within error bars although the proton beam value is high. The ratio of η production in π^- to proton beams is 0.85 ± 0.3. The cross sections lie between published cross sections. Figure 54 shows E706 data overlayed with other experiments. The change in cross section is due to scaling violations in QCD.[9] [10] [11] [12] [13]

The comparison of our data to other experiments asummes a A^1 dependence since the other experiments had a proton target. It is possible that we have effects from using our nuclear target, but the statistics are too small to make a comment. The data agree reasonably well with the published cross sections. For the pion data the E706 inclusive cross section lies above the others since it is at a higher $\sqrt{s}$. For the proton data we see that the cross section is between those experiments at higher and lower $\sqrt{s}$.

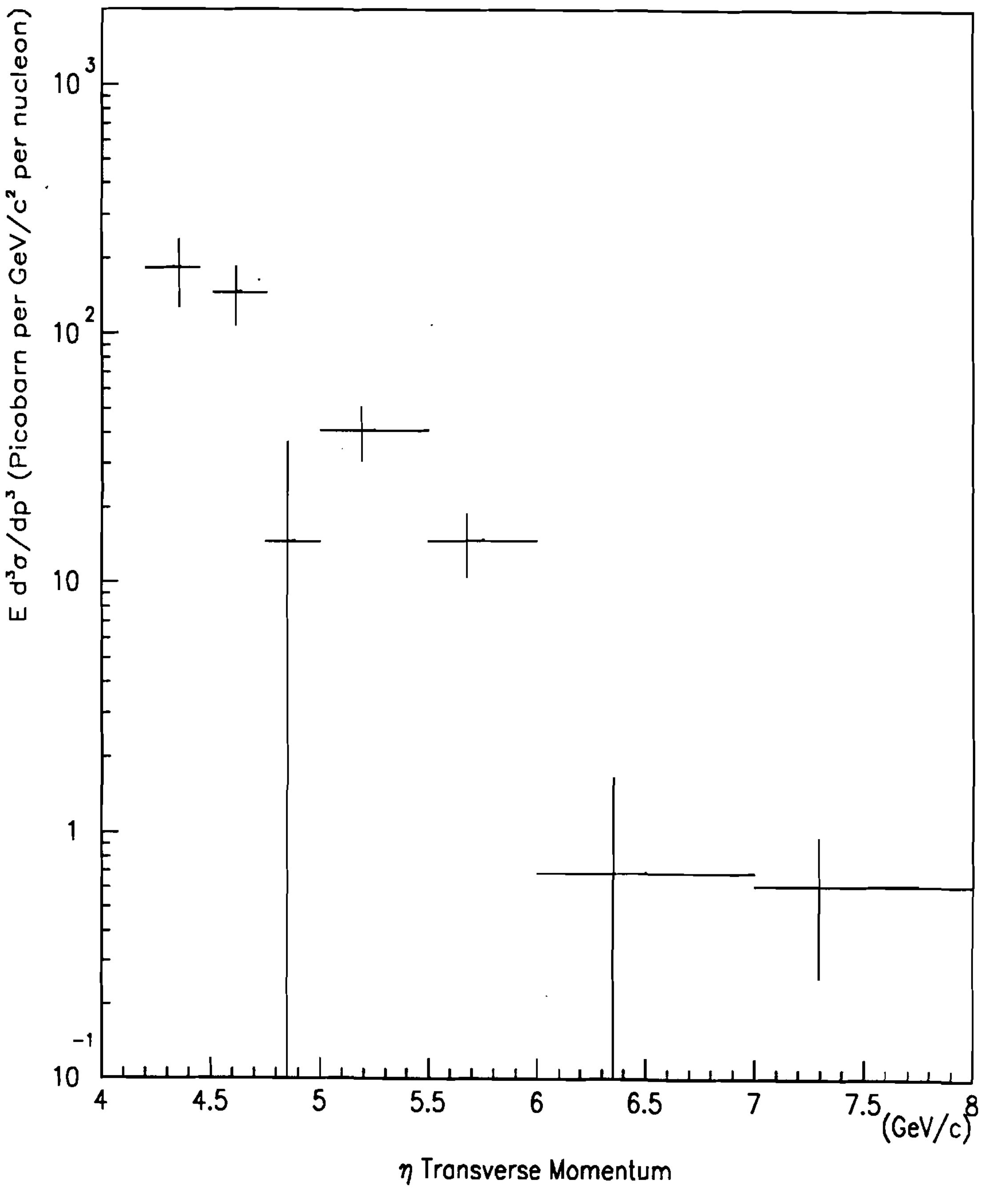

Figure 51: $E\frac{d^3\sigma}{d^3p}(p + Be \rightarrow \eta + X)$ as a function of P_T for P_T greater than 4. GeV/c .

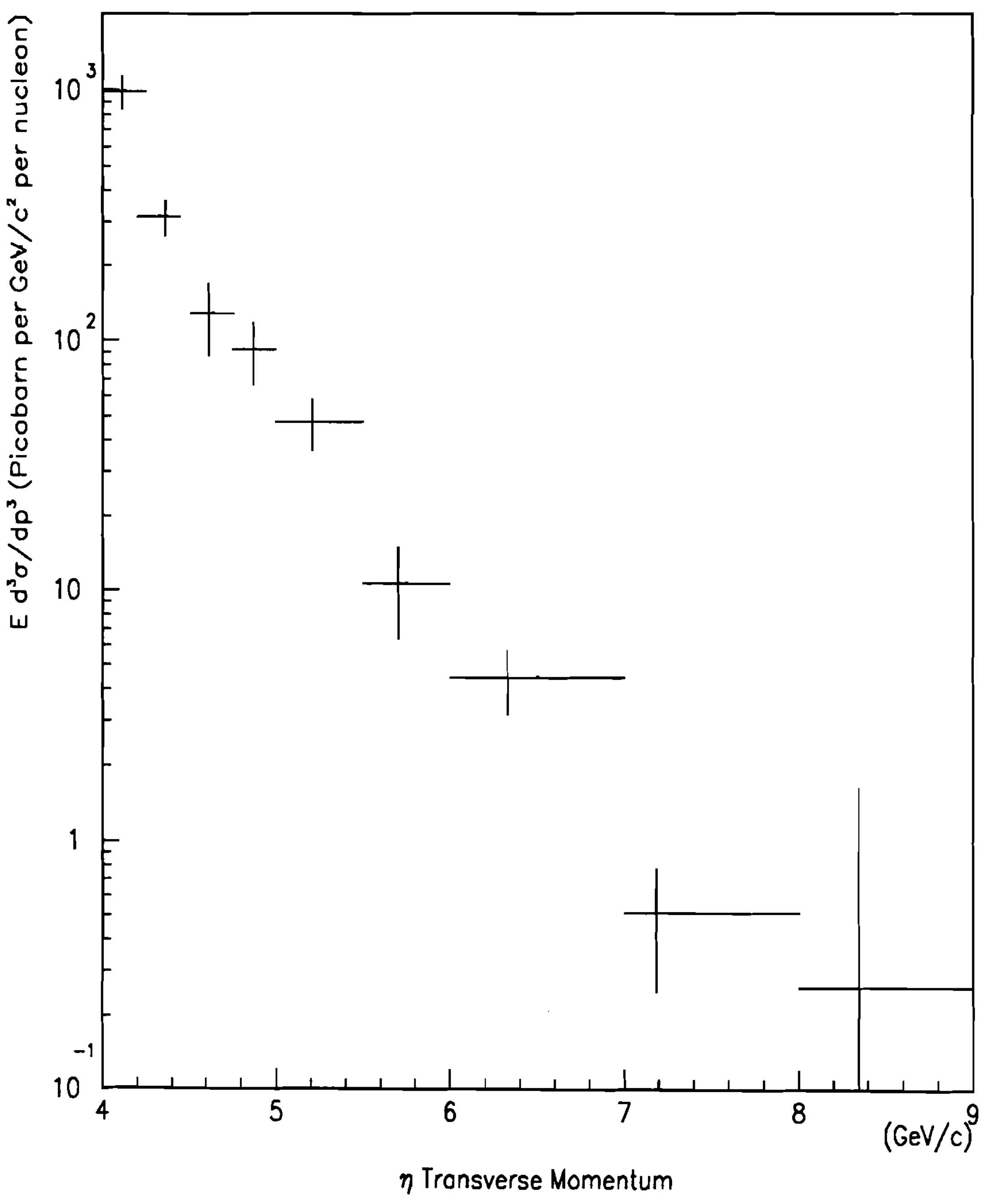

Figure 52: $E\frac{d^3\sigma}{d^3p}(\pi^- + Be \rightarrow \eta + X)$ as a function of P_T for P_T greater than 4. GeV/c .

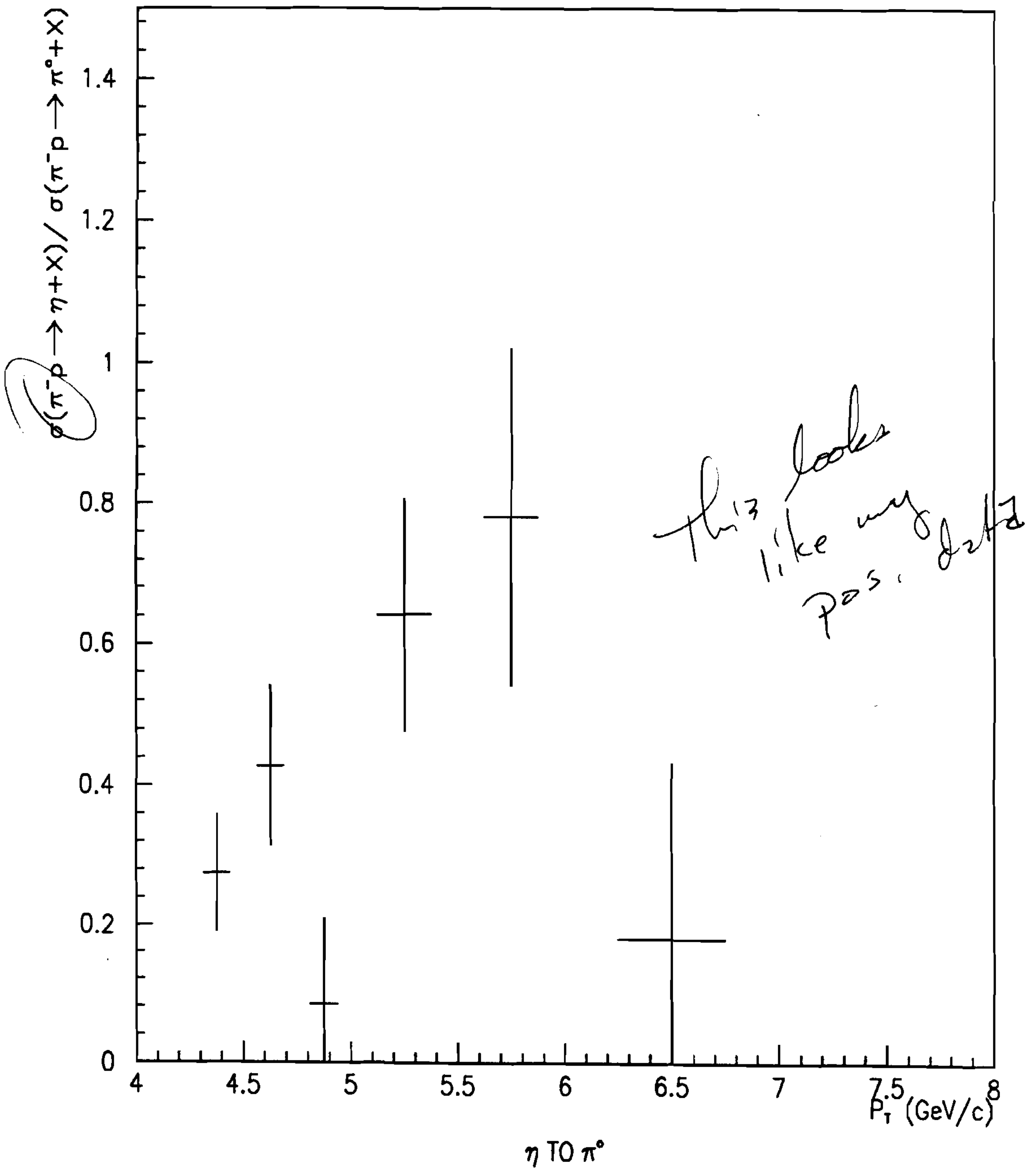

this looks like my pos. data

Figure 53 B: Ratio of η to π^0 as a function of P_T with incident proton.

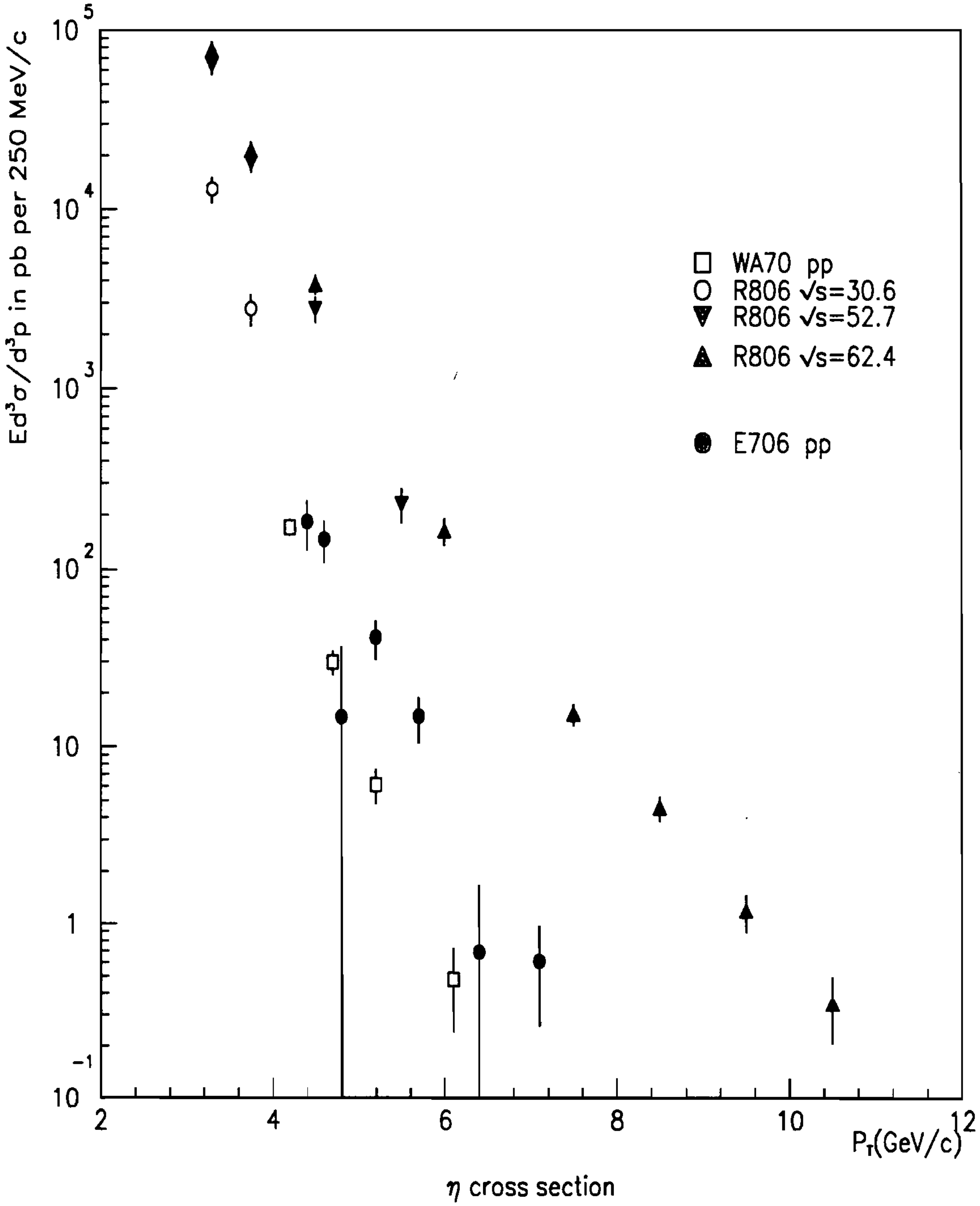

Figure 13 A: Comparison of η production for proton data.

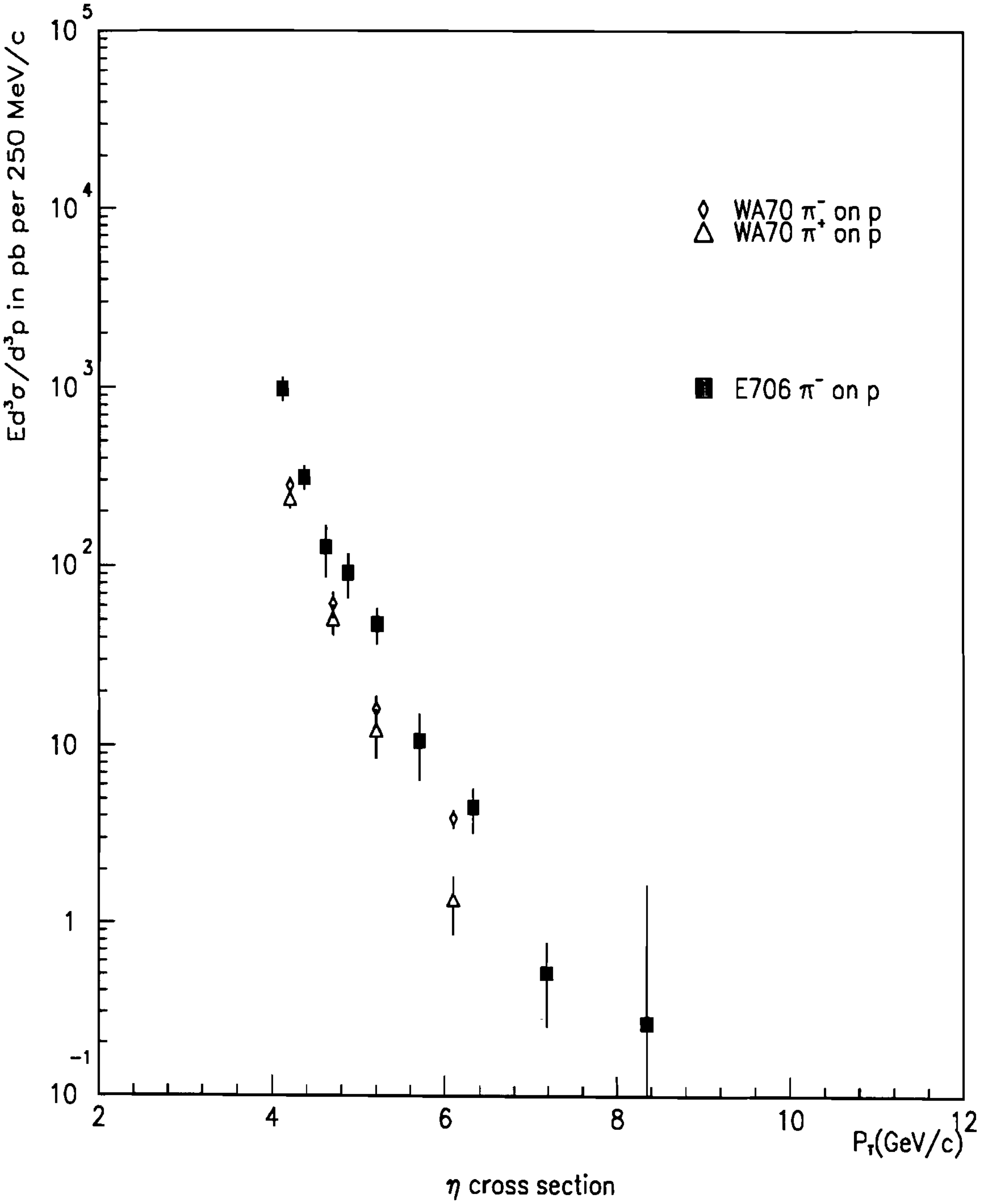

Figure 13 B: Comparison of η production for π^- data.

p_T	$E\frac{d^3\sigma}{d^3p}$	
	π^- N	pN
4.1	986.56 ± 148.0	-
4.4	313.19 ± 50.06	183.27 ± 56.1
4.6	127.17 ± 41.26	146.46 ± 38.48
4.9	91.54 ± 25.61	14.59 ± 22.04
5.2	47.37 ± 10.93	40.99 ± 10.22
5.7	10.64 ± 4.29	14.71 ± 4.22
6.5	4.47 ± 1.27	0.689 ± 0.97
7.2	0.51 ± 0.264	0.608 ± 0.35
8.3	0.26 ± 11.39	-

Table 26

p_T	ratio
4.4	1.708 ± 0.590
4.6	0.868 ± 0.362
4.9	6.274 ± 9.63
5.2	1.115 ± 0.392
5.7	0.723 ± 0.358
6.5	6.49 ± 9.34
7.2	0.846 ± 0.634

Table 27

P_T	$E\frac{d^3\sigma}{d^3p}$	
	π^- N	pN
4.1	0.555 ± 0.085	-
4.4	0.376 ± 0.060	0.275 ± 0.084
4.6	0.284 ± 0.093	0.427 ± 0.11
4.9	0.361 ± 0.102	0.084 ± 0.12
5.2	0.397 ± 0.093	0.642 ± 0.16
5.7	0.311 ± 0.130	0.78 ± 0.23
6.5	0.882 ± 0.270	0.178 ± 0.25
7.2	0.630 ± 0.360	2.82 ± 2.3

Table 28

P_T	$E\frac{d^3\sigma}{d^3p}$	
	π^- N	pN
4.1	0.555 ± 0.085	-
4.4	0.376 ± 0.060	0.275 ± 0.084
4.6	0.284 ± 0.093	0.427 ± 0.11
4.9	0.361 ± 0.102	0.084 ± 0.12
5.2	0.397 ± 0.093	0.642 ± 0.16
5.7	0.311 ± 0.130	0.78 ± 0.23
6.5	0.882 ± 0.270	0.178 ± 0.25
7.2	0.630 ± 0.360	2.82 ± 2.3

Table 28

REFERENCES

1. Gross and Wilczek, 1973, Phys. Rev. Letts. 43, 1065, and Gross and Wilczek, 1974, Phys. Rev. D9, 980.
2. High-P_T production of direct photons and jets in quantum chromodynamics, L. Cormell, J.F. Owens, Phys. Rev. D22,N7,(1609)
3. Photon-Photon Production in Hadron-Hadron Collisions, R.D. Field, Proceedings of the 5th International Workshop on Photon Collisions, 13-16 April 1983, Aachen, Germany.
4. Structure of direct-photon events, F. Halzen, M. Dechantsreiter and D.M. Scott, Phys. Rev. D22,N7,(1617).
5. High-P_T production of direct photons and jets in quantum chromodynamics, L. Cormell, J.F. Owens, Phys. Rev. D22,N7,(1609)
6. T. Ferbel and W.R. Molzon, Direct Photon Production in High-Energy Collisions., Reviews of Modern Physics, April, 1984.

7. Large Momentum Transfer Production of Direct Photons, Jets and Particles, J.F. Owens., Reviews of Modern Physics Vol 59 No. 2 April 1987
8. J.P. Mansour Thesis, University of Rochester.
9. M. Bonesini et al., High Transverse Momentum η production in π^- p, π^+ p, and pp interactions at 280 GeV/c , Z. Phys. C 42,527-532(1989)
10. C. Kourkoumelis et al., Inclusive η production at high P_T at the ISR, Phy. Lett., 84B,No. 2,June 1979
11. T. Akesson et al., A comparison of direct photon, π° , and η production in $\bar{p}p$ and pp interactions at the CERN ISR.
12. J. Antille et al., A measurement of the inclusive π° and η production cross sections at high P_T in $\bar{p}p$ and pp collisions at $\sqrt{s}$ =24.3 GeV/c .
13. G. Donaldson et al., Inclusive η production at Large Transverse Momenta
14. C. Yosef *et al.*, "A Study of Direct Photon Production in Hadronic Collisions" in *Proceedings of the Second International Course on Particle Physics, Bogata, Columbia, August 1988* (submitted for publication).
15. G. Ginther *et al.*, "Preliminary Results from Fermilab Experiment E706 A Study of Direct Photon Production in Hadronic Interactions" in *Proceedings of the XXIVth Rencontres de Moriond - New Results in Hadronic Interactions, Les Arcs, Savoie, France, March 12-18 1989* (to be submitted for publication by Editions Frontières).
16. P. Lukens *et al.*, "Preliminary Results from Fermilab Experiment E-706 - A Study of Direct Photon Production in Hadronic Collisions" in *Proceedings of the DPF meeting, Storrs, Aug 15-18 1988* (submitted for publication).

17. E. Engels Jr., *et al.*, "Performance Characteristics and Radiation Damage Results from the Fermilab E706 Silicon Microstrip Detector System", *Nucl. Instr. and Meth.* **A279** (1989), 272.

18. G. Alverson, *et al.*, "Preliminary Results from Fermilab Experiment E-706 - A Study of Direct Photon Production in Hadronic Collisions", in *XXIVth International Conference on High Energy Physics*, R. Kotthaus and J.H. Kühn, eds., (1988), 719.

19. W. F. Baker *et al.*, "A-Dependence of Leading Particle Production by 800 GeV Protons", *ibid.*, p. 1400.

20. G. Ginther *et al.*, "Current Status of Fermilab E-706 A Direct Photon Study" in *New Data and Theoretical Trends - Proceedings of the XIXth International Symposium on Multiparticle Dynamics 1988, Arles, France, June 13-17 1988* edited by D. Schiff and J. Tran Thanh Van, (Editions Frontières) 217-222.

21. G.K. Fanourakis, *et al.*, "Direct Photon Studies: Current Status of Experiment E706 (Fermilab)", *Proc. of the Advanced Research Workshop on QCD Hard Hadronic Processes*, St. Croix, (1987) (in press).

22. E. Engels Jr., *et al.*, "A Silicon Microstrip Vertex Detector for Direct Photon Physics", *Nucl. Instr. and Meth.* **A253** (1987), 523.

23. P. Gutierrez, *et al.*, "E706 Liquid Argon Calorimeter", *Proc. of the International Europhysics Conf. on High Energy Physics*, Bari, L. Nitti and G. Preparata, eds., (1986).

24. F. Lobkowicz, *et al.*, "A Large Liquid Argon Photon/Hadron Calorimeter at FNAL", *Nucl. Instr. and Meth.* **A235** (1985), 332.

25. G. Alverson, *et al.*, "Investigation of Direct Photon Production at Fermilab", *Proc. of the 18th International Conference on Cosmic Rays*, P.V. Ramana Murthy, ed., (1983).